Signal Processing Algorithms
for Ultra-Wideband Wireless Communications

PROEFSCHRIFT

ter verkrijging van de graad van doctor
aan de Technische Universiteit Delft,
op gezag van de Rector Magnificus Prof. dr. ir. J.T. Fokkema,
voorzitter van het College voor Promoties,
in het openbaar te verdedigen
op vrijdag 15 februari 2008
door

Quang Hieu Dang

elektrotechnisch ingenieur
geboren te Hai Duong, Vietnam.

Dit proefschrift is goedgekeurd door de promotor:

Prof. dr. ir. A.-J. van der Veen

Samenstelling promotiecommissie:

Rector Magnificus	voorzitter
Prof. dr. ir. A.-J. van der Veen	Technische Universiteit Delft, promotor
Dr. ir. G.J.T. Leus	Technische Universiteit Delft
Prof. dr. J.C. Arnbak	Technische Universiteit Delft
Prof. dr. ir. R.L. Lagendijk	Technische Universiteit Delft
Prof. dr. ir. J.W.M. Bergmans	Technische Universiteit Eindhoven
Prof. dr. ir. E.R. Fledderus	Technische Universiteit Eindhoven
Dr. ir. O. Rousseaux	Holst Centre

To my parents and my sister.

Contents

Glossary

ALS	Alternating Least Squares
BER	Bit Error Rate
CDMA	Code Division Multiple Access
CM	Chanel Model
DH	Delay Hopped
DS	Direct Sequence
FDMA	Frequency Division Multiple Access
IFI	Inter-frame Interference
IPI	Inter-pulse Interference
ISI	Inter-symbol Interference
LOS	Line-of-Sight
LS	Least Squares
MF	Matched Filter
ML	Maximum Likelihood
MSE	Mean Square Error
MUI	Multiuser Interference
NBI	Narrowband Interference
NLOS	Non-Line-of-Sight
OFDM	Orthogonal Frequency Division Multiplexing
PAM	Pulse Amplitude Modulation
PPM	Pulse Position Modulation
SNR	Signal to Noise Ratio
SVD	Singular Value Decomposition
TR	Transmit-Reference
UWB	Ultra-Wideband
WLAN	Wireless Local Area Network
WPAN	Wireless Personal Area Network
ZF	Zero Forcing

Chapter 1

Introduction

The only way to discover the limits of the possible is to go beyond them into the impossible.

Arthur C. Clarke

Since the introduction of the simple wireless telegraph using Morse code and the (wired) telephone lines in the 19-th century, telecommunication has revolutionized the world. Recent years have seen a tremendous growth in both technologies and applications for wireless communications. The wireless local area networks (WLANs) and the third generation mobile phones have become a common and integral part of our daily lives. Furthermore, telecommunication in general or wireless communication technologies in particular are also present in many specialized applications like the global positioning systems, transportation, medical systems, under water communications, etc. Ultra-Wideband (UWB) radio is among the most recently developed technologies for wireless communications, and gains strong attention in both academia and industries in the world these days. In this chapter, the UWB technology is briefly introduced in the background of current general technological challenges and opportunities. The main problems of the thesis are subsequently formulated. Finally, the thesis' contributions are shortly presented in the chapters' outline of the thesis.

1.1 Background

In this ever-growing hi-tech world, there are unlimited demands on wireless communication systems to support higher speeds (data rates), higher precision, more reliable connections, more simultaneous users, etc. Meanwhile, the frequency resource is always limited. By definition, wireless communication is the transfer of information over a distance without any wire, by transmitting (and receiving) electromagnetic waves over a radio propagation channel. Depending on the characteristics of the radio channels, the distances, other requirements of the applications, and most importantly, the requirement to avoid interference to other systems, these electro-magnetic waves, also called wireless signals, need to operate in certain frequency bands. For example, the Global System for Mobile Communications (GSM) networks usually operate in 900 MHz and 1800 MHz frequency bands, or 850 MHz and 1900 MHz in North America. The WLAN signal is allowed to operate in the 2.4 GHz - 2.5 GHz band according to the IEEE 802.11g standard under Part 15 of the Federal Communications Commission (FCC) Rules and Regulations. As a result of increasing demands from all the commercial, industrial, scientific and government applications, the whole radio frequency spectrum, ranging from 3 KHz to 300 GHz, is now virtually occupied, from the broadcasting radio AM (in LF bands) to mobile satellite and radio astronomy (in EHF bands) [4].

This leads to a question: *"How can we support an unlimited demand (of throughput, users, etc.) with a limited (frequency) supply?"* The idea of frequency allocation originates from the Frequency Division Multiple Access (FDMA) technology. By dividing the whole frequency bandwidth into separate sub-bands, and allocating separate systems / users into these bands, we can avoid the (frequency) interferences between them. However, there are other technologies that also support multiple access like Time Division Multiple Access (TDMA) and Code Division Multiple Access (CDMA). The idea of spread spectrum CDMA technology is that all the signal are transmitted under the same (wide) frequency spectrum with some embedding codes, which can be used later at receiver by some signal processing algorithms to differentiate them. This technology has proven to have a higher overall network capacity in most 3G mobile communication networks today.

Ultra-Wideband (UWB) technology arrives as an alternative to partly solve the frequency resource scarcity problem mentioned above. By virtually covering the whole radio frequency spectrum with an ultra-wide frequency band (from 500 MHz to 30GHz or more), all the current radio systems including the so-called wideband CDMA become “narrowband” when compared to UWB signal (as illustrated in Fig. 1.1). Although this overlay approach does not solve the problem completely, it does not require a new licensed frequency allocation, which is always rare and expensive. The interference from UWB signals to the existing wireless systems is minimized by imposing limitations on the UWB radiated emission powers under different frequency ranges, while the interferences from existing wireless signals (with high power levels) to the UWB system remain as a problem to solve when implementing UWB transceiver schemes. These features - ultra-wide frequency bandwidth and ultra-low power - characterize the UWB signals. As a result, each node in the network using UWB technology can have only a short range coverage, which, similar to cellular network concept, turns out to be beneficial in terms of interferences from other adjacent nodes and improves overall capacity.

Not only does UWB technology avoid the frequency resource scarcity problem, but it also brings many new promising features compared to the existing “narrowband” wireless systems. Naturally, the ultra-wide bandwidth signal suggests a better obstacle penetration, higher data rate, and higher precision ranging (at

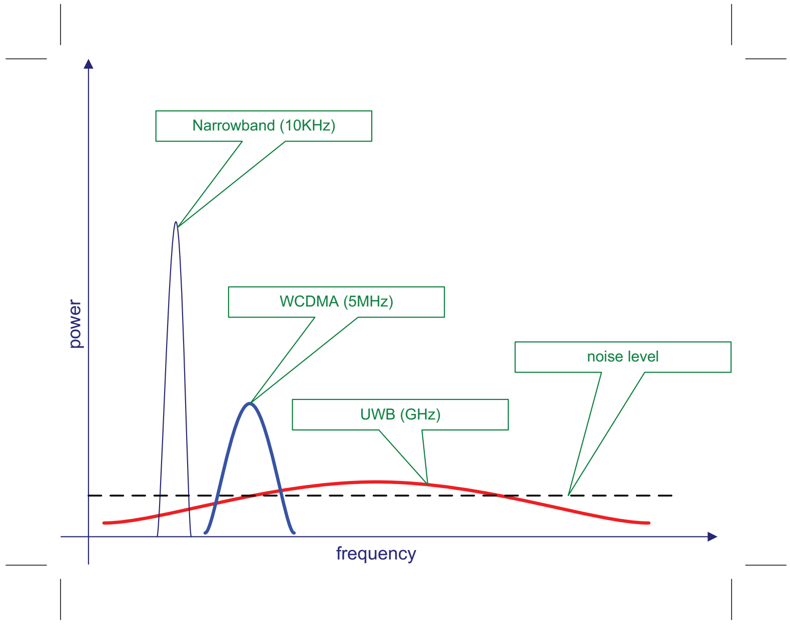

Figure 1.1: *UWB spectrum compared to existing narrowband systems.*

centimeter level) applications. Impulse Radio (IR) UWB systems, which use ultra-short pulses (sub-nanosecond duration), has the ability to resolve multipath channels. Moreover, IR UWB can operate independently in baseband (without a carrier), which, unlike the traditional narrowband systems, eliminates the need for up/down converters in the transmitter/receiver analog circuits. These features together make UWB an ideal candidate for low-complexity, low-power, short-range wireless communication systems.

1.2 Problem statement

Traditionally, the first step in all digital receivers for wireless communication (after the analog frontend) is to discretize (and quantize) the received signal into samples, which in turn become the inputs to the digital signal processing VLSI circuit. This chip can perform one or several tasks, e.g. channel estimation and equalization, single/multiuser detection, synchronization, etc. In order to perfectly reconstruct the analog received signal, the sampling rate should be, according to the famous Nyquist theorem, at least two times of the signal bandwidth. Sampling below the

Nyquist rate causes a signal aliasing problem, which significantly degrades the receiver performance. In UWB radio, due to its ultra-wide bandwidth, the Nyquist sampling rate is now ultra-high (can be as high as 20 GHz or even more). The resulting ultra-high sampling rates may be available in present-day ADCs or in the near future thanks to advances in semiconductor technology, but the cost will be too high with respect to the achieved data rates.

Transmit-Reference (TR) UWB scheme, which uses a sub-Nyquist sampling rate (can be as low as one sample per chip/symbol), is a well-known low complexity solution for IR-UWB. However, due to several implicit assumptions on channel length, channel correlation, and pulse spacing (e.g. no inter-pulse/frame interference IPI/IFI), it can, as originally proposed, only support very low data rates (at Kbps level) [37].

Not only does the issue of IFI relate to the data rates (bandwidth efficiency), but it also affects the bit-error-rate (BER) performance. Consider a transmission of UWB signals in a simple IR-UWB system. One data symbol spread over several frames, while each frame has one or two ultra-short pulse(s). In IR-UWB, these ultra-short pulses are transmitted (without any carrier) through a multipath wireless channel, under a certain noise level. Assuming a fixed symbol rate and given a fixed signal to noise ratio (SNR), the more frames (per symbol) are used the higher the resulting bit energy over noise power density (E_b/N_0) will be, and this is known to result in a better BER. Therefore, in power-limited UWB applications, it is more efficient to have as many frames per symbol as possible. However, the frame period cannot be chosen arbitrarily small because of two reasons: (i) pulse spacing should be large enough (normally larger than the inverse of the channel + antenna bandwidth) to avoid unwanted correlations, (ii) the average signal power is also upper bounded by FCC regulations. Despite these two reasons, given a fixed symbol rate and a practical channel length, if we can find a proper way to resolve the interframe interferences (caused by the fact that frame period is shorter than the channel length), the overall BER performance certainly improves.

Therefore, the first question arises: *"How to design a transceiver scheme for IR-UWB that uses sub-Nyquist sampling frequencies to reduce the receiver's complexity while it can still resolve IPI and IFI to achieve relatively high data rates?"*

Apart from the additive thermal noise, the radio propagation channel is the main source of unknown, unwanted distortions and attenuations on the signal in any wireless communication system. Similar to many other wireless systems, UWB signals can propagate through many paths before reaching the UWB receiver. A RAKE receiver, which will be introduced in the next chapter, matches a shifted template waveform with the individual reflected version of the transmitted pulse to estimate all the individual channel multipath components. Although IR-UWB benefits from the multipath fading immunity due to ultra-short pulses [1], its channel estimation is still a challenging task. UWB channels in practice can be very long (up to 200 ns) and with dense multipath (400 channel coefficients or more), which significantly affects the RAKE receiver's complexity (not to mention that this kind of receiver uses Nyquist sampling rate).

Meanwhile, the original TR-UWB scheme [70] goes to the other extreme when channel estimation is avoided completely by either ignoring the channel effect or implicitly assuming that the pulse spacing is larger than the channel length and that the channel is completely uncorrelated.

The second question is: *"Is there a third solution that neither ignores channel estimation nor estimates all the individual multipath channel coefficients, while providing a good and flexible trade-off between performance and complexity?"*

Although UWB technology seems simple and clean at first glance, it does have many small but important practical considerations. The use of ultra-narrow pulses poses a stringent requirement in time synchronization algorithms because only a small timing error would miss all or a large part of the signal's pulse. Secondly, due to the strong dominance of the first arrival line-of-sight (LOS) path, a small error in hardware, especially in the analog delay lines (which are mandatory in many IR-UWB schemes) would cause the loss of most of the received signal energy, and thus degrades the signal detection performance. Furthermore, antenna imperfections, e.g. the antenna bandwidth is not ultra-wide enough, and other frequency selective effects can distort the received pulses seriously and degrades the receiver performance, especially those that use matched filter operations like RAKE receivers. Finally, as mentioned before, the existing "narrowband" wireless systems are major sources of interferences to UWB radio due to their high power levels compared to UWB signal power. These interferences, called narrowband interferences (NBI), should be considered in all practical UWB schemes.

The third question is: *"How to build a IR-UWB scheme that effectively deals with NBI and other hardware imperfection issues mentioned above?"*

The capabilities to deal with multiuser interferences (MUI) as well as multiuser detection are crucial in any modern wireless system as more and more devices (or users) are required to communicate with each other simultaneously. Problems arise when the user signals collide or are not properly aligned. Moreover, the complexities of the corresponding receiver algorithms grow rapidly (even exponentially in some cases) as the number of users increases.

Finally, here comes the fourth question: *"How to derive efficient linear signal pro-*

[1] The multipath fading effect is when several copies of a transmitted signal are overlapped in time at the receiver, and thus cause unwanted waveform's distortion and attenuation. However, since UWB pulses are ultra-short, these multipath copies are generally not overlapped.

cessing models and receiver algorithms to include multiple users and have an acceptable complexity?"

These questions will be dealt either separately or together in the following chapters as summarized in the next section.

1.3 Thesis outline

The thesis is organized into five main content chapters: a robust TR-UWB scheme that deals with random channels and accepts small discrepancies in delay lines (chapter 3), a higher rate TR-UWB scheme that resolves both interpulse interference and interframe interference (chapter 5), a multiuser CDMA system that has a linear data model in matrix form and implements blind iterative receiver algorithms with low complexity (chapter 6), and a solution to mitigate narrowband interference (chapter 7). Although many of the proposed receiver algorithms are based on the iterative Alternating Least Square (ALS), which is presented in details in chapter 6, each chapter can be read independently. More specifically, the content of each individual chapter is briefly described as follows.

Chapter 2 presents some basic concepts and characteristics in UWB radio. Two main popular transceiver schemes, i.e. RAKE and TR schemes, are introduced. The research challenges are discussed in more detail.

Chapter 3 proposes a novel TR-UWB scheme that estimates the channel correlation parameters (in the form of a channel correlation matrix). An exact data model is obtained and receiver algorithms are derived. The incorporation of the channel correlation matrix guarantees the robustness of the system against random UWB channels and some small misadjustments in the delay lines.

Chapter 4 investigates some typical correlation aspects of both the measured UWB channels and the IEEE proposed channel models. Their implications on the signal model and on other system parameters are presented.

Chapter 5 uses oversampling (together with an "integrate and dump" operator) to deal with interframe interference. The unknown channel parameters are now the energies of the channel segments, which can be estimated either blindly or iteratively by using a linear data model and its corresponding decorrelating receiver algorithms. This scheme supports multiple users, is more flexible and robust against synchronization error (up to a sampling period). By resolving IFI, it can support higher data rates than other TR-UWB schemes.

Chapter 6 presents the same fundamental signal processing model and algorithms that have been used extensively in the previous chapters. It shows how the CDMA concept can apply in UWB and how efficient (low complexity) algorithms can be implemented based on the sparse structures of the matrices in the data models.

Chapter 7 considers narrowband interference (NBI) in TR-UWB scheme. The statistics of many cross terms are briefly studied and simulated. It is shown under certain circumstances that the dominant NBI terms can be put into the data model and can be mitigated digitally in the receiver algorithm.

Chapter 8 concludes the thesis with a summary of the main results. Open problems and future research are also discussed.

1.4 Context

The research for this thesis was conducted within the VICI project ”Signal processing for future wireless communications” and partly sponsored by the AIRLINK project.

- VICI (September 2003 - September 2008). The VICI project ”Signal processing for future wireless communications” is implemented within the CAS group, EEMCS faculty, TU Delft. It aims at developing new signal processing algorithms for source seperation problem and ad hoc networks, in which UWB radio technology is an ideal candidate with unlicensed, very large spectrum and many promising features.

- AIRLINK (August 2002 - April 2004). The AIRLINK project ”Ad-hoc Impulse Radio: Local Instantaneous Networks” aims exclusively at the IR-UWB technology. Researchers from many groups in the EEMCS faculty are gathered to deal with different work packages, which cover almost all areas of UWB, from practical measurement/modeling of the UWB channels, implementation of the UWB antennas, UWB pulse generators to developing signal processing algorithms in UWB transceiver schemes, channel coding and ad-hoc network protocols.

1.5 List of publications

Journals

- Q.H. Dang and A.J. van der Veen. ”A low-complexity blind multiuser receiver for long-code CDMA” Eurasip Journal on Wireless Communications and Networking, Vol. 2004, No. 1, pp. 113-122, Aug. 2004.

- Q.H. Dang, A. Trindade, A.J. van der Veen, and G. Leus. ”Signal model and receiver algorithms for a transmit-reference ultra-wideband communication system” IEEE Journal on Selected Areas in Communications, Vol. 24, No. 4, pp. 773-779, April 2006.
- Q.H. Dang and A.J. van der Veen. ”A decorrelating multiuser receiver for TR-UWB communication systems” IEEE Journal on Selected Topics in Signal Processing, Vol. 1, Issue. 3, pp. 431-442, Oct 2007.

Conferences

- Q.H. Dang and A.J. van der Veen. ”Single- and multi-user blind receiver for long code WCDMA,” in Proc. IEEE Workshop on Signal Processing Advances in Wireless Communications, (Rome, Italy), Jun 2003.
- A. Trindade, Q.H. Dang, and A.J. van der Veen. ”Signal processing model for a transmit reference UWB wireless communication system,” in Proc. IEEE Conference on Ultra Wideband Systems and Technologies, (Reston, Virginia), Oct. 2003.
- A.J. van der Veen and Q.H. Dang, ”Complexity Analysis of an Efficient Blind Long-Code WCDMA Receiver” In IEEE SPS Benelux workshop, Hilvarenbeek, The Netherlands, pp. 125-128, April 2004.
- Q.H. Dang, A.J. van der Veen and A. Trindade. ”Statistical analysis of a transmit-reference UWB wireless communication system,” in Proc. IEEE International Conference on Acoustics, Speech, and Signal Processing (ICASSP), (Philadelphia, PA), Vol. 3, Mar 2005.
- A. Trindade, Q.H. Dang and A.J. van der Veen. ”Signal processing model for a transmit-reference UWB wireless communication system” In IEEE SPS Benelux workshop, Hilvarenbeek, The Netherlands, pp. 129-132, April 2004.
- Q.H. Dang, A. Trindade and A.J. van der Veen. ”Considering delay inaccuracies in a transmit-reference UWB communication system” in Proc. IEEE International Conference on Ultra-Wideband. (ICU 2005) (Zurich, Switzerland). Sept 2005.
- Q.H. Dang and A.J. van der Veen. ”Resolving inter-frame interference in a transmit-reference ultra-wideband communication system” Proceedings. 2006 IEEE International Conference on Acoustics, Speech and Signal Processing (ICASSP) , (Toulouse, France), Vol. 4, May 2006.

- Q.H. Dang and A.J. van der Veen. ”Narrowband interference mitigation for a transmitted-reference ultra-wideband receiver” in Proc. Eusipco, Florence (IT), September 2006.
- Q.H. Dang and A.J. van der Veen. ”Signal processing for Transmit-Reference UWB”, In Proc. 3rd Annual IEEE Benelux/DSP Valley Signal Processing Symposium, Antwerp (BE), IEEE, pp. 55-61, March 2007.
- Q.H. Dang and A.J. van der Veen. ”Signal Processing Model and Receiver Algorithms for a Higher Rate Multi-User TR-UWB System” in Proc. IEEE International Conference on Acoustics, Speech and Signal Processing (ICASSP), Vol. 3, (Honolulu, Hawaii), Apr 2007.

Chapter 2

Preliminaries

Think big, start small.

Anonymous

In this chapter, the basic concepts of Ultra-Wideband (UWB) radio are presented. The transmit-reference scheme is motivated and discussed as a potential candidate for a low complexity and feasible UWB systems. The research challenges are introduced with more detail. Some (known) mathematic notations and algorithms in linear algebra are briefly listed.

2.1 An introduction to Ultra-Wideband Radio

Ultra-Wideband communication systems are characterized by the fact that the transmission bandwidth B is greater than 500 MHz or more than 20% of the center frequency f_c, where $B := f_H - f_L$ and $f_c := (f_H - f_L)/2$, f_H and f_L are respectively the -10dB upper and lower frequencies [3]. Therefore, an UWB signal centered at 2.5 GHz has 500 MHz bandwidth at least, and a UWB signal centered at 5 GHz should have a minimum bandwidth of about 1 GHz, which are really ultra-wide compared to other "traditional" wireless communication systems. This ultra-wide bandwidth feature promises much higher data rates and several attractive features in many wireless applications.

Since April 2002, UWB technology is legally allowed in the United States to operate without license in the frequency band 3.110.6 GHz as long as the UWB signal meets a spectral mask provided by FCC [3], which sets the upper limits of the power emission levels of the signal under different frequency ranges. This spectral mask requires that the UWB signal must not be too strong to cause any serious interference to other existing "narrowband" systems, e.g. GSM, GPS, WLAN. In fact, under this spectral mask, the UWB signal strength is so low that it is almost embedded below the noise floor.

Later, in March 2005, the European Electronic Communications Committee (ECC) also proposed a frequency spectral mask for UWB signal [5]. This spectral mask is

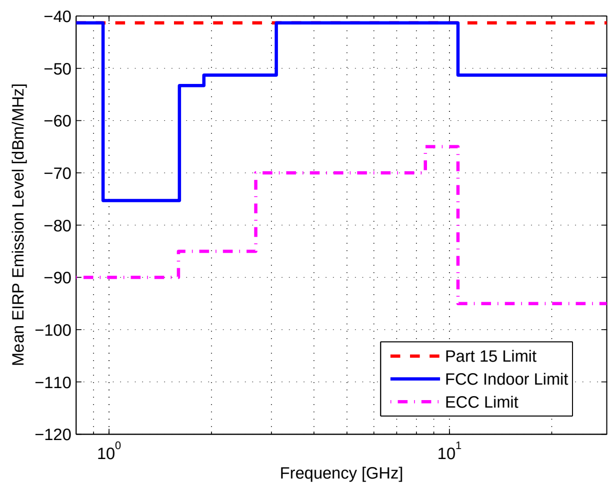

Figure 2.1: *FCC (indoor) and ECC spectral masks for UWB radio.*

even more strict on the UWB signal's bandwidth and power levels (illustrated in Fig. 2.1).

2.1.1 Impulse Radio Ultra-Wideband

So far, there are two main approaches to implement a UWB system: MultiBand OFDM (MB-OFDM) and Impulse-Radio UWB (IR-UWB), which is also known as Direct-Sequence UWB (DS-UWB). The first approach uses OFDM technology to divide the whole bandwidth into several subbands of approximately 500 MHz. A signal symbol is spread over all the subbands, modulated and transmitted by all the subcarriers simultaneously. One big advantage of this approach is that all the results of OFDM, a pretty mature technology, can be applied immediately. By dividing the whole bandwidth into subbands, the signal can be shaped to fit virtually any spectral mask.

The second approach comes from the very basic duality between time and frequency. The ultra-wide (frequency) bandwidth suggests the use of ultra-short (in time duration) pulses. In IR-UWB, these pulses are transmitted discontinuously, without any carrier, at very low power. The proposed schemes for UWB systems in this thesis belong to this IR-UWB approach.

The most widely used pulses in IR-UWB are the Gaussian monocycles and their

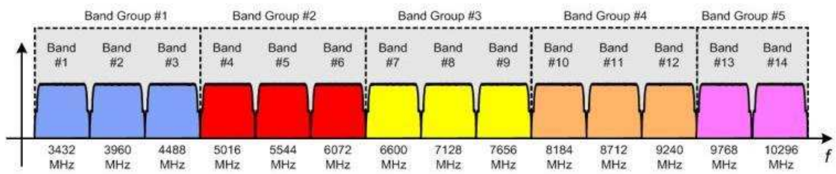

Figure 2.2: *MB-OFDM band plan.*

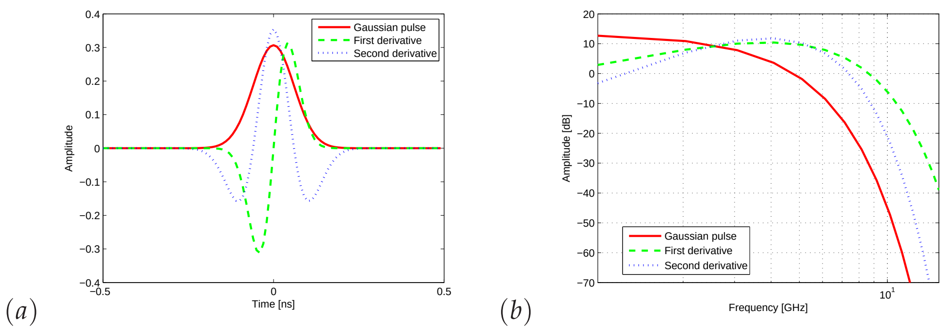

Figure 2.3: *UWB monocycles as derivatives of Gaussian pulse.*

derivatives because of their superior localization both in time and frequency, and easier antenna implementation [59]. The basic Gaussian monocycle is defined as

$$g_o(t) = e^{2\pi(\frac{t}{t_p})^2}$$

and its k-th derivative is

$$g_k(t) = \epsilon_k \frac{d^k}{dt^k}(e^{2\pi(\frac{t}{t_p})^2})$$

where t_p is a parameter that determines the pulse's duration T_p ($T_p \approx 2 \cdot t_p$), and ϵ_n is introduced to normalize the pulse energy. The derivatives are used because in first order approximation, antennas act like a differentiator (chapter 6 in [54], and in [31]).

As shown in Fig. 2.3, these derivatives of Gaussian pulses have -10dB frequency bandwidth greater than 20% of the center frequency. More over, the first order derivative pulses tend to shift more to the higher frequency region, which better fit in the FCC spectral mask.

2.1.2 Standardization and applications

One main application of UWB technology is in Wireless Personal Area Network (WPAN), which is within the coverage of the IEEE 802.15 Working Group. Two task groups have been created to develop WPAN standards under two different contexts, both of which opt to use UWB technology in physical layer. Therefore, the UWB standardization job has been implicitly given to this working group.

- The 802.15.3a task group (TG3a - WPAN High Rate Alternative PHY) aims to define a new physical layer in high speed WPANs. Although UWB technology has been proposed, but no agreement has been reached on which approach: MB-OFDM (supported by WiMedia Alliance) or DS-UWB (supported by UWB Forum). On January 19, 2006 IEEE 802.15.3a task group (TG3a) members voted to withdraw the December 2002 project authorization request (PAR) that initiated the development of high data rate UWB standards. One of the important achievements of this task group is the IEEE radio channel models, which are used widespread in UWB research community for simulations.

- The 802.15.4a task group (TG4a - WPAN Low Rate Alternative PHY) is working on an amendment to the existing 802.15.4 standard on low rate WPAN by "providing communications and high precision ranging / location capability (1 meter accuracy and better), high aggregate throughput, and ultra low power; as well as adding scalability to data rates, longer range, and lower power consumption and cost" [2]. Similar IEEE channel models are proposed with some modifications particularly for low rate context.

In addition to the two task groups mentioned above, there is another 802.15.3c task group (TG3c), which also aims to amend the 802.15.3 standard but in the millimeter-wave-based alternative PHY. "This mmWave WPAN will operate in the new and clear band including 57-64 GHz unlicensed band defined by FCC 47 CFR 15.255. The millimeter-wave WPAN will allow high coexistence (close physical spacing) with all other microwave systems in the 802.15 family of WPANs" [1]. Although the signal in this band is, by definition, not exactly ultra-wideband, some results e.g. the channel statistics can be useful especially when UWB signal is allowed to operate in higher (and wider) frequency bands in the future.

Similarly, the main applications of UWB technology can also be roughly categorized as follows.

- High rate WPAN. The next generation wireless USB is proposed to use UWB technology. Ultra-high speed wireless connections become viable between personal computers, the peripherals and other portable electronic devices in a short-range ad hoc indoor environment. This enables a wireless virtual home / office with high quality real time entertainment / data transferring system in the most mobile and convenient ways.

- Low rate sensor networks. Because of its ultra-low power consumption nature and the ultra-wide bandwidth in which the connection's range and performance can be easily traded for data rate, UWB radio becomes an ideal technology for wireless sensor networks that requires reliable radio connections between spatially distributed autonomous devices. Various applications can be found in health monitoring system, traffic control, inventory tracking, military surveillance, etc. Ultra-short pulses allow localization at sub-centimeter resolution. Moreover, their strong penetration enables localization through walls, building blocks.

2.1.3 UWB channels

As in any wireless system, the UWB channel is a multipath channel, i.e. a signal arrives at the receiver via several different paths with different received powers, delays, fading and other frequency selective effects. The main difference to the traditional "narrowband" wireless systems is that the transmission of an ultra-short pulse through the multipath wireless channel will result in a combination of several distorted pulses, arrived at discrete time instants (no overlap between consecutive pulses, which will be shown later not always true for some scenarios with dense multipath channels) as illustrated in Fig. 2.4. Therefore, a simple circuit can simply sample and collect all these multipath components and thus effectively detect the transmitted signal.

Let $h_p(t)$ be the (physical) multipath channel impulse response. The UWB indoor channel models proposed by IEEE 802.15.3a Task Group [28, 52] are based on the famous multipath Saleh-Valenzuela model [58], in which the multipath components arrive at the receiver in clusters,

$$
\begin{aligned}
h_p(t) &= \sum_{n=0}^{\infty} a_n \delta(t - \tau_n) && (2.1)\\
&= \sum_{\ell=0}^{L} \sum_{k=0}^{K_\ell} a_{k\ell} \delta(t - T_\ell - \tau_{k,\ell}) && (2.2)
\end{aligned}
$$

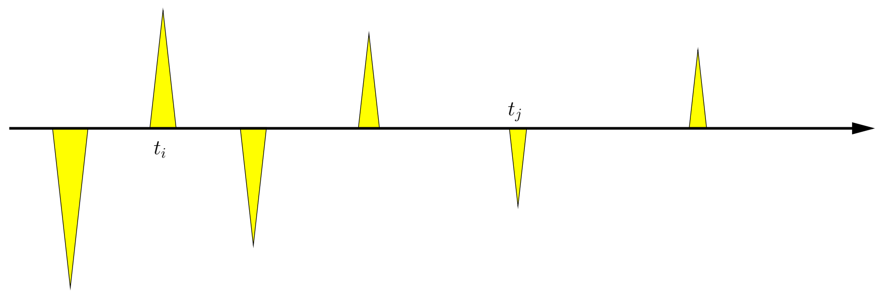

Figure 2.4: *The received signal when transmitting a single UWB pulse through a simplified multipath channel.*

where $\delta(\cdot)$ is the dirac delta function, L is the total number of clusters and K_ℓ is the total number of rays in the ℓ-th cluster. The scalars $a_{k\ell}$, $\tau_{k\ell}$ denote the complex amplitude and delay of the k-th ray of the ℓ-th cluster, while T_ℓ is the delay of the ℓ-th cluster. Equation (2.2) is used when we want to highlight the cluster structure of the UWB channel. Otherwise, we use the more general equation (2.1), where a_n is the amplitude of the ray (also called as "channel tap") at delay τ_n.

UWB channels will be discussed in more details later in chapter 4.

2.2 Transceiver schemes for IR-UWB

The generic unit that carries information in IR-UWB is a frame of a constant duration T_f, in which only one or two UWB pulses are transmitted typically. The frames' information can be either the pulses' amplitudes / polarities (Pulse Amplitude Modulation - PAM) or the relative time position of the pulse(s) within a frame period (Pulse Position Modulation - PPM). Because each pulse is transmitted at a very low power, several frames may be needed to convey one data symbol. To accommodate multiple users, superimposing CDMA-like chip codes can be used. In this case, each symbol consists of several chips, each chip of period T_c may have one or more frames.

Fig. 2.6 and Fig. 2.5 illustrate the PAM and PPM modulated pulse sequences for one data symbol. Each symbol consists of N_f chips, and each chip consists of just one frame (in this case the chip and frame terminologies are interchangeable). Some UWB applications trade the bit rate for higher bit energy over noise density (E_b/N_0) by transmitting several identical frames per chip.

A transmitted pulse sequence for a single user with PAM modulation, one frame per chip $c_i \in \{+1, -1\}$ and N_f chips per symbol $s_{\lfloor i/N_f \rfloor}$ can be written as

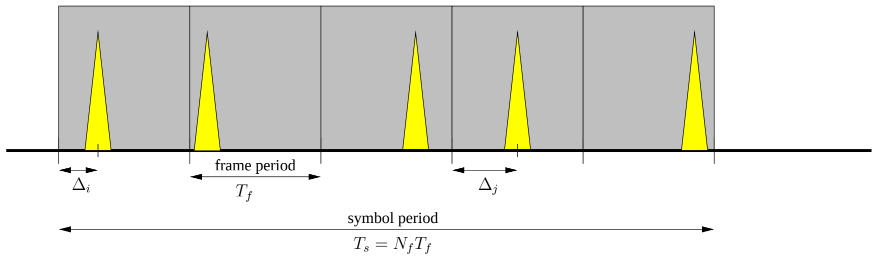

Figure 2.5: *Pulse Position Modulation (PPM).*

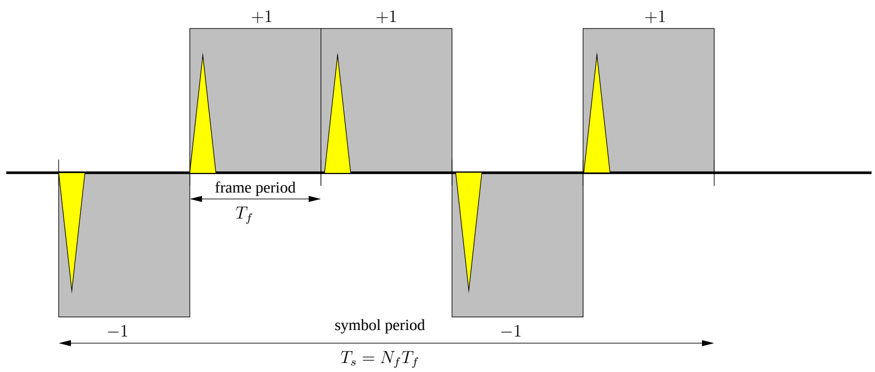

Figure 2.6: *Pulse Amplitude Modulation (PAM) when $M = 2$.*

$$x_{tx} = \sqrt{\epsilon} \sum_{i=0}^{\infty} s_{\lfloor i/N_f \rfloor} c_i g(t - iT_f) \tag{2.3}$$

where T_f is the frame period, ϵ is the user's transmitted energy per pulse. Later, for simplicity and clarity reason, this term ϵ is often omitted in our equations. In this case, in order to highlight the frame sequence structure and shorten the equation, symbols' indices are expressed as a function of the frame index i using the floor operator.

Most transceiver schemes in IR-UWB exploit the strong penetration of the UWB pulses over a short distance and the unique multipath channel characteristics described in the preceding section. The typical UWB transceivers, apart from the antennas and some bandpass/lowpass analog filters, are expected to have very simple circuit e.g. just some delay and sampling circuit, without the upconverter in the transmitter and the downconverter in the receiver, and the rest of the detection, estimation, equalization will be implemented digitally.

2.2.1 RAKE receivers

The most well-known approach to deal with multipath wireless channels is to use RAKE receivers, as implemented successfully in the "traditional" wideband CDMA systems. Therefore, it is straightforward to apply this concept for channel estimation in IR-UWB. Basically, a RAKE receiver consists of multiple correlators (also called RAKE fingers). Each finger matches (correlates) the received pulse sequence (spread by the multipath channel) with a delayed version of a template pulse $g(t-\tau_n)$. The correlator's output is an estimate of the amplitude a_n of the corresponding channel tap (from equation (2.1)).

Consider the PAM modulated pulse sequence expressed in (2.3), transmitted over a multipath channel described in (2.1). Ignoring the non-ideal antenna effect, the received signal is

$$r(t) = \sqrt{\epsilon}\sum_{i=0}^{\infty} s_{\lfloor i/N_f \rfloor} c_i h(t - iT_f) + n(t)$$

where $n(t)$ is the additive noise, $h(t)$ is the composite channel response $h(t) := h_p(t) * g(t)$.

$$h(t) = \sum_{n=0}^{\infty} a_n g(t-\tau_n)$$

Matching the received signal with a template pulse, which is a delayed copy of the transmitted pulse $g(t)$, the correlator's output for a RAKE finger corresponding to the multipath component at τ_n delay in the i-th frame will be

$$\begin{aligned} x_{i,n} &= \int r(t) g(t - iT_f - \tau_n) dt \\ &= \int \sqrt{\epsilon} \cdot s_{\lfloor i/N_f \rfloor} c_i h(t - iT_f) g(t - iT_f - \tau_n) dt + n'_{in} \\ &= \sqrt{\epsilon} \cdot s_{\lfloor i/N_f \rfloor} c_i a'_n + n'(t) \end{aligned}$$

where $n'_{in} := \int n(t) g(t - iT_f - \tau_n) dt$, and $a'_n = a_n \int g^2(t - iT_f - \tau_n) dt$ is the amplitude of the corresponding channel multipath component (at delay τ_n of the i-th frame) scaled by a positive constant. Subsequently, outputs from all RAKE fingers will be combined to detect the transmitted symbols as in any usual RAKE-CDMA system. At the same time, channel taps can be estimated blindly (along with data symbols) or by training in various ways [72], [50].

In order to avoid interference between pulses or frames, this step assumes that the maximum channel delay spread T_h is smaller than the frame period T_f, and spacing between two consecutive multipath components must be two times larger than the pulse duration T_p.

The RAKE receiver is a matched filter (the received pulse is matched with a template that has the same waveform) and therefore (with known channel coefficients) optimum with respect to the BER performance, and it also benefits from the fact that many results in existing literature on RAKE receivers for wireless communication systems e.g. WCDMA can still apply. However, there are some serious practical issues in this kind of receiver.

- The Nyquist sampling frequency used in this approach may be too costly under the current ADC technology, which can be as high as 40 GHz.

- Some measured channels can spread very long (up to 200 ns) and have dense multipath components (400 channel taps or more), which greatly increases the receiver's complexity in channel estimation and synchronization. Very often, only a subset of "RAKE fingers" is used giving an approximation of the matched filter. The ignored paths will result in interferences.

- In the above example, the template pulse $g(t - \tau_n)$ is assumed known and generated locally. But in practice, due to non-ideal antennas (at the transmitter and receiver) and other frequency selective effects, the received pulse is distorted in unwanted and unknown ways. This significantly affects the receiver performance.

2.2.2 Transmit reference scheme

While the RAKE concept is used to estimate individual multipath components of the channel, the Transmit-Reference (TR) systems were devised as a method of communicating in unknown or random channels [57], under the assumption that the channel is stationary during the transmission of the reference signal followed by the message signal. Luckily, UWB pulses are ultra-short in time duration and they are supposed to be transmitted at much higher rates (than the traditional narrowband systems), which allows the channel to be stationary over an even longer time span e.g. frame or symbol period.

It is known that, in general, the problem of single user optimal detection leads to the use of a matched filter, i.e., a convolution by the transmitted waveform including the effects of the channel. This waveform is not known and would need to be estimated. The idea of a TR system is that by transmitting a reference signal through

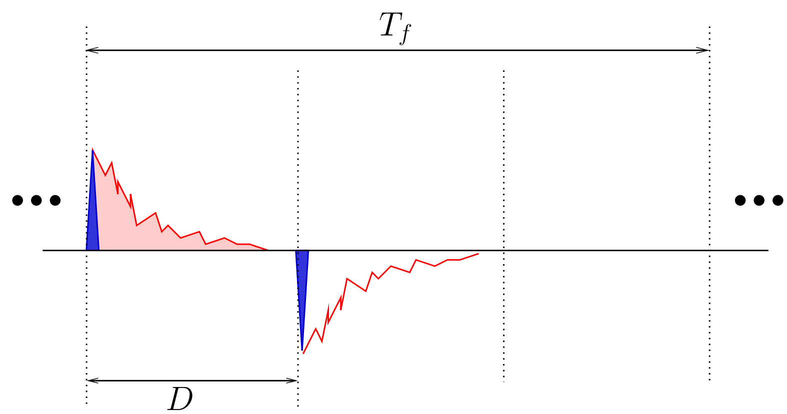

Figure 2.7: *One received signal frame in TR-UWB.*

the same channel as the message, it can be used in the convolution, so that channel state information is not needed to estimate the information.

For example, we consider a simple transmission of a pulse pair (also called a doublet) consisting of a reference pulse $g(t)$ and an information-bearing pulse $s \cdot g(t-D)$. After being sent through a multipath channel (2.1), the received signal is

$$r(t) = h(t) + s \cdot h(t-D) \tag{2.4}$$

where s is the data symbol, $h(t)$ is the composite channel. Fig. 2.7 illustrates the received signal and the basic receiver structure of a TR-UWB system.

Assuming $T_h + T_p < D$ so that there will be no interpulse interference, the data symbol can be detected by crosscorrelating the signal with the delay-by-D version of itself, which can be viewed as matched filter with a noisy template,

$$\hat{s} = \text{sign}\left\{ \int r(t)r(t-D)dt \right\}$$

In this TR-UWB scheme, the data symbols can be detected without channel estimation. No synchronization is needed at the analog part of the receiver (the data and the reference pulse are always spaced at a fixed and known time interval D). Furthermore, no matter how the UWB pulses are distorted, their distortions as well as the channel spread are the same, and only one sample is needed per frame for the detection.

"Transmit Reference" is an old idea that goes back to the processing of random signals in the 1950s. The problem of partitioning the energy between the reference

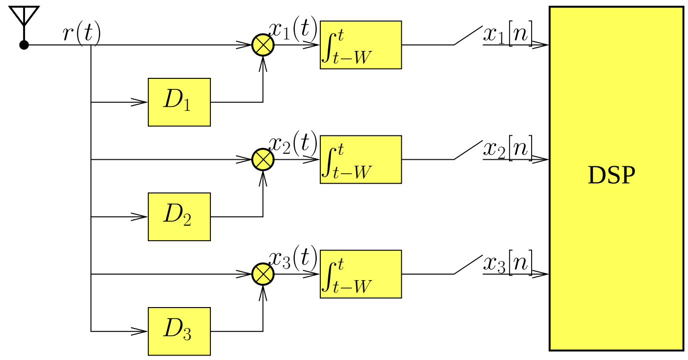

Figure 2.8: *The TR-UWB receiver with a bank of correlators prosposed by Hoctor and Tomlinson.*

and the message or information-bearing signals was subsequently addressed in [35], where the correlation receiver was proposed as a good approximation of the optimal receiver in AWGN. Further analysis of a crosscorrelator receiver with bandpass inputs was conducted in [9]. It is recognized that TR systems may be an inefficient means of transmitting information in a bandlimited system [32], with a 3-dB poorer SNR when compared to locally generated reference systems (LGR).

Nevertheless, its combination with UWB and the processing constraints of receivers in very high data rate transmissions make this trade-off worthwhile, as it allows simpler synchronization and channel estimation, especially when compared to RAKE receivers. Furthermore, it is possible to increase the efficiency of TR systems by re-using one reference template for estimating the message in several information-bearing pulses, as suggested in [80]. TR-UWB systems are therefore a practical technique to side-step channel estimation, especially at very high data rates in portable devices where processing power and power consumption are limited.

The first TR-UWB system that can be considered practical for an ad-hoc communication scheme was proposed by Hoctor and Tomlinson [70, 36], and called delay-hopped (DH) transmitted reference (TR) system. It could be implemented as an impulse radio or as a more traditional spread-spectrum carrier-based system. An experimental setup demonstrated the validity of the concept for short-range low-power communications [70], and a detailed analysis can be found in [37]. The spacing between the pulses in a doublet can vary, which serves as a user code. The receiver correlates the received data with several shifts of it using a bank of correlation lags, integrates, samples and digitally combines the outputs of the bank. The receiver structure is illustrated in Fig. 2.8.

As in [70, 36], by using the several repetition frames per chip per symbol with no

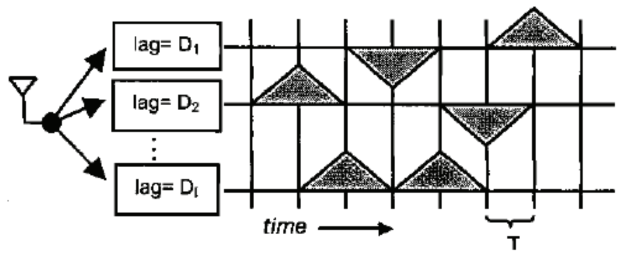

Figure 2.9: *The signal output at the TR-UWB receiver prosposed by Hoctor and Tomlinson (copied from [36]).*

interframe interference, and by using sliding window integration, the signal at the receiver output (before being sampled) has the triangular shapes (Fig. 2.9), which will simplify the synchronization at the receiver, sampling and digital processing at a feasible rate. The receiver complexity is also reduced by the use of straightforward non-adaptive analog components.

2.3 Research challenges in IR-UWB

After having introduced the basic concepts of UWB technology, the main research challenges in IR-UWB are listed in more detail as follows.

- Synchronization. Since IR-UWB uses ultra-short pulses, the synchronization task to estimate τ_0 (from equation (2.1)) or the offset of the first arrival signal in high data rate applications becomes a challenging task.

- High data rate. One of the main applications of UWB technology is the high data rate wireless USB, where IR-UWB (or DS-UWB) faces a strong challenge from MB-OFDM approach. Not to mention all the implicit assumptions on the upper limit of the frame rate in many IR-UWB research papers, the implementation of such high rate IR-UWB schemes, as directly pointed out by the MB-OFDM consortium, suffer losses caused by finite precision ADC, the aliasing (due to sub-Nyquist sampling) and timing synchronization errors. → see chapter 3 and chapter 5.

- Computational complexity. One of the main claims of IR-UWB over MB-OFDM is that IR-UWB can provide transceiver schemes with much lower complexity. However, as the UWB channels are longer, more dense multipath, and the selective frequent fading gets more serious, the RAKE receiver (because of Nyquist sampling, estimating individual channel taps), or even some TR-UWB schemes becomes infeasible. Meanwhile, although some TR-UWB schemes like the one proposed by Hoctor and Tomlinson are simple enough, they can only support applications with low requirements (lower data rate or low BER performance). There comes a need of more flexible schemes, which can adjust the performance / complexity tradeoff more directly and robustly. → see chapter 5.

- Narrowband interference (NBI). As a UWB signal covers almost all the available frequency spectrum, the existing wireless communication signal GSM, GPS, WLAN becomes “narrowband”. While the UWB signal must be kept at very low power emission levels (under the spectral mask provided by regulations) so that it will not damage the current wireless systems, these narrowband systems do cause unavoidable interference to the UWB signal. These intereferences are narrowband but with much higher power emission levels than that of the UWB signal, which degrades the performance of the UWB system. The problem becomes more serious for TR-UWB schemes because of the autocorrelation step, which results in many cross-terms between the signal and the various sources of interference. This NBI effect should be carefully taken into account in constructing the data models as well as in deriving receiver algorithms. → see chapter 7.

2.4 Mathematic notations and algorithms

In this thesis, ^{T} is the matrix transpose, ^{H} the matrix complex conjugate transpose, $\dagger$ the matrix pseudo-inverse (Moore-Penrose inverse). $\mathbf{I}$ (or $\mathbf{I}_p$) is the $(p \times p)$ identity matrix. $\mathbf{0}$ and $\mathbf{1}$ are vectors for which all entries are equal to 0 and 1, respectively. δ_{ij} is the Kronecker delta, $\delta(t)$ is a dirac unit impulse.

vec$(\mathbf{A})$ is a stacking of the columns of a matrix $\mathbf{A}$ into a vector. For a vector, diag$(\mathbf{v})$ is a diagonal matrix with the entries of $\mathbf{v}$ on the diagonal. For a matrix, vecdiag$(\mathbf{A})$ is a vector consisting of the diagonal entries of $\mathbf{A}$. $\odot$ is the Schur-Hadamardt (entry-wise) matrix product, $\otimes$ is the Kronecker product, $\circ$ is the Khatri-Rao product, which is a column-wise Kronecker product:

$$\mathbf{A} \circ \mathbf{B} = [\mathbf{a}_1 \otimes \mathbf{b}_1 \quad \mathbf{a}_2 \otimes \mathbf{b}_2 \quad \cdots] .$$

$\mathrm{E}(\cdot)$ denotes the expectation operator, $\mathrm{cov}(\cdot)$ the covariance and $\mathrm{var}(\cdot)$ the variance operator.

2.4.1 Band matrices in linear systems

Through out this thesis, we will have to solve several linear systems of the form $\mathbf{x} = \mathbf{A}\mathbf{s}$ (where $\mathbf{s}$ is unknown) repeatedly. This is usually the step that requires most operations in the receiver algorithms. However, if we can exploit the sparse structure of $\mathbf{A}$, the complexity can be reduced significantly. In this section, we will give a simple example where $\mathbf{A}$ is a band square banded matrix.

The standard solution to this linear system is the famous Gaussian Elimination method. First, $\mathbf{A}$ is LU factorized into a product of a lower triangular matrix $\mathbf{L}$ and an upper triangular matrix $\mathbf{U}$

$$\mathbf{A} = \mathbf{L}\mathbf{U}\,.$$

Then the linear system is solved in two steps,

$$\mathbf{x} = \mathbf{L}\mathbf{y}\,, \quad \mathbf{y} = \mathbf{U}\mathbf{s}\,,$$

each of which can be solved by a simple forward / back substitution.

When $\mathbf{A}$ is a full $n \times n$ square matrix, the number of operations needed is $2n^3/3$ (ignoring some lower order terms, e.g. back substitution takes $O(n^2)$ operations) (see chapter 3 in [33]). There are more computationally efficient techniques [62, 14] but the Gaussian Elimination is still a prefered method for its simplicity.

Consider the case when $\mathbf{A}$ is a band matrix: $a_{ij} = 0$ for $|i - j| > d$, where $d \ll n$ is defined as the "bandwidth" of $\mathbf{A}$. Obviously, this reduces the storage from n^2 (for the full $n \times n$ matrix) to only $n(2d + 1)$. Similarly, we can solve the linear system by applying LU factorization and a foward/back substitution. Due to the band structure of $\mathbf{A}$, it can be easily computed that the complexity for this case (by using Gaussian Elimination) will be $O(nd^2)$ instead of $O(n^3)$.

When the band matrix $\mathbf{A}$ is sparse within the band, there are known techniques which use permutations to minimize the bandwidth, which results in further reduced complexity.

2.4.2 Singular value decomposition

The singular value decomposition (SVD) is one of the most important tools in signal processing [33, 53]. It can provide robust solutions to various problems including the signal estimation problem in the presence of noise and interference. The SVD theorem can be briefly stated as follows.

Every matrix $\mathbf{X} \in \mathbb{C}^{m\times n}$ can be factored as

$$\mathbf{X} = \mathbf{U}\mathbf{\Sigma}\mathbf{V}^H ,$$

where $\mathbf{U} = [\mathbf{u}_1, \ldots, \mathbf{u}_m] \in \mathbb{C}^{m\times m}$, $\mathbf{V} = [\mathbf{v}_1, \ldots, \mathbf{v}_n] \in \mathbb{C}^{n\times n}$ are unitary matrices, and $\mathbf{\Sigma} \in \mathbb{R}^{m\times n}$ is a real diagonal matrix

$$\mathbf{\Sigma} = \mathrm{diag}(\sigma_1, \sigma_2, \ldots, \sigma_p) ,$$

where $p = \min(m, n)$, the real positive σ_i are called the singular values of $\mathbf{X}$, which are often ordered as

$$\sigma_1 \geq \sigma_2 \geq \cdots \geq \sigma_p .$$

If $\mathbf{X} \in \mathbb{R}^{m\times n}$ then the 2-norm and the Frobenius norm of $\mathbf{X}$ are

$$\begin{aligned} \|\mathbf{X}\|_2 &= \sigma_1 , \\ \|\mathbf{X}\|_F &= \sqrt{\sigma_1^2 + \cdots + \sigma_p^2} . \end{aligned}$$

The best rank-d approximation $\hat{\mathbf{X}}$ of $\mathbf{X}$ is obtained by taking the SVD of $\mathbf{X}$ and setting all but the first d singular values in $\mathbf{\Sigma}$ equal to zeros:

$$\hat{\mathbf{X}} = \sum_{i=1}^{d} \sigma_i \mathbf{u}_i \mathbf{v}_i^H .$$

where $\mathbf{u}_i$ and $\mathbf{v}_i$ are the i-th columns of $\mathbf{U}$ and $\mathbf{V}$ respectively.

Therefore, a rank-1 approximation corresponds to taking the first singular value σ_1 and setting

$$\hat{\mathbf{X}} = \sigma_1 \mathbf{u}_1 \mathbf{v}_1^H .$$

This rank-1 approximation by the SVD will be used almost exclusively in all of the proposed blind algorithms. Efficient implementations of SVD have already been developed [34] and integrated in many signal processing software and hardware.

In addition, SVD is also an efficient way to find the pseudo-inverse when solving the Least Squares (LS) problem for a rank-deficient matrix,

$$\min_{\mathbf{s}} \|\mathbf{x} - \mathbf{A}\mathbf{s}\|^2$$

The solution is given as

$$\mathbf{s} = \mathbf{A}^{\dagger}\mathbf{x} ,$$

where $\mathbf{A}^{\dagger} = (\mathbf{A}^H\mathbf{A})^{-1}\mathbf{A}^H$ is the pseudo-inverse of the tall and full rank matrix $\mathbf{A}$. However, if $\mathbf{A}$ is rank-deficient, $(\mathbf{A}^H\mathbf{A})$ is not invertible. In this case, if k is the rank of the matrix, by taking the SVD of $\mathbf{A}$, we can find the Moore-Penrose inverse of $\mathbf{A}$:

$$\mathbf{A}^{\dagger} = \mathbf{V}_0\mathbf{\Sigma}_0^{-1}\mathbf{U}_0^H$$

where $\mathbf{\Sigma}_0 = \mathrm{diag}(\sigma_1, \sigma_2, \ldots, \sigma_k)$, $\mathbf{U}_0$ and $\mathbf{V}_0$ consist of the first k columns of $\mathbf{U}$ and $\mathbf{V}$ respectively.

This Moore-Penrose inverse will also be used extensively in our receiver algorithms presented in the next chapters.

Part of this chapter was published as: Q.H. Dang, Antonio Trindade, A-J van der Veen and Geert Leus – *"Signal Model and Receiver Algorithms for a Transmit-Reference Ultra-Wideband Communication System,"* IEEE Journal on Selected Areas in Communications, Vol. 24, No. 4, pp. 773-779, April 2006 [19].

Chapter 3

A robust TR-UWB scheme

A communication system based on Transmit-Reference (TR) Ultra-Wideband (UWB) is studied and further developed. Introduced by Hoctor and Tomlinson, the aim of the TR-UWB transceiver is to provide a straightforward impulse radio system, feasible to implement with current technology, and to achieve either high data rate transmissions at short distances or low data rate transmissions in typical office or industrial environments. Our main contribution is the derivation of a signal processing model that takes into account the effects of the radio propagation channel, and an analysis of the effect of additive noise on the model. Several receivers based on the CDMA-like properties of the proposed model are derived, and the performance of the algorithms is tested in a simulation.

3.1 Introduction

As introduced in the previous chapter, the proposed TR-UWB scheme in [70, 36] does not take the effect of the propagation channel into account. It is also implicitly assumed in [70, 36, 81, 83] that the channel length T_h is shorter than the spacing D between two pulses in a doublet. Meanwhile, measured channels can spread up to about 200 ns [12, 29]. This causes problems in both the system design and the receiver algorithm performance perspectives. Firstly, if the frames are designed such that $D > T_h$, the received pulses do not overlap but the overall data rate of the system will reduce significantly. Another complication is that, in this case, such long ultra-wideband delay lines are more difficult to implement with high accuracy in practice [7]. Secondly, if $D < T_h$, the interpulse interferences (IPI) will introduce unwanted correlation terms when deriving data models and thus degrade the performance of the corresponding detection algorithms unless they are taken into account properly. Both cases – no IPI ($D > T_h$) and with IPI ($D < T_h$) – are illustrated in Fig. 3.1.

In this chapter, we will investigate the case when pulses in a doublet are closely spaced, i.e. $D \ll T_h$ by modeling the "new" correlation terms in a more accurate signal processing data model. Based on this model, the derived receiver algorithms are shown to be more superior in BER performance and more robust with respect to

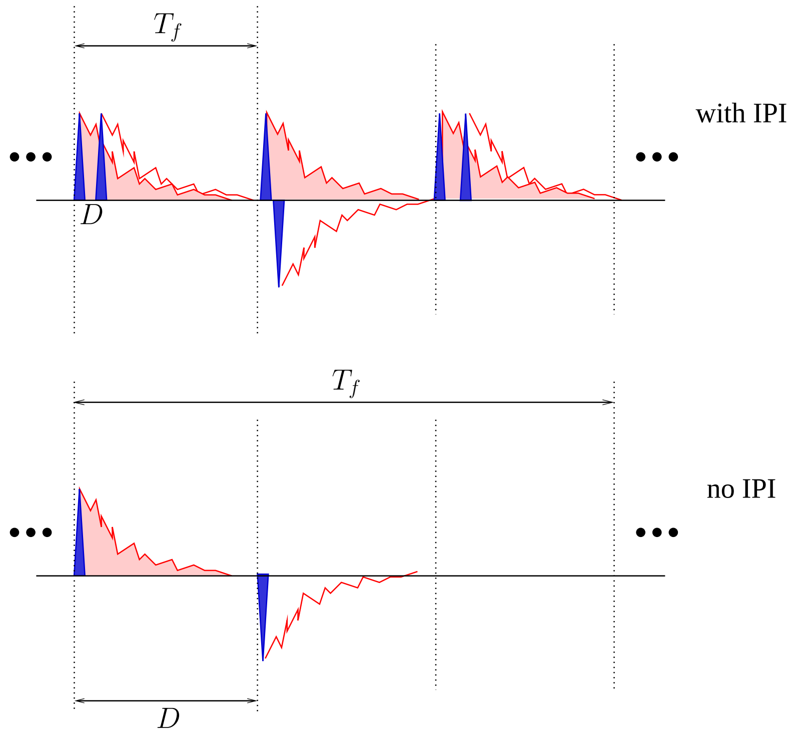

Figure 3.1: *The interpulse interference in TR-UWB.*

some small shifted errors in delay lines than the simple scheme in [70, 36].

This chapter is organized as follows. Firstly, a detailed data model for a TR UWB system is derived (section 3.2). Based on this, several receiver algorithms are introduced (section 3.3). The proposed algorithms are blind or semi-blind: the channel parameters (in this case correlations) are estimated along with the data. Finally, section 3.4 shows the simulated performance of the algorithms.

3.2 Data Model

We consider a single-user delay-hopped transmit reference system as originally proposed in [36], and develop its signal processing model (as in [69]). The transmitted signal symbol consists of a sequence of N_c chips, each of duration T_c. Each chip has only one frame ($T_c = T_f$) in which a pulse pair (doublet) is transmitted. For lower

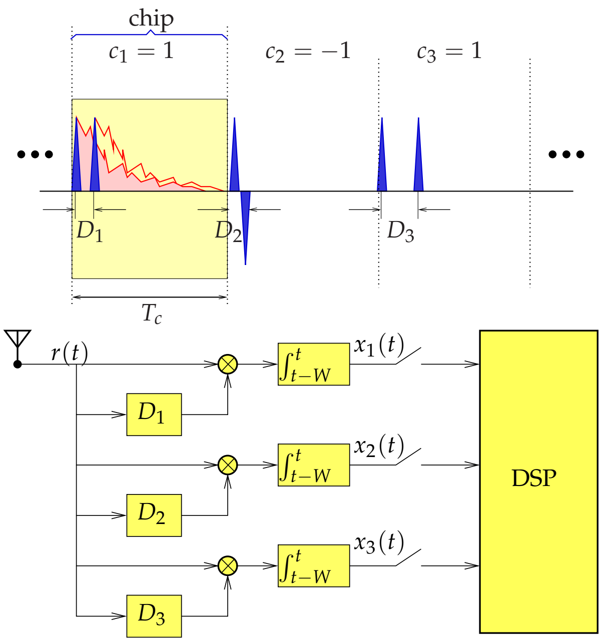

Figure 3.2: (a) *Structure of the transmitted data burst,* (b) *Structure of the auto-correlation receiver.*

data rate (with longer range) applications, several repeated frames may be needed per chip. The data model can be easily extended to cover that case.

At the moment, to simplify the presentation, we will first consider the data model for a single chip, which has a single frame, and then extend this model to multiple chips.

3.2.1 Single Chip

As depicted in figure 3.2(a), for each chip a pair (doublet) of narrow pulses $g(t)$ is transmitted, spaced by a time interval of duration d_i, selected from a collection $\{D_1, \ldots, D_M\}$, where we assume $D_1 < D_2 < \cdots < D_M$. The values of these delays range from sub-nanosecond to a few nanoseconds, which are much smaller than the typical UWB channel lengths (hundreds of nanoseconds). The first pulse is fixed, whereas the second pulse is modulated by the chip value $c \in \{+1, -1\}$. For the jth chip, which is transmitted at time instant $t = jT_c$, the chip value is c_j and the selected delay is $i = i(j)$ (following a user-dependent chip sequence and index function), and can be written as

$$c_j(t) = g(t - jT_c) + c_j\, g(t - jT_c - d_i). \tag{3.1}$$

Let $h_p(t)$ be the impulse response of the physical channel, and T_h be the channel length. Define the composite channel $h(t)$ as the convolution between a UWB pulse and $h_p(t)$: $h(t) = g(t) * h_p(t)$. Since the pulse duration (at nanosecond) is much smaller than the channel length, we can safely cut out the last pulse at the tail of the composite channel, which is usually at a very small amplitude (comparable to the noise floor), and assume the composite channel to have the same channel length T_h. Ignoring the additive noise, the received signal for the transmitted chip (3.1) can then be expressed as

$$r_j(t) = h(t - jT_c) + c_j\, h(t - jT_c - d_i). \tag{3.2}$$

At the receiver $r_j(t)$ is passed through a bank of M correlators, each correlating the signal with a delayed version of itself at lags D_m, $m = 1, \cdots, M$. Subsequently, the outputs of the correlators are integrated over a sliding window of duration $W \geq T_c$, as in figure $3.2(b)$. The output of the m-th correlator and integrator branch for the received signal (3.2) can then be written as

$$\begin{aligned} x_{m,j}(t) &= \int_{t-W}^{t} r_j(\tau) r_j(\tau - D_m)\, d\tau \\ &= \int_{t-jT_c-W}^{t-jT_c} r_j(\tau + jT_c) r_j(\tau + jT_c - D_m)\, d\tau \\ &= \kappa(t - jT_c, D_m) + \kappa(t - jT_c - d_i, D_m) \\ &\quad + c_j \left[\kappa(t - jT_c - d_i, D_m - d_i) + \kappa(t - jT_c, D_m + d_i)\right], \end{aligned} \tag{3.3}$$

where

$$\kappa(t, \tau) = \int_{t-W}^{t} h(\tau) h(\tau - \tau)\, d\tau\,. \tag{3.4}$$

Assuming that the integration duration W [1] is larger than the channel length T_h, it is straightforward to derive that

$$\kappa(t, \tau) = \begin{cases} 0, & t \leq 0 \\ \rho(\tau), & T_h < t < W \\ 0, & t > W + T_h \end{cases}, \tag{3.5}$$

[1]In practical implementation of this low data rate TR-UWB scheme, W is often chosen as the chip duration T_c, which is much larger than T_h

where $\rho(\tau)$ is the channel autocorrelation function

$$\rho(\tau) = \int_{-\infty}^{\infty} h(t)h(t-\tau)\,dt, \tag{3.6}$$

and with interpolating values in the unspecified intervals in (3.5). Assuming furthermore that W is not just larger but much larger than the channel duration T_h, it is thus seen that $\kappa(t,\tau)$ is well approximated by a scaled "brick function" $p(t)$ which is independent of τ,

$$p(t) = \begin{cases} 0, & t \le 0,\ t \ge W \\ 1, & 0 < t < W \end{cases}, \tag{3.7}$$

so that

$$\kappa(t,\tau) \approx p(t)\,\rho(\tau). \tag{3.8}$$

Under this approximation, and assuming that W is also much larger than the maximal delay D_M, which implies $\kappa(t - jT_c - d_i, \tau) \approx \kappa(t - jT_c, \tau)$, the output of the m-th correlator and integrator branch (3.3) can be rewritten as

$$\begin{aligned} x_{m,j}(t) &= p(t - jT_c)\{2\rho(D_m) + c_j\,[\rho(D_m - d_i) + \rho(D_m + d_i)]\} \\ &= p(t - jT_c)(c_j\,\alpha_{m,i} + \beta_m), \end{aligned} \tag{3.9}$$

where

$$\begin{aligned} \alpha_{m,i} &= \rho(D_m - d_i) + \rho(D_m + d_i), \\ \beta_m &= 2\rho(D_m). \end{aligned} \tag{3.10}$$

Note that $\alpha_{m,i} = \alpha_{i,m}$, while β_m only depends on D_m. We may interpret α_{mi} as a channel gain, whereas β_m is an offset. These unknown parameters replace the usual channel coefficients. Similarly, the "brick function" $p(t)$ plays the role of "pulse shape function" in the model for $x_{m,j}(t)$.

If $\alpha_{m,i} = \alpha\delta_{m,i}$ where $\alpha = \int h^2(t)\,dt$ is the channel energy, and if $\beta_m = 0$, then we obtain the data model considered by Hoctor and Tomlinson in [70, 36]. In this case, we simply have $x_{m,j}(t) = p(t - jT_c)\alpha\delta_{m,i}$, with a nonzero output only if the transmit delay matches the receiver delay. For channels with a short duration T_h (compact support for the correlation function), this model is a good approximation. For channels with a longer impulse response (in the order of the maximal delay D_M, or larger), this model may be too simple. The statistics of these parameters will be further studied in section 4.2.1.

$$\mathbf{P} = \begin{bmatrix} 1 & & & \\ 1 & & & \\ 1 & 1 & & \\ 1 & 1 & & \\ & 1 & 1 & \\ & 1 & 1 & \\ & & 1 & 1 \\ & & 1 & 1 \\ & & & 1 \\ & & & 1 \end{bmatrix}$$

Figure 3.3: *Structure of the matrix* $\mathbf{P}$ *(size* $N \times N_c$*), shown for* $W = 2T_c$*,* $P = 2$*,* $N_c = 4$*.*

3.2.2 Multiple Chips – Matrix Formulation

Let us now consider transmitting a symbol $s \in \{+1, -1\}$. This is done by transmitting N_c consecutive chips $\mathbf{c} = [c_0, \ldots, c_{N_c-1}]^T$ multiplied by the symbol s. Each chip is transmitted using one of the delays $D_1, \cdots, D_M$ and is received using a bank of M correlators at delays $D_1, \cdots, D_M$. Based on (3.9), and assuming T_c is larger than the channel duration T_h plus twice the maximal delay D_M ($T_c > T_h + 2D_M$), in order to avoid overlap between consecutive chips after correlation, we can write the output of the m-th correlator and integrator branch for the symbol s as

$$x_m(t) = \sum_{i=1}^{M} \sum_{j=0}^{N_c-1} p(t - jT_c)(\alpha_{m,i} J_{i,j} c_j s + \beta_m J_{i,j}), \tag{3.11}$$

where

$$J_{i,j} = \begin{cases} 1, & \text{if chip } j \text{ is transmitted at delay } d_i \\ 0, & \text{else} \end{cases} \tag{3.12}$$

Assume that the outputs of the integrators are sampled at P times the chip rate, where P is the oversampling rate (typically $P = 2$). The sampled data at the instances $t = nT_c/P + \epsilon$ is then given by

$$x_{m,n} = x_m(nT_c/P + \epsilon) = \sum_{i=1}^{M} \sum_{j=0}^{N_c-1} p_{n,j}(\alpha_{m,i} J_{i,j} c_j s + \beta_m J_{i,j})$$

where $p_{n,j} = p(nT_c/P + \epsilon - jT_c)$. Here, n is an integer and ϵ is a fractional offset, $\epsilon \in [0, T_c/P)$. Synchronization algorithms (as in [22]) should be able to either tolerate the unknown ϵ or estimate it along with the integer offset at the beginning of the chip. Here we assume perfect synchronization with known ϵ (often chosen at either 0 or $T_c/(2P)$).

To obtain a matrix model for the symbol s, we will collect $N = N_c P$ temporal samples at the output of the m-th correlator and integrator branch into the vector

$\mathbf{x}_m = [x_{m,0}, \ldots, x_{m,N-1}]^T$. Let us further define the $M \times 1$ channel vector $\mathbf{a}_m$ as $[\mathbf{a}_m]_i = \alpha_{m,i}$ and the $M \times M$ channel matrix $\mathbf{A}$ as $[\mathbf{A}]_{m,i} = \alpha_{m,i}$ (note that $\mathbf{A} = \mathbf{A}^T$ since $\alpha_{m,i} = \alpha_{i,m}$). In addition, we define the $M \times 1$ channel vector $\mathbf{b}$ as $[\mathbf{b}]_m = \beta_m$. To describe the delay code, we also define the $M \times N_c$ selector matrix $\mathbf{J}$ as $[\mathbf{J}]_{i,j+1} = J_{i,j}$. It has for each column only one nonzero entry, corresponding to the transmitted delay index at that chip. Therefore, $\mathbf{J}^T \mathbf{1}_M = \mathbf{1}_{N_c}$. Finally, define the $N \times N_c$ sampled pulse matrix $\mathbf{P}$ as $[\mathbf{P}]_{n+1,j+1} = p_{n,j}$, the structure of which is shown in Fig. 3.3.

The above definitions allow us to express $\mathbf{x}_m = [x_{m,0}, \ldots, x_{m,N-1}]^T$ as

$$\begin{aligned}
\mathbf{x}_m &= \sum_{i=1}^{M} \sum_{j=0}^{N_c-1} \mathbf{p}_j (\alpha_{m,i} J_{i,j} c_j s + \beta_m J_{i,j}) \\
&= \sum_{j=0}^{N_c-1} \mathbf{p}_j (\mathbf{a}_m^T \mathbf{h}_j c_j s + \beta_m \mathbf{1}_M^T \mathbf{h}_j) \\
&= \sum_{j=0}^{N_c-1} \mathbf{p}_j c_j \mathbf{h}_j^T \mathbf{a}_m s + \mathbf{p}_j \mathbf{h}_j^T \mathbf{1}_M \beta_m \\
&= [\mathbf{p}_0 c_0, \ldots, \mathbf{p}_{N_c-1} c_{N_c-1}] \mathbf{J}^T \mathbf{a}_m s + [\mathbf{p}_0, \ldots, \mathbf{p}_{N_c-1}] \mathbf{J}^T \mathbf{1}_M \beta_m \\
&= \mathbf{P} \mathrm{diag}(\mathbf{c}) \mathbf{J}^T \mathbf{a}_m s + \mathbf{P} \mathbf{1}_{N_c} \beta_m,
\end{aligned} \tag{3.13}$$

where $\mathbf{p}_j$ and $\mathbf{h}_j$ are the $(j+1)$-st columns of $\mathbf{P}$ and $\mathbf{J}$, respectively. Collecting all vectors $\mathbf{x}_m$ into a matrix $\mathbf{X} = [\mathbf{x}_1, \ldots, \mathbf{x}_M]$ gives

$$\mathbf{X} = \mathbf{P} \mathrm{diag}(\mathbf{c}) \mathbf{J}^T \mathbf{A}^T s + \mathbf{P} \mathbf{1}_{N_c} \mathbf{b}^T .$$

Finally, if we transmit multiple symbols $\mathbf{s} = [s_0, \cdots, s_{N_s-1}]^T$, and assume there is no overlap between consecutive symbols (this can be obtained by inserting a $\lceil W/T_c \rceil$ blank chips in between every two symbols), we have for the k-th symbol

$$\mathbf{X}_k = \mathbf{P} \mathrm{diag}(\mathbf{c}) \mathbf{J}^T \mathbf{A}^T s_k + \mathbf{P} \mathbf{1}_{N_c} \mathbf{b}^T \tag{3.14}$$

$$= \mathbf{P} [\mathrm{diag}(\mathbf{c}) \mathbf{J}^T, \mathbf{1}_{N_c}] [\mathbf{A} s_k, \mathbf{b}]^T. \tag{3.15}$$

For simplicity, we assumed here that periodic codes are used. In this model, $\mathbf{X}_k$ is measured, $\mathbf{c}$ is known (user code), $\mathbf{J}$ is known (delay code), and $\mathbf{P}$ is known and data independent (this assumes synchronization; without synchronization an unknown number of zero rows are stacked on top but this can be estimated and resolved, see [22]). $\mathbf{A}$ and $\mathbf{b}$ are unknown (channel correlation coefficients), and s_k is the data symbol to be detected.

3.2.3 Remarks and Extensions

For the simple data model considered by Hoctor and Tomlinson [36,70], i.e., assuming no correlations for unmatched delays, we obtain $\mathbf{A} = \alpha \mathbf{I}$ and $\mathbf{b} = 0$. For channels with an impulse response longer than D_M, this may not be a valid assumption. This is studied in more detail in chapter 4.

The advantage of the analog part of the receiver structure is that it is data independent and non-adaptive. Even synchronization is not needed in the analog domain; this can be done in the DSP based on the received data model [22]. With $P = 2$ times oversampling of the integrator output, there is no loss of information. Details on chip-level synchronization for the considered set-up can be found in [22, 24, 21] and [60].

The typical duration of the integration window is $W = T_c$. If the receiver uses an integrate-and-dump operation (which resets the integrator after sampling), then without oversampling ($P = 1$) the model remains the same. Technologically, such integrators have the advantage that the integration length is easily modified (related to an external clock), rather than being fixed by an RC integration network.

In some descriptions of TR systems, multiple repetition frames (doublets) per chip are considered. This may be useful for very low power/low data rate applications. It is a special case of the above model, with duplicate values for the chips and delays. In this case, when all the "brick" functions (each corresponds to a frame) are stacked together, by sliding window integration, they becomes a triangular "tent shape" for $p(t)$ [69] (only matrix $\mathbf{P}$ changes).

As an example, Figure 3.2.3 shows the output sequences $x_i(t)$ for each receiver correlation lag (1–4 ns), in a noise-free case. The transmitted chip values and delay lags are shown at the top. It is clear that, due to the cross-correlations in the channel, the received chips do not only have a response at the matching delays, but also at other delays. The simple data model ($\mathbf{A} = \alpha\mathbf{I}$, $\mathbf{b} = \mathbf{0}$) does not take the effect of the channel into account, hence assumes a response only at the matching delay. For the simulated channel, the deviations can be significant. The new model (shown as '+') is almost indistinguishable [2] from the actually received data, hence provides a very good match. The values of $\mathbf{A}$ and $\mathbf{b}$ were estimated from the received data as described in [69] and also in the next section.

At the receiver, it is essential that a lowpass filter be used prior to the correlation, to limit the noise. Ideally a filter matched to the monopulse waveform is used, but this shape is not accurately known (antenna-dependent), and the resulting convolution may be hard to implement. Another technique to limit the noise is to split the integration window into multiple windows per chip, and adaptively weigth and combine the results. This is discussed in [44].

Finally, in practical systems it is advisable to randomize the polarity of the first (reference) pulse as well, which will reduce spectral lines. In the noise-free case this has no influence on the model after the correlator.

[2] There can be synchronization error when the fractional offset ϵ is unknown.

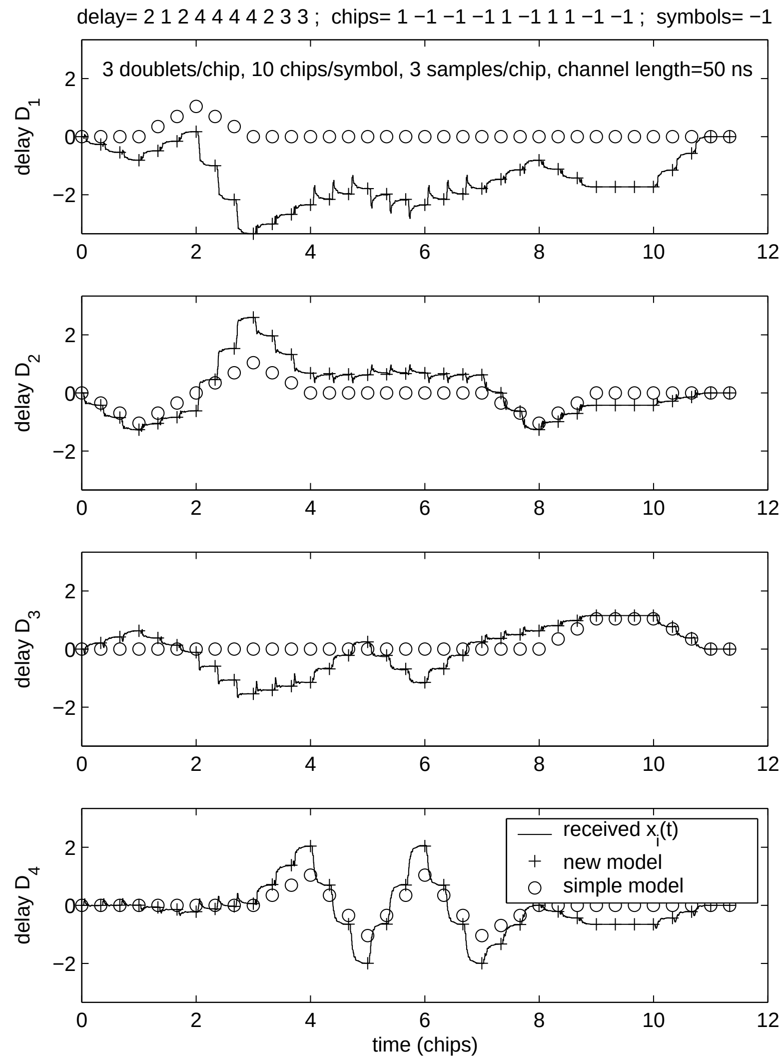

Figure 3.4: *The correspondence of the actually received data to 'o' the simple model and '+' the proposed data model.*

3.3 Receiver Algorithms

Based on the data model derived in the previous section, we can now develop a few detection algorithms. Let us first recall (3.15) including a noise term $\mathbf{N}_k$:

$$\mathbf{X}_k = \mathbf{P}\text{diag}(\mathbf{c})\mathbf{J}^T\mathbf{A}s_k + \mathbf{P}\mathbf{1}_{N_c}\mathbf{b}^T + \mathbf{N}_k,$$

The problem now is, given the received signal $\mathbf{X}_k$, estimate the data symbol s_k along with the unknown channel matrix $\mathbf{A}$ and channel vector $\mathbf{b}$. Depending on the knowledge we have on the statistics of $\text{vec}(\mathbf{N}_k)$ (this knowledge could be obtained by training), we can choose to whiten the noise or not. The algorithms listed below will for simplicity assume that $\mathbf{N}_k$ is white.

3.3.1 Simple Matched Filter Receiver

A simple receiver can be derived if we assume that the channel does not have temporal correlations ($\alpha_{m,i} = \alpha\delta_{m,i}$). The channel matrix and vector, thus, will be $\mathbf{A} = \alpha\mathbf{I}$, $\mathbf{b} = \mathbf{0}$, where $\alpha > 0$ is the only unknown constant (the channel power). The simplified data model then is

$$\mathbf{X}_k = \mathbf{P}\text{diag}(\mathbf{c})\mathbf{J}^T\alpha s_k + \mathbf{N}_k\,, \tag{3.16}$$

and the corresponding data symbol can be estimated as

$$\alpha\hat{s}_k = \text{tr}[\mathbf{J}\text{diag}(\mathbf{c})\mathbf{P}^T\mathbf{X}_k]\,, \tag{3.17}$$

where $\text{tr}(\cdot)$ is the trace operator. Since α is always positive, it does not change the detected symbol ($s \in \{+1, -1\}$) and, thus, it does not need to be estimated.

3.3.2 Blind Multiple Symbol Receiver

If $\mathbf{A}$ and $\mathbf{b}$ are unknown, they can be estimated along with the data $\mathbf{s} = [s_0, \cdots, s_{N_s-1}]^T$ in a blind scheme as follows. Write the model as

$$[\mathbf{X}_0, \ldots, \mathbf{X}_{N_s-1}] = \mathbf{P}[\text{diag}(\mathbf{c})\mathbf{J}^T, \mathbf{1}]\begin{bmatrix}\mathbf{A}^T s_0 & \cdots & \mathbf{A}^T s_{N_s-1}\\ \mathbf{b}^T & \cdots & \mathbf{b}^T\end{bmatrix} + [\mathbf{N}_0, \ldots, \mathbf{N}_{N_s-1}]. \tag{3.18}$$

Since $\mathbf{Q} := \mathbf{P}[\text{diag}(\mathbf{c})\mathbf{J}^T, \mathbf{1}]$ is completely known, we can remove its effect by multiplying both sides with the left pseudo-inverse of $\mathbf{Q}$:

$$\begin{aligned}[\mathbf{Y}_0, \ldots, \mathbf{Y}_{N_s-1}] &:= \mathbf{Q}^\dagger[\mathbf{X}_0, \ldots, \mathbf{X}_{N_s-1}]\\ &= \begin{bmatrix}\mathbf{A}^T s_0 & \cdots & \mathbf{A}^T s_{N_s-1}\\ \mathbf{b}^T & \cdots & \mathbf{b}^T\end{bmatrix} + \mathbf{Q}^\dagger[\mathbf{N}_0, \ldots, \mathbf{N}_{N_s-1}]\\ &=: \begin{bmatrix}\mathbf{A}^T s_0 & \cdots & \mathbf{A}^T s_{N_s-1}\\ \mathbf{b}^T & \cdots & \mathbf{b}^T\end{bmatrix} + [\mathbf{V}_0, \ldots, \mathbf{V}_{N_s-1}].\end{aligned}$$

It is then clear that the channel vector $\mathbf{b}$ can be estimated as

$$\hat{\mathbf{b}}^T = \frac{1}{N_s} \sum_{k=0}^{N_s-1} [\mathbf{Y}_k]_{M+1,:}\,.$$

To estimate $\mathbf{A}$ and $\mathbf{s}$, we vectorize the matrices $[\mathbf{Y}_k]_{1:M,:}$ into vectors $\mathbf{y}_k = \mathrm{vec}([\mathbf{Y}_k]_{1:M,:})$ of size $M^2 \times 1$, and define $\mathbf{Y}' = [\mathbf{y}_0, \cdots, \mathbf{y}_{N_s-1}]$. This matrix has model

$$\mathbf{Y}' = \mathrm{vec}(\mathbf{A}^T)\mathbf{s}^T + \mathbf{V}', \tag{3.19}$$

where $\mathbf{V}'$ is similarly defined as $\mathbf{Y}'$. Hence, the channel matrix $\mathbf{A}$ and the source symbol vector $\mathbf{s}$ can be estimated up to a scaling factor by computing a rank-1 decomposition (using the SVD) of $\mathbf{Y}'$. The symmetry of $\mathbf{A}$ is easily exploited by introducing a small modification of the $\mathrm{vec}(\cdot)$ operator such that the identical entries get averaged into a single entry.

3.3.3 Iterative Receiver

In the preceding receiver algorithm, the inversion of $\mathbf{Q}$ may be undesirable (e.g., Q may not be very tall, and it colors the noise). Improved performance can be obtained by a two-step iterative receiver which is initialized by the receiver of the preceding section: (i) assume $\mathbf{s}$ is known, estimate $\mathbf{A}$ and $\mathbf{b}$; (ii) assume $\mathbf{A}$ and $\mathbf{b}$ are known, estimate $\mathbf{s}$. For the first step, we rewrite the data model (3.18) as

$$\begin{bmatrix} \mathbf{X}_0 \\ \vdots \\ \mathbf{X}_{N_s-1} \end{bmatrix} = \begin{bmatrix} \mathbf{P}[s_0 \mathrm{diag}(\mathbf{c})\mathbf{J}^T \ \ \mathbf{1}] \\ \vdots \\ \mathbf{P}[s_{N_s-1} \mathrm{diag}(\mathbf{c})\mathbf{J}^T \ \ \mathbf{1}] \end{bmatrix} \begin{bmatrix} \mathbf{A}^T \\ \mathbf{b}^T \end{bmatrix} + \begin{bmatrix} \mathbf{N}_0 \\ \vdots \\ \mathbf{N}_{N_s-1} \end{bmatrix}, \tag{3.20}$$

from which $\mathbf{A}$ and $\mathbf{b}$ can be estimated using least squares as

$$\begin{bmatrix} \hat{\mathbf{A}}^T \\ \hat{\mathbf{b}}^T \end{bmatrix} = \begin{bmatrix} \mathbf{P}[s_0 \mathrm{diag}(\mathbf{c})\mathbf{J}^T \ \ \mathbf{1}] \\ \vdots \\ \mathbf{P}[s_{N_s-1} \mathrm{diag}(\mathbf{c})\mathbf{J}^T \ \ \mathbf{1}] \end{bmatrix}^{\dagger} \begin{bmatrix} \mathbf{X}_0 \\ \vdots \\ \mathbf{X}_{N_s-1} \end{bmatrix}. \tag{3.21}$$

The matrix which is inverted has size $NN_s \times (M+1)$ and should be tall. For the second step, we partition $\mathbf{Q}$ in (3.18) as $\mathbf{Q} = [\mathbf{Q}', \mathbf{q}]$ and obtain

$$\mathrm{vec}(\mathbf{X}_k) = \mathrm{vec}(\mathbf{Q}'\mathbf{A}^T)s_k \ + \ \mathbf{b} \otimes \mathbf{q} + \mathrm{vec}(\mathbf{N}_k) \tag{3.22}$$

Therefore, a least squares solution for s_k is

$$\hat{s}_k = [\mathrm{vec}(\mathbf{Q}'\mathbf{A}^T)]^{\dagger}(\mathrm{vec}(\mathbf{X}_k) - \mathbf{b} \otimes \mathbf{q}),$$

which is straightforward to evaluate.

3.4 Simulation Results

We simulate the transmission of $N_s = 20$ symbols over the UWB channels [3]. We consider the IEEE CM-1 (LOS) channel, convolved with a Gaussian pulse and twice with the measured antenna/bandpass filter response; furthermore we consider the API-3 measured channel convolved with the same Gaussian pulse. We use 100 Monte Carlo runs to obtain the bit-error-rate (BER) versus SNR plots for the various receiver algorithms while the channel is kept fixed. Here, the SNR (signal-to-noise-ratio) is defined as the average received energy in a symbol over the white Gaussian noise power density.

The system uses $M = 3$ delay positions, and $N_c = 5$ chips per symbol. The transmitted Gaussian pulse has duration parameter $\tau_m = 0.2$ ns. The two pulses in a doublet are separated by $D_m \in \{0.5, 1.0, 1.5\}$ ns, and the doublets are separated by $T_c = 70$ ns to avoid inter-frame interference. The integration interval is taken as $W = T_c$, and no oversampling is used ($P = 1$).

The receiver algorithms which are tested are the Simplified Matched Filter Receiver (section 3.3.1), which uses a single (matched) delay per received chip, the Blind Multiple Symbol Receiver (section 3.3.2), which uses the complete bank of receiver delays for each received chip, and the Iterative Receiver (section 3.3.3), which uses the complete data model and is initialized by either one of the two noniterative receivers.

Figure 3.5(a) shows the BER versus the SNR for various algorithms for the IEEE CM-1 channel. The channel matrices in this case are

$$\mathbf{A} = \begin{bmatrix} 0.969 & -0.071 & -0.038 \\ -0.071 & 0.993 & -0.092 \\ -0.038 & -0.092 & 0.962 \end{bmatrix}, \quad \mathbf{b} = \begin{bmatrix} -0.207 \\ -0.061 \\ 0.066 \end{bmatrix}.$$

Similarly, Figure 3.5(c) shows the results for the API-3 measured channel, for which

$$\mathbf{A} = \begin{bmatrix} 0.984 & 0.171 & -0.003 \\ 0.171 & 1.013 & -0.015 \\ -0.003 & -0.015 & 1.038 \end{bmatrix}, \quad \mathbf{b} = \begin{bmatrix} 0.008 \\ -0.032 \\ 0.335 \end{bmatrix}.$$

In both cases, the figures show that the simplified Matched Filter receiver is more accurate than the Blind Multi-Symbol Receiver. Postprocessing with the iterative algorithm (which uses the full signal model) provides little advantage. Thus the assumption that $\mathbf{A} = \alpha\mathbf{I}$ and $\mathbf{b} = \mathbf{0}$ is sufficiently accurate. The relatively poor performance of the BMSR is explained from the fact that $\mathbf{Q}$ in this case has size

[3] The UWB channel models, standard and statistics will be discussed in more detail in chapter 4

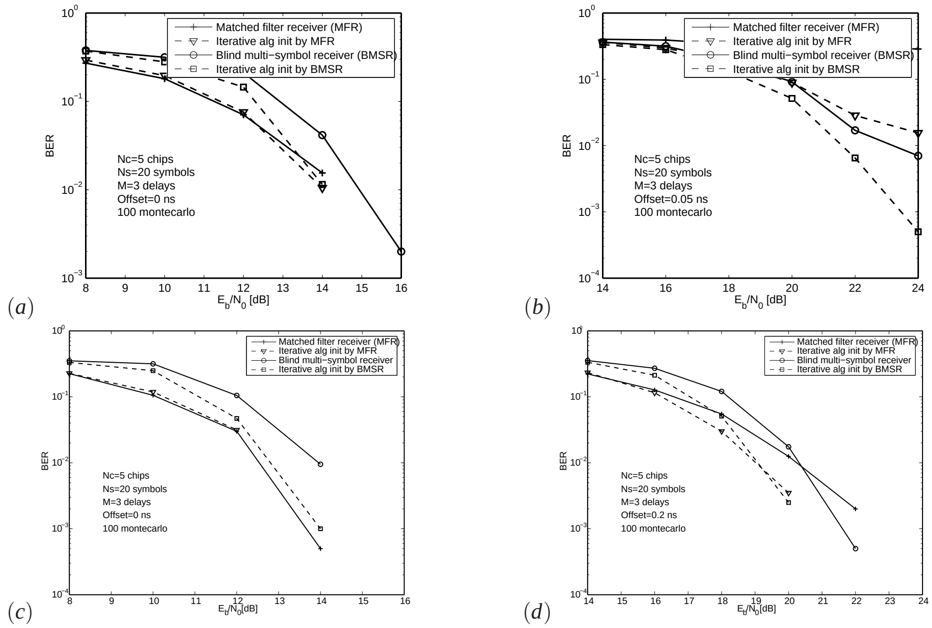

Figure 3.5: *BER vs. SNR for different receiver algorithms. IEEE CM-1 channel (LOS) including antenna/filter response:* (a) *no delay mismatch,* (b) *delay mismatch 0.05 ns. Measured channel ("API 3", LOS):* (c) *no delay mismatch,* (d) *delay mismatch 0.2 ns.*

5×4, which is not very tall; thus, some noise enhancement will occur. The Iterative Receiver instead inverts a matrix which grows with the number of samples and therefore experiences less noise enhancement in the estimation of $(\mathbf{A}, \mathbf{b})$ in (3.21). The detection step (3.22) involves the "inversion" of a vector which is always well conditioned as it only depends on the total amount of energy collected in the correlation bank.

We next consider the case where there is a small timing offset in each receiver delay due to component inaccuracies. For the IEEE CM-1 channel model, we take the offset as small as 0.05 ns, for the measured API channel, we take it perhaps more realistically equal to 0.2 ns. As discussed in chapter 4, due to this offset the diagonal dominance property of the channel matrix $\mathbf{A}$ is affected. The resulting channel correlation matrix is for the IEEE CM-1 channel

$$\mathbf{A} = \begin{bmatrix} -0.225 & -0.121 & 0.081 \\ 0.246 & -0.214 & -0.117 \\ 0.043 & 0.197 & -0.241 \end{bmatrix}, \quad \mathbf{b} = \begin{bmatrix} -0.256 \\ 0.069 \\ 0.014 \end{bmatrix},$$

and for the measured API-3 channel

$$\mathbf{A} = \begin{bmatrix} 0.311 & 0.148 & 0.008 \\ -0.149 & 0.415 & 0.058 \\ 0.018 & -0.240 & 0.391 \end{bmatrix}, \quad \mathbf{b} = \begin{bmatrix} 0.115 \\ -0.097 \\ 0.182 \end{bmatrix}.$$

Figure 3.5(*b*,*d*) shows the results. It is seen that, for the CM-1 channel, the Simplified Matched Filter Receiver completely breaks down since it assumes $\mathbf{A} = \alpha\mathbf{I}, \mathbf{b} = \mathbf{0}$ which is not at all accurate, whereas the Blind Multi-Symbol Receiver, which takes into account all the elements of matrices **A** and **b**, maintains a fair performance. A less strong conclusion holds for the API channel. In both cases, the iterative algorithm gives a significant performance improvement over both non-iterative algorithms. The values of $(\mathbf{A}, \mathbf{b})$ strongly depend on precisely which delays (values of τ) are selected. Only receivers which use the full data model are expected to be resilient to this.

3.5 Conclusions

We have proposed an accurate signal processing model for a transmit-reference UWB system taking into account the interpulse interference (IPI) caused by the long channel delay spread. In fact, the pulses in a doublet are spaced so closely that there is always IPI caused by the channel spread at receiver. This feature allows easier hardware implementation [7] and supports higher data rate.

The extra correlation terms are modeled as the "new" channel correlation coefficients in **A** and **b**, which can be estimated from a single symbol and used in a simple matched filter receiver or in a more advanced iterative receiver. Since no assumption is made on these unknown coefficients, and they are to be estimated in receiver algorithms, our scheme can work in any scenario under any random channel.

Moreover, the system is designed to tolerate hardware imperfection (more specifically, the small shifted in delay lines) by incorporating the error into the unknown parameters **A**, **b**. Therefore, it is more robust than the TR-UWB scheme that assumes $\mathbf{A} = \mathbf{I}$ and $\mathbf{b} = \mathbf{0}$.

Although pulses in a doublet are moved closer, the proposed scheme still cannot support higher data rate transmission because of the assumption that there is no interframe interference (IFI) $T_f > T_h + D + T_p$. However, by allowing IPI but no IFI, we can easily see that, given a fixed chip rate e.g. $T_c \approx 3T_h$, the proposed scheme can accommodate 3 frames (with 6 pulses) instead of just 1 frame (with 2 pulses) as before in the Hoctor-Tomlinson schemes, which results in a higher signal to noise ratio.

In the next chapter, we will investigate in more detail the UWB channel. Based on the typical characteristics of these UWB channel models and measurements, a higher rate TR-UWB scheme that allows IFI will be motivated and developed.

Chapter 4

UWB channel statistics

In theory, there is no difference between theory and practice;
In practice, there is.

Chuck Reid

In this chapter, we study in more detail some statistical properties of the typical indoor UWB channels and their implications on the signal processing data model and on other parameters in a system design perspective. More specifically, we focus on the correlation properties in both measured channels and the IEEE channel models. The effects caused by non-ideal antennas and other pulse shaping filters are included as well.

4.1 Introduction

In chapter 3, we made no assumption on the channel statistics when deriving a signal processing data model, which means that the model is applicable to virtually any random channel (as long as the channel length T_h is shorter than the frame period T_f). However, more insights in the practical UWB channels helps to develop more efficient schemes, and receiver algorithms.

In section 3.2.1, it was shown that, by correlation and integration, the effect of the propagation channel on the data model will reduce to the parameters α_{mi} and β_m, which depend on the effective channel auto-correlation function $\rho(\Delta)$, see equation (3.10). In this chapter, characteristics of this autocorrelation function under various assumptions and based on measurement data are studied. The IEEE channel models are also presented.

The impact of these characteristics on the data model and receiver algorithms will then be discussed. Finally, based on the uncorrelated tap property of the UWB channels, we will motivate a new TR-UWB scheme, which is more practical and supports higher data rates.

4.1.1 Multipath channel model

A physical multipath channel impulse response can be generically modeled as a sum of discrete delta pulses as follows

$$h_p(t) = \sum_{i=0}^{\infty} a_i \delta(t - \tau_i), \tag{4.1}$$

where a_i is the i-th ray's amplitude, and τ_i is its delay. Generally, these parameters are considered as random variables with different statistical assumptions depending on the specific channel model. A typical channel model for UWB is assumed to be time-invariant [1] and to have uncorrelated ray amplitudes a_i, and its ray amplitudes are assumed negligibly small for large τ_i [28], [58].

4.1.2 Multipath channel parameters

The channel length is defined as the total time interval during which reflected paths with significant energy (within 10dB from the strongest path) arrive, i.e.

$$T_h := \max_i \tau_i - \min_i \tau_i \tag{4.2}$$

However, T_h is often not well defined (dependent on the observable channel response when transmitting a pulse under a given SNR). For example, when the noise level is high enough (compared to the signal strength), the trailing paths will be embedded in noise. They can be ignored, which shortens the channel length.

The RMS delay spread is defined as the standard deviation value of the delays of the reflected paths, weighted proportionally to all the paths' powers, i.e.

$$\tau_{rms} := \sqrt{\overline{\tau^2} - \overline{\tau}^2} \tag{4.3}$$

where

$$\begin{aligned} \overline{\tau^2} &:= \frac{\sum_i \tau_i^2 a_i^2}{\sum_i a_i^2}, \\ \overline{\tau} &:= \frac{\sum_i \tau_i a_i^2}{\sum_i a_i^2}. \end{aligned}$$

[1] Usually the channel parameters a_i, τ_i changes randomly in time, but their rates of variations are so slow that they can be considered constant in a frame period, or even in a symbol period. In this context, these parameters can be regarded as time-invariant random variables.

The channel length and the channel RMS delay spread are the main parameters that determine the maximum data rate of the whole system. Normally, they set the upper limit on the symbol (pulse) period so that there is no inter-symbol interference (or inter-pulse interference).

The power delay profile (PDP) is the expected power per unit of time received with a certain excess delay (with respect to the first arrival path). It is obtained by averaging a large set of impulse responses.

4.2 Channel autocorrelation function

The channel auto-correlation function depends on the physical channel response, the transmitted UWB pulse $g(t)$, antenna response and other frequency selective effects. With the physical channel model in (4.1), assuming an ideal antenna (omnidirectional, ultra-wideband, with no angle or frequency dependent effects), the effective channel response is

$$h(t) := g(t) * h_p(t) = \sum_{i=0}^{\infty} a_i g(t - \tau_i)$$

Define the channel auto-correlation as

$$\rho(\Delta) = \int_{-\infty}^{\infty} h(\tau)h(\tau - \Delta)\, d\tau\,. \tag{4.4}$$

The expected value of $\rho(\Delta)$ is

$$E[\rho(\Delta)] = \int_{-\infty}^{\infty} E[h(\tau)h(\tau - \Delta)]d\tau\,.$$

Since UWB channel taps are generally assumed uncorrelated, i.e. $E[a_i a_j] = 0$ for $i \neq j$, we have

$$E[\rho(\Delta)] = P_0 \phi_g(\Delta) \tag{4.5}$$

where P_0 is the total received power in $h_p(t)$, whereas

$$\phi_g(\Delta) := \int_{0}^{\infty} g(\tau)g(\tau - \Delta)d\tau\,. \tag{4.6}$$

is the autocorrelation of the transmitted UWB pulse. Note that $\phi_g(\Delta) = 0$ for $\Delta \geq T_g$, where T_g is the pulse duration. For typical UWB pulses, T_g will be short. For typical TR-UWB receivers, only evaluation of $\rho(\Delta)$ at a discrete set of lags Δ is needed, equal to the sums and differences of the delays used in the transceiver. Assuming the minimum difference in lags is larger than T_g, effectively $E[\rho(\Delta)]$ is nonzero only for $\Delta = 0$.

Table 4.1: *Value of Φ for some pulses with normalized energy ($\Psi = 1$)*

Pulse type	Width	Φ
Rectangular	T	$2/3T$
Manchester	T	$1/3T$
Gaussian	$\approx 4\tau_m$	$\tau_m\sqrt{\pi}$
Gaussian monocycle	$\approx 3\tau_m$	$\approx 0.94\tau_m$

4.2.1 Channel taps with exponential decay

The case of an exponentially decaying power delay profile in relation to a transmit-reference UWB system was studied in detail in [75], and some of their resulting expressions are summarized below.

Assume that the channel has an exponentially decaying power delay profile with parameters γ plus a line-of-sight component with power ratio (Ricean factor) K. Furthermore, the arrival density of rays is assumed to be λ rays/s. The variance of $\rho(\Delta)$ for $\Delta > T_g$ is then shown to be

$$\mathrm{var}[\rho(\Delta)] = \gamma P_0^2 \Phi \frac{2K+1}{2(K+1)^2} e^{-\gamma\Delta}$$

where $\Phi := \int_{-\infty}^{\infty} \phi_g^2(\kappa) d\kappa$. For $\Delta = 0$,

$$\mathrm{var}[\rho(0)] \approx \frac{\gamma P_0^2}{(K+1)^2}\left[\Phi(2K+1) + \frac{\Psi}{\lambda}\right]$$

where

$$\Psi := \int_{-T_g}^{T_g} \phi_{g^2}(\epsilon)\, d\epsilon = \int_{-T_g}^{T_g}\int_0^{T_g} g^2(t) g^2(t-\epsilon)\, dt\, d\epsilon$$

Φ and Ψ depend only on the transmitted pulse; for a unit-energy pulse, $\Psi = 1$. For such a pulse, some typical values of Φ are shown in table 4.1. In the table, τ_m is the parameter of the Gaussian monocycle (or second derivative of a Gaussian pulse), i.e., $g(t) := [1 - 4\pi(t/\tau_m)^2]e^{-2\pi(t/\tau_m)^2}$.

The derivation is based on the uncorrelated taps assumption of the channel. In this case, the expected value of $\rho(\Delta)$ depends on the total received energy of channel and the energy of the UWB pulse, while the variance is influenced by channel parameters, pulse properties Φ, Ψ and the delay Δ.

Based on the statistics of $\rho(\Delta)$, it is straightforward to derive the expectations and variances of α_{mi} and β_m developed in chapter 3. Substituting the mean values

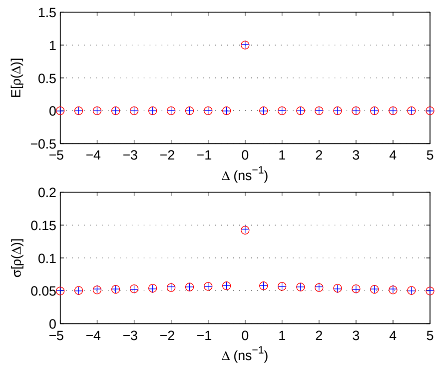

Figure 4.1: *Statistics of $\rho(\Delta)$ according to the uncorrelated exponentially decaying multipath model*

of $\rho(\Delta)$ into (3.10), we have

$$E[\alpha_{mi}] = \begin{cases} 0, & \text{for } m \neq i \\ P_0\phi_g(0), & \text{for } m = i \end{cases} \tag{4.7}$$

$$E[\beta_m] = 0 \tag{4.8}$$

Similarly, the variances become

$$\sigma^2[\alpha_{mi}] = \begin{cases} \frac{\gamma \ell P_0^2}{2}\Phi\left(e^{-\gamma(|D_i-D_m|)} + e^{-\gamma(D_m+D_i)}\right), & \text{for } m \neq i \\ \gamma P_0^2 \ell \left[\Phi\left(1+\frac{1}{2}e^{-2\gamma D_m}\right) + \frac{\Psi}{2\lambda(K+1)}\right], & \text{for } m = i \end{cases} \tag{4.9}$$

$$\sigma^2[\beta_m] = 2\gamma \ell P_0^2 \Phi e^{-\gamma D_m} \tag{4.10}$$

where $\ell = \frac{2K+1}{(K+1)^2}$.

Figure 4.1 shows the resulting expected values and variances of $\rho(\Delta)$ for a Gaussian monocycle ($\tau_m = 0.2$ ns), and a multipath channel with parameters $P_0 = 1$ (normalized channel power), $K = 0$ (non-line-of-sight channel), $\tau_{rms} = 1/\gamma = 15$ ns, $\lambda = 5$ ns^{-1}. In the figure, '$+$' denotes a simulated value, whereas '$\circ$' is the analytical result. According to this model, $\rho(\Delta)$ is significant only for $\Delta = 0$, which gives credibility to the model assumptions [2] considered by Hoctor and Tomlinson [70,36].

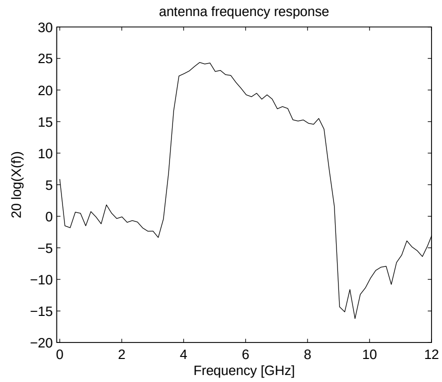

Figure 4.2: *The frequency response of a practical antenna.*

4.2.2 Antenna effect

If the antenna effect is taken into account, $\phi_g(\Delta)$ in (4.5) and (4.6) is replaced by the autocorrelation of the received UWB pulse spread by the non ideal antenna response. Since the UWB pulses are "ultra" narrow (only sub-nanosecond duration), the non ideal antenna effect (mostly because the antenna is not wideband enough) turns out to be the dominant factor in $\rho(\Delta)$. To illustrate this effect, we simulate a transmission of a UWB monocycle (first derivative of Gaussian pulse, duration 0.25 ns as shown in Fig. 2.3) and use a measured practical antenna [3] of which frequency response is shown in Fig. 4.2.2.

From Fig. 4.3, we can see that most of the channel correlation is introduced by the antenna. This can be explained if we view the UWB monocycle and the antenna response in the frequency domain. Their convolution in time domain equals their product in frequency domain. In this case, it can be seen from Fig. 4.2.2 and Fig. 2.3b that the antenna frequency band is merely comparable or even embedded in that of the UWB pulse. Therefore the antenna plays the more dominant role in shaping the frequency response of the convolved UWB signal.

[2] It is assumed [70, 36] that only matched delays at receiver have significant information while the unmatched delays are ignored. This leads to two implicit assumptions: (i) channel length T_h is shorter than the delay D between 2 pulses in a doublet; or (ii) uncorrelated (composite) channel taps.

[3] This antenna was used in various experiments carried by Z. Irahhauten et. al. within the Airlink project [42, 41].

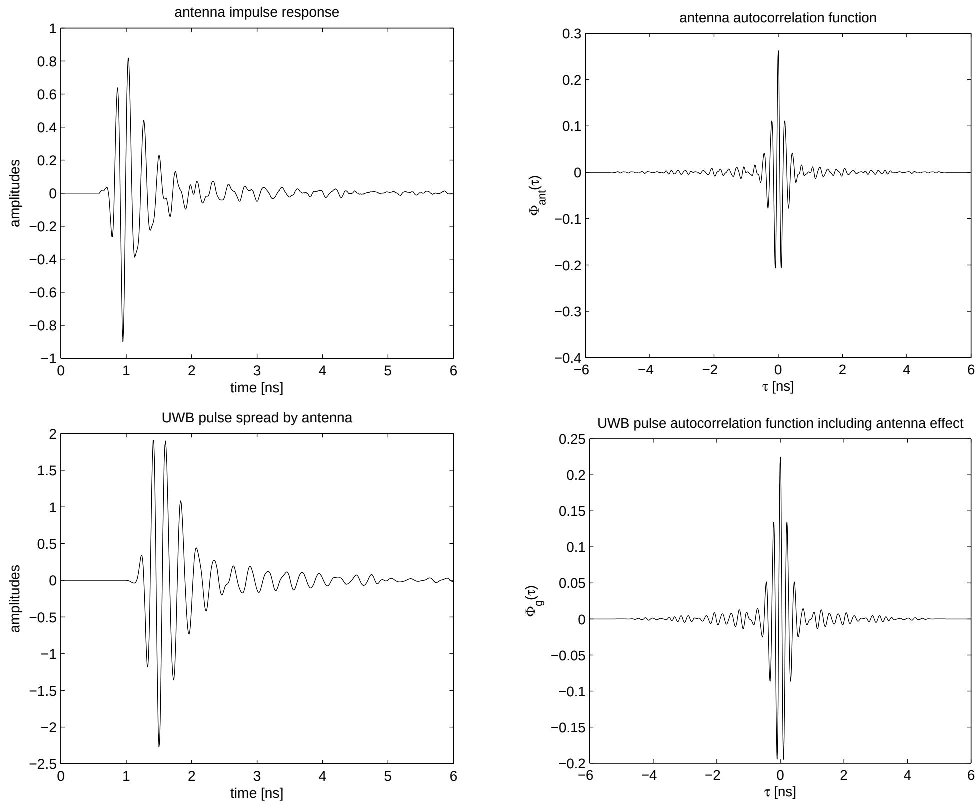

Figure 4.3: *The effect of antenna on the UWB pulse and its autocorrelation function*

4.2.3 The IEEE channel models

Although much research attention has been paid on UWB channel measurement and modeling in the last few years, there has not been a complete and official IEEE standard on the UWB channel models so far. However, as in [28, 52], the channel modeling subgroup of IEEE 802.15.3a has derived channel models under various scenarios and environments (see Table. 4.2.3). Matlab-generated data on the corresponding channel impulse responses is provided as well.

The proposed IEEE channel model is the multi-cluster version of the generic model in (4.1), which assumes independent fading for each cluster as well as each ray within the cluster. It is the extension of the well-known Saleh-Valenzuela (S-V) model [58]. The channel is modeled as [28]

$$h(t) = \sum_{\ell=0}^{L} \sum_{k=0}^{K_\ell} a_{k\ell} \delta(t - T_\ell - \tau_{k,\ell}) \tag{4.11}$$

where $\delta(\cdot)$ is the dirac delta function, L is the total number of clusters and K_ℓ is the total number of rays in the ℓ-th cluster. The scalars $a_{k\ell}$ and $\tau_{k\ell}$ denote the complex amplitude and delay of the k-th ray of the ℓ-th cluster. Finally, the scalar T_ℓ is the delay of the ℓ-th cluster. Two hidden parameters are Λ - the cluster arrival rate, and λ - the ray arrival rate (within the cluster).

The distribution of cluster arrival time and the ray arrival time are given by

$$\begin{aligned} p(T_\ell | T_{\ell-1}) &= \Lambda e^{-\Lambda(T_\ell - T_{\ell-1})}, \\ p(\tau_{k\ell} | \tau_{(k-1)\ell}) &= \lambda e^{-\lambda(\tau_{k\ell} - \tau_{(k-1)\ell})} \end{aligned}$$

The channel coefficients are defined as follows

$$\begin{aligned} \alpha_{k\ell} &= p_{k\ell} \xi_\ell \beta_{k\ell}, \\ |\xi_\ell \beta_{k\ell}| &= 10^{(\mu_{k\ell} + n_1 + n_2)/20}. \end{aligned}$$

where $n_1 \sim N(0, \sigma_1^2)$ and $n_2 \sim N(0, \sigma_2^2)$ are independent and correspond to the fading on each cluster and ray, respectively, and

$$E[|\xi_\ell \beta_{k\ell}|^2] = \Omega_0 e^{-T_\ell/\Lambda} e^{-\tau_{k\ell}/\gamma}$$

where Ω_0 is the mean energy of the first path (ray) of the first cluster, and $p_{k\ell}$ is the equiprobable $\{+1, -1\}$ to account for the signal polarity inversion due to the reflections. Then $\mu_{k\ell}$ is given by

$$\mu_{k\ell} = \frac{10 \ln(\Omega_0) - 10 T_\ell/\Gamma - 10 \tau_{k\ell}/\gamma}{\ln(10)} - \frac{(\sigma_1^2 + \sigma_2^2) \ln(10)}{20}.$$

In the above equations, ξ_ℓ and $\beta_{k\ell}$ reflect the fading associated with the ℓ-th cluster and the k-th ray of the ℓ-th cluster. Γ and γ are respectively the cluster and ray decaying factors.

Table 4.2.3 shows different standard channel models and their parameters under different scenarios and environments proposed by IEEE 802.15.3a task group [52,28]. These channel models are used extensively for simulations in most of the proposed UWB schemes and receiver algorithms in this thesis.

The IEEE 802.15.3c channel modeling subcommittee has also proposed an extension of the model in (4.11) to the angular domain assuming that the spatial and temporal domains are independent and thus uncorrelated.

Table 4.2: *Different channel models and their main parameters.*

	CM1	CM2	CM3	CM4
Targeted channel characteristics				
Mean excess delay (ns) (τ_m)	5.05	10.38	14.18	
RMS delay (ns) (τ_{rms})	4.28	8.03	14.28	25
NP (10dB)			35	
NP (85%)	24	36.1	61.54	
Model parameters				
Λ (1/ns)	0.0233	0.4	0.0667	0.0667
λ (1/ns)	2.5	0.5	2.1	2.1
Γ	7.1	5.5	14.00	24.00
γ	4.3	6.7	7.9	12
σ_1 (dB)	3.3941	3.3941	3.3941	3.3941
σ_2 (dB)	3.3941	3.3941	3.3941	3.3941
Model characteristics				
Mean excess delay (ns) (τ_m)	5.0	9.9	15.9	30.1
RMS delay (ns) (τ_{rms})	5	8	15	25
NP (10dB)	12.5	15.3	24.9	41.2
NP (85%)	20.8	33.9	64.7	123.3
Channel energy mean (dB)	-0.4	-0.5	0.0	0.3
Channel energy standard (dB)	2.9	3.1	3.1	2.7

CM1: LOS model 0-4m.
CM2: NLOS model 0-4m.
CM3: NLOS model 4-10m.
CM4: NLOS model under extreme conditions.
NP (10dB): number of paths within 10dB of the peak.
NP (85%): number of paths capturing 85% of the energy.

$$h(t,\varphi) = \sum_{\ell=0}^{L}\sum_{k=0}^{K_\ell} a_{k\ell}\delta(t - T_\ell - \tau_{k,\ell})\delta(\varphi - Q_\ell - w_{k,\ell}) \tag{4.12}$$

where $w_{k\ell}$ denotes the azimuth of the k-th ray of the ℓ-th cluster and Q_ℓ is the mean angle-of-arrival (AOA) of the ℓ-th cluster.

When a directive antenna is used in LOS scenarios, there is strong LOS path on top of all the clusters described in (4.12). In this case, the channel model becomes

$$h(t,\varphi) = b\delta(t,\varphi) + \sum_{\ell=0}^{L}\sum_{k=0}^{K_\ell} a_{k\ell}\delta(t - T_\ell - \tau_{k,\ell})\delta(\varphi - Q_\ell - w_{k,\ell}) \tag{4.13}$$

In the NLOS scenarios, the channel model is assumed the same, but without the LOS component.

Since our interest is merely about the channel correlation, we summarize here a few related characteristics of the IEEE channel models (and measurements):

- Although the proposed channel models in (4.11) and (4.13) look more complicated than the generic model in (4.1), they preserve the uncorrelated property of the channel taps (rays, clusters). Therefore, most of the results in the previous sections can still apply.
- The average number of clusters, as shown in measurements, does not follow any particular distribution. But this number can be calculated for different scenarios, which typically is from $L = 3$ to 14. The cluster arrival and ray arrival times are described as two Poisson processes as usual. However, the small scale fading distributions are not modeled by Rayleigh (for LOS) and Rician (for NLOS) as in other "traditional" narrowband communication systems. Instead, the proposed distribution is log-normal for most environments with different measurement system bandwidths. This might lead to a difference in the calculation of the variance of the autocorrelation function compared to the result derived in Section. 4.2.1.

Fig. 4.4 shows the simulated data for one random realization of channel model CM2 in both cases: the physical channel impulse response, and the one for effective channel including the UWB pulse and antenna effect (as used before in Section. 4.2.2). The autocorrelation of the effective channel is shown in Fig. 4.5. It can be seen that the autocorrelation function does have some local maxima, which means that there are some lags that introduce correlation to the channel. This happens for densely multipath channel cases when there are two or more rays arriving during one pulse duration spread by the antenna.

4.2.4 Remarks

We have investigated the correlation property of the UWB channels for various models. The results can be summarized as follows.

- UWB physical channels are multipath channels with highly uncorrelated taps. The number of clusters and number of rays per cluster, which defines the channel length and multipath density, depends on the particular scenario (LOS or

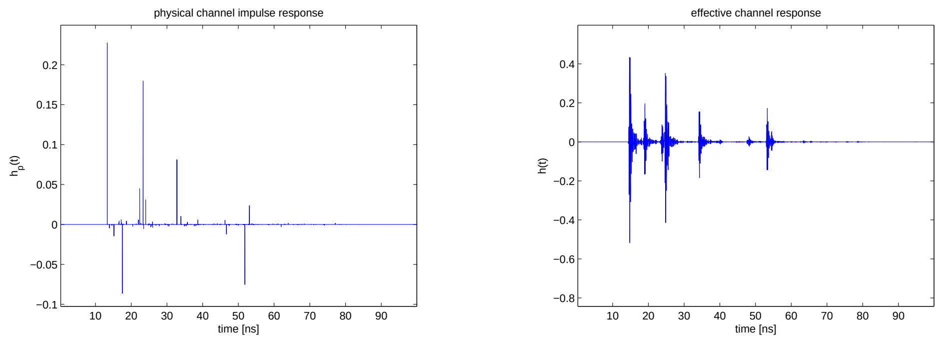

Figure 4.4: *The channel impulse response without and with UWB pulse, antenna effect for CM2.*

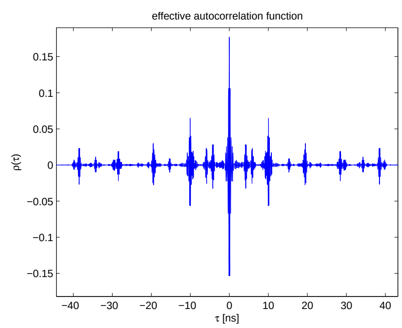

Figure 4.5: *The autocorrelation of the effective channel model CM2.*

NLOS) and environment (residential, office, libary, or desktop, etc.). In some extreme cases, the dense multipath UWB channel can be as long as 200 ns.

- The physical channel taps are assumed uncorrelated. The effective channel correlation is mainly caused by the UWB pulses and the non ideal antenna effect (either at transmitter or receiver), which is visual from (wide) main lobes and side lobes of the channel autocorrelation curve.

- The width of the lobes in the autocorrelation curve is defined by the antenna frequency bandwidth, while the decaying rate is determined by the slopes of the antenna's frequency response.

4.3 Statistics of the data model's parameters

In chapter 3, we have derived a signal processing data model and the corresponding receiver algorithms for a low rate TR-UWB scheme. The unknown "channel" parameters in this model are the **A** and **b** matrices, which consist of α_{mi}, and β_m. These parameters are, in turn, directly related to the channel autocorrelation function $\rho(\Delta)$ as in equation (3.10),

$$\begin{aligned}\alpha_{m,i} &= \rho(D_m - d_i) + \rho(D_m + d_i),\\ \beta_m &= 2\rho(D_m).\end{aligned}$$

More specifically, the diagonal of **A** contains matched delay elements ($d_i = D_m$), which equal channel power or the value of the autocorrelation function at $\Delta = 0$. The off-diagonal elements in **A** and the elements in **b** are the values of autocorrelation function at different nonzero lags.

Obviously, for a UWB channel with an ideal antenna, as discussed in the previous section, **A** will be a diagonal matrix and $\mathbf{b} = \mathbf{0}$. However, that is not the case in practice. Although **A** is diagonally dominant, its off-diagonal entries are nonzero, and **b** is a nonzero vector. This suggests that we can use $\mathbf{A} = \mathbf{I}$ and $\mathbf{b} = \mathbf{0}$ as the initial estimates for the channel matrices, and use the iterative algorithm to jointly estimate the data symbols and the full channel matrices as in section 3.3.3. For complexity reasons, we can always reduce **A** to a band matrix while still maintaining a fairly good BER performance.

Robustness against delay discrepancies

One practical issue in TR-UWB is the implementation of the analog delay lines. It is widely known that a long delay line is hard to implement with high accuracy [7], not to mention that it will reduce the overall data rate of the system. However, as discussed above, too short delays will introduce correlation into the channel. Moreover, because of the ultra-wideband nature of pulses and the antennas, the width of the main lobe in the channel autocorrelation function is usually very narrow, which means that only a small shift ϵ in the delay lines between the transmitter and receiver would cause dramatic changes in the value of $\rho(0 + \epsilon)$. To make the point clear and at the same time verify the theoretical results on the correlation property of the UWB channel models, we study a case with measured channel data.

Within the AIRLINK project at TU Delft, recently the first channel impulse response measurements have been conducted [41]. An example impulse response, frequency spectrum and autocorrelation function is shown in figure 4.6. The measurement data has not been deconvolved, it includes the convolution by the pulse

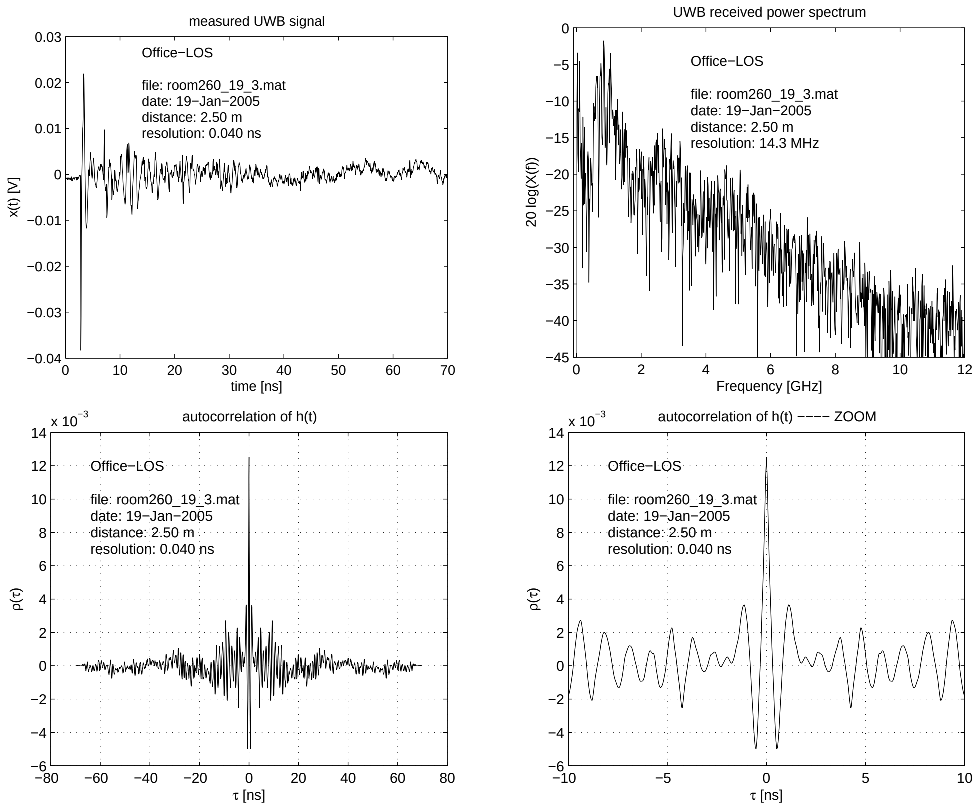

Figure 4.6: *Measured UWB channel—Office, LOS*

shape and the distortion by the biconical antennas. The sampling period is 10 ps, achieved using stroboscopic sampling. However, the effective bandwidth is about 10 GHz, as above this frequency the signal is masked by the noise. The transmitted pulse is about 50 ps, but it is immediately distorted by the antenna to a nonsymmetric monocycle with a duration of about 1.5 ns. In the frequency plot, it is seen that frequencies above 1.5 GHz are significantly attenuated; this shows up in the correlation function as a quasi-periodicity with a period of slightly more than 1 ns.

Our preliminary data includes 7 indoor experiments: four line-of-sight (LOS) at distances of 1.5 to 4 m, two non-line-of-sight (NLOS) from an office to a neighboring office (thin concrete wall), and one NLOS from office to corridor. Table 4.3 shows specific values of $\rho(\tau)$ for each of the experiments, at a spacing of 0.5 ns.

It is seen that $\rho(0)$ is dominant and typically 3 to 5 times larger than the other

Table 4.3: *Measured channel correlations $\rho(\tau + \text{offset})$, normalized to $\rho(0)$, for 7 channels*

	no offset					offset 0.2 ns				
τ [ns]	0	0.5	1.0	1.5	2.0	0	0.5	1.0	1.5	2.0
LOS 1	1.000	-0.430	0.236	0.095	-0.100	0.171	-0.186	0.165	0.093	-0.088
LOS 2	1.000	-0.346	0.208	0.183	-0.066	0.198	-0.141	0.255	0.043	0.008
LOS 3	1.000	-0.380	0.259	0.097	0.036	0.207	-0.197	0.261	0.019	0.000
LOS 4	1.000	-0.478	0.422	-0.066	0.056	0.182	-0.261	0.281	-0.179	0.096
NLOS 5	1.000	-0.516	0.273	0.053	0.006	0.167	-0.316	0.368	-0.291	0.219
NLOS 6	1.000	-0.376	0.063	0.238	-0.032	0.197	-0.266	0.197	0.133	-0.139
NLOS 7	1.000	-0.100	0.268	0.115	0.086	0.383	-0.001	0.204	0.127	0.004

values of $\rho(\tau)$. However, the correlation peak at 0 is very narrow (about 200 ps). Typical affordable delay lines have tolerances which are higher than this. To show the effect of an inaccurate delay at the receiver, a second column in table 4.3 shows values of $\rho(\tau + 0.2 \text{ ns})$ for each of the experiments. In this case, the correlation peak is missed, and all values of ρ have about the same magnitude.

Therefore, any simple model that is based on the assumption that **A** is diagonally dominant and that **b** is zero will not work anymore. However, since our data model in chapter 3 deals with **A** and **b** as the arbitrary matrices, the receiver algorithms can still operate smoothly, of which the results have been shown in simulations from the previous chapter.

The reason we call our low rate TR-UWB developed in chapter 3 a robust system is that it not only can work with random channels, but also is immune to a small shift in delay lines, which is a common problem in practical UWB systems.

4.4 Oversampled UWB channels

One of the main directions of UWB radio is towards high data rate applications, e.g. wireless USB. However, since the UWB channel can be very long and contain dense multipath, we cannot achieve this goal if the frame period is chosen longer than the channel length and low sampling rates are used (only one sample per frame or even per symbol). There appears the need to have a higher sampling rate by using integrate and dump to have multiple samples per frame, while the frame period is shorter than the channel length. Therefore, if we transmit a UWB pulse $g(t)$ through a multipath physical channel $h_p(t)$, after being convolved with the antenna response(s) $a(t)$, the resulting composite channel $h(t) = g(t) * h_p(t) * a(t)$ will be spread over multiple samples. In this case, the sampling operation will take neither only one sample per composite channel (as in the "original" TR-UWB schemes) nor all the individual channel taps (as in RAKE receivers). The received composite channel $h(t)$ is now oversampled at the rate $T_{sam} = T_f/P$ (the number of samples per channel is T_h/T_{sam}). That is why we name this case: "oversampled channel".

Consider the transmission of a single frame by one user, using one delay. The resulting discrete signal (after sampling) at the receiver is

$$\begin{aligned} x[n] &= \int_{(n-1)T_{sam}}^{nT_{sam}} x(t)dt \\ &= \int_{(n-1)T_{sam}}^{nT_{sam}} h^2(t-D)dt + \int_{(n-1)T_{sam}}^{nT_{sam}} [h(t)h(t-D) + h(t-D)h(t-2D)]dt \\ &\quad + \int_{(n-1)T_{sam}}^{nT_{sam}} h(t)h(t-2D)dt \end{aligned} \tag{4.14}$$

We can see that the first term (denoted as the matched term), the second term and the third term (the unmatched terms) in (4.14) are directly related to $\rho(0)$, $\rho(D)$ and $\rho(2D)$, where $\rho(\tau)$ defined in (4.4) is the autocorrelation function of the "composite" channel (including antenna effect).

4.4.1 Matched term vs. unmatched terms

As studied in section 4.2, when antenna effect is ignored, it can be concluded that $\rho(\tau)$ is significant only at $\tau = 0$, i.e., the matched delay term, while all the mismatched delay terms have zero means and very small variance.

In the left hand side of table 4.3 the measurement data (including a practical antenna response) also shows that when τ increases, $\rho(\tau)$ approaches zero. So there exists a certain small value τ_0 (about 1 ns) such that $\rho(\tau)$ becomes negligible for $\tau > \tau_0$.

However, since we use oversampling, the integration length T_{sam} is now much shorter, only a fraction of a frame period T_f. There might be not enough samples to reach a similar statistical conclusion as above. Therefore, we have to compare the matched terms against unmatched terms entry by entry from simulations. Fig. 4.7 shows the simulated plots to compare the matched delay terms ($\mathbf{h}_0$) and the mismatched delay terms ($\mathbf{h}$ with delay $D = 0.5$ ns) for the IEEE channel models CM1 and CM3, under different sampling rates. The resulting plots are the average over 100 realizations of the UWB channel models including pulse shape and a measured antenna response.

From these plots, we can see that even when oversampling is used, these mismatched terms are so small compared to the matched term that we can omit them, i.e. regard them as noise, in (4.14). It is also interesting to note that the matched term

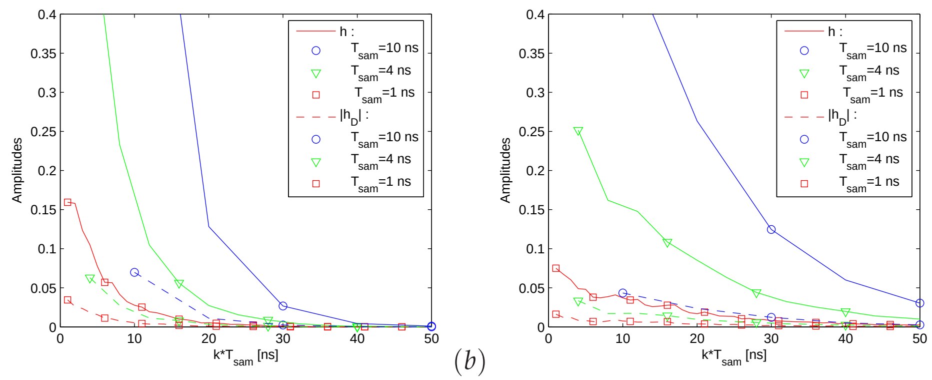

(*a*) (*b*)

Figure 4.7: *Matched and unmatched terms for* (a) *CM1 and* (b) *CM3.*

becomes more dominant when the integration length increases. This is because the matched terms, which are always positive, are added together while the unmatched terms can be either positive or negative. Another reason is that the longer the integration length, the more closely these terms approach the channel autocorrelation function. Therefore, as we reduce the sampling rate, the model error (assuming that the unmatched terms are negligible) will decrease, but at the same time we will lose some IFI resolving ability.

4.4.2 Minimum lag and the delay set selection

It is concluded in the previous section that there exists a certain minimum lag τ_0, which is often quite small, such that the channel autocorrelation can be ignored for correlation lags longer than that value, i.e. $\tau \geq \tau_0$. The value of τ_0 depends on the combined frequency response of the UWB pulse, the transmitting and receiving antennas, and associated filtering (and negligibly on the channel statistics).

More specifically, assume an "ideal" rectangular bandpass frequency response with bandwidth B, centered at frequency f_c, the autocorrelation function has the shape of a modulated squared "sinc" function.

$$R(\tau) = \frac{1}{2B}\cos(2\pi f_c \tau)\mathrm{sinc}(B\tau)$$

Similar to filter design theory, the bandwidth defines the width of the main lobe (around the origin) of its envelope before it approaches zero, and the slopes of the frequency response determine how quickly the side lobes approach zero. For the unmatched terms to be small enough to be negligible, the chosen delay(s) should be longer than τ_0.

From this expression or more visually from its plot, we can find the experimental result of τ_0 as a function of both f_c and B (B is more important because it defines the envelope). The value of τ_0 can be further reduced when the slope of the antenna is designed properly. It is well-known in literature that the raised cosine filter is designed such that its the side lobes can quickly reduces to zero. Therefore, the raised cosine filter with the roll-off factor $\beta = 1$, not the "ideal" rectangular shape, is among the best candidates in this case [56].

For multiple delays, there will be unmatched terms when a transmitted doublet with spacing d_i passes through a correlator bank with delay D_j at the receiver, another condition must be satisfied: $|d_i - D_j| \geq \tau_0$ for all $i \neq j$.

These two conditions set the limit of how close two pulses in a doublet can be, and how far the chosen delays should be separated. Therefore, the most closely spaced set of possible delays is $\{\tau_0, 2\tau_0, \ldots\}$. Obviously, this will directly affect the data rate of the system. Luckily, the value of τ_0 is often very small, less than a nanosecond, and it will decrease as the antenna technology advances.

4.5 Conclusions

In this chapter, we have studied in brief some typical characteristics of the UWB channels. It can be concluded that the UWB physical channels are quite similar to the familiar wideband (radio) channels (S-V multipath channel model, uncorrelated channel taps). The main differences are that UWB channels have more dense multipaths and can be very long in some extreme NLOS cases, they normally do not have overlapping paths (due to ultra-short pulse nature), and the small scale fading is not modeled as Rayleigh or Rician but log-normal distributions.

Practical antennas (not ultra-wide enough in frequency bandwidth) can have a deciding role in shaping the UWB pulses, and thus influence the effective channel autocorrelation statistics. The antenna bandwidth and its slopes can set the minimum lag τ_0 at which the effective channel can be considered as uncorrelated. The "ideal" rectangular shape (or with sharp transition slopes) in this case causes the worst τ_0 (biggest value), while an antenna response with smooth transition slopes in the frequency domain provide the best τ_0 (smallest value).

Therefore, if all delay lags in the TR transceiver are chosen to be larger than τ_0, we can implement in the next chapter a simple and feasible scheme for a higher rate TR-UWB, which uses oversampling and allows interframe interference. Also in the next chapter, we will point out the importance of τ_0 or the antenna frequency response on the scheme's maximum achievable data rates.

Published as: Q.H. Dang, A-J van der Veen – "*A Decorrelating Multiuser Receiver for Transmit-Reference UWB Systems,*" IEEE Journal on Selected Topics in Signal Processing, Vol. 1, Issue. 3, pp. 431-442, Oct 2007 [17].

Chapter 5

A higher rate TR-UWB scheme

See simplicity in the complicated. Achieve greatness in little things.

Lao Tzu

Transmit-reference (TR) is known as a realistic but low data rate candidate for ultra-wideband (UWB) communication systems. This chapter proposes a new TR-UWB scheme that uses a decorrelating receiver to enable higher data rates with only a reasonably small increase in complexity while still maintaining the ease of synchronization of the original. Integrate and dump with oversampling is used to derive an approximate signal processing data model in a multiuser context. An iterative and a blind receiver algorithm are introduced and tested in simulations. Multiple reference delays are used to further improve the system performance similar to the role of multiple antennas in communication systems. The receiver's complexity and other practical issues in transceiver design are also discussed.

5.1 Introduction

Since 2002, ultra-wideband (UWB) has received special research interest as a promising technology for high speed, high precision, strong penetration short-range wireless communication applications. The fact that impulse radio (IR) UWB transmission uses ultra-short low-power pulses, helps resolve multipath, simplifies the receiver's structure and complexity (no analog up/down converter is required), and allows co-existence with other traditional "narrow-band" communication systems.

However, there are significant challenges in developing feasible IR-UWB schemes. Typical UWB channels can be as long as 200 ns, and can be characterized by dense multipath with thousands of components for some NLOS scenarios [12], [28], which greatly increases the complexity of the RAKE receiver that tries to estimate individual channel taps. Sampling an UWB signal at Nyquist rate is not very cost effective in view of its much lower data (symbol) rate, especially when considering the limitations in sampling rates and/or number of quantization levels of current ADC technologies. Moreover, catching the ultra-short pulses (with a duration of only a fraction of a nanosecond) requires strict timing synchronization [64]. Non-ideal ultra-wideband antennas and other frequency-selective effects cause unwanted distortion on the received UWB pulses.

The transmit-reference (TR) scheme, first proposed for UWB in [36], [13] emerges as a realistic candidate that can effectively deal with these challenges. By transmitting pulses in pairs (or doublets) in which both pulses are distorted by the same channel, and using an autocorrelation receiver, the total energy of the channel is gathered to detect the signal without having to estimate individual channel multipath components. The simple delay (at transmitter), correlation and integration operations (at receiver) ease the timing synchronization requirements [6] and reduce the transceiver's complexity. Already a single sample may be sufficient to detect one data symbol. Other techniques [40], [39] are proposed to further reduce the receiver complexity in TR-UWB schemes by using mono-bit digital ADCs, which allows parallel sampling configuration to avoid the error propagation issue in a serial ADC case.

However, TR-UWB also has some disadvantages. It is often considered as a low data rate scheme because of implicit assumptions that the pulse spacing D in a doublet should be longer than the channel length T_h to prevent inter-pulse interference (IPI), and the frame period T_f should be chosen such that there is no inter-frame interference (IFI): together this leads to $T_f > 3T_h$. Since both pulses in a doublet go through the same noisy channel, the correlating operation enhances (and colors) the noise, which degrades the bit error rate (BER) performance. In most TR-UWB schemes, signals are integrated over the full frame or symbol period, which may accumulate noise, especially at the end of the frame (or the tail of the multipath channel) where the signal strength is much weaker or even absent.

Wideband delay lines longer than a few pulse widths are difficult to implement with high accuracy [7]. Therefore, in [19], we have considered a TR-UWB scheme where the pulse spacing D is very short, much shorter than the channel length T_h. However, the frame length T_f was still taken larger than T_h. In chapter 3 and [16], we have lifted this assumption and considered $T_f < T_h$, and introduced equalization schemes to remove the IPI and IFI. As a result, the frame rate can be at least three times higher than in the preceding schemes. In [18] we have extended this scheme to a CDMA-like multiuser context.

To improve the tradeoff between energy capture and noise accumulation, various authors have considered oversampling, which means to take multiple samples per frame by speeding up the integrate and dump operation. E.g., in [30], oversampling was used in combination with a GLRT receiver–IPI was assumed to be absent. In [44, 45], the noise problem was reduced by oversampling and optimized combining of weighted samples. However, the scheme did not allow IFI and is hard to generalize to the multiuser case where user signals are not properly aligned. In the present paper, we use oversampling to get P samples per frame, but all the samples are treated in parallel instead of immediately combining them. This helps to resolve the IFI and makes it easier to extend the data model to the multiuser, multiple delay case.

The IFI problem was also considered in [74], where a data model based on second-order Volterra systems is developed for a frame differential UWB system. The algorithm's complexity quickly grows in longer (and more practical) UWB channels and in a multiuser context. Here, we develop a data model in matrix form and propose receiver algorithms exploiting the sparse structure of these matrices, of which the complexity only grows linearly with the channel length.

Finally, in [78], a multiuser system was proposed for TR-UWB, which considers all digital TR, template averaging, etc. This scheme accepts IPI, which also increases the data rate. However, IFI is not considered and perfect frame synchronization is assumed.

In this paper, we develop a multiuser TR-UWB system that admits both IPI and IFI. Users are allowed to transmit signals asynchronously as in CDMA systems [66], [15]. No synchronization is necessary in the analog part of the receiver: it is running data-independently. In the digital part of the receiver, we will assume without loss of generality that the time offset of each user is known up to an integer multiple of the sampling period—the estimation of this offset is outside the scope of the paper.

It is known that the use of multiple antennas facilitates the equalization problem in communication systems. In this paper, we make use of multiple delays between the two pulses in a doublet. This creates a multi-channel scenario that has similar effects as multiple antennas and oversampling. Simulation results show that it gives a significant improvement over the single delay case.

The chapter is organized as follows. Section 5.2 derives, for clarity, a generic data model for the transmission of a single frame, and subsequently for multiple frames, based on approximations of which the validity is analyzed and simulated in chapter 4. The model is extended in section 5.3 to a general model that includes oversampling, multiple delays, and multiple users. Based on these signal processing data models, blind and iterative receiver algorithms are derived in section 5.4, and their performance is shown in simulations in section 5.5. As conclusion, section 5.6 summarizes some design considerations of the proposed TR-UWB scheme in relation to practical system design.

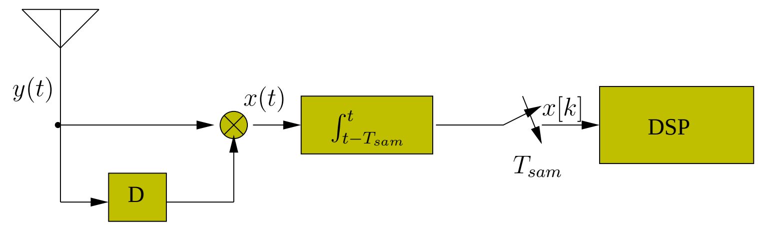

Figure 5.1: *Autocorrelation receiver*

5.2 Data model - Preliminaries

5.2.1 Single frame

To make the model derivation steps easier to follow and to simplify the expressions, we start from a generic transmission of a single frame of duration T_f.

When a UWB pulse $g(t)$ is transmitted through a UWB physical channel $h_p(t)$ of length T_h, the received signal at the antenna's output (possibly after some band-pass/lowpass received filters) will be

$$h(t) = h_p(t) * g(t) * a(t) \tag{5.1}$$

where $a(t)$ is the antenna response. From now on, $h(t)$ will be regarded as the "composite" channel impulse response.

In TR-UWB systems, pulses are transmitted in pairs (called doublets), one doublet per frame. Within a frame, the first pulse is fixed, while the second pulse, delayed by D seconds, has information in its polarity: $s_0 \in \{-1, +1\}$. The received signal at the antenna output due to one transmitted frame is

$$y_0(t) = h(t) + s_0 \cdot h(t - D)\,.$$

The receiver structure for a single frame is shown in Fig. 5.1, in which $y_0(t)$ is multiplied with a delayed (by D) version of itself before being integrated and dumped. The sampling period is T_{sam}, and we use oversampling by taking P samples per frame: $T_{sam} = \frac{T_f}{P}$. The resulting signal at the multiplier's output is

$$\begin{aligned}
x_0(t) \quad &:= \quad y_0(t)y_0(t-D) \\
&= \quad [h(t) + s_0 h(t-D)][h(t-D) + s_0 h(t-2D)] \\
&= \quad [h(t)h(t-D) + h(t-D)h(t-2D)] + s_0[h^2(t-D) + h(t)h(t-2D)]
\end{aligned}$$

Define the channel autocorrelation function as

$$R(\tau, n) = \int_{(n-1)T_{sam}}^{nT_{sam}} h(t)h(t-\tau)dt\,.$$

After integrate-and-dump, the received samples are

$$x_0[n] = [R(0, n - \frac{D}{T_{sam}}) + R(2D, n)]s + [R(D, n) + R(D, n - \frac{D}{T_{sam}})]\,. \tag{5.2}$$

In equation (5.2), the dominant term is the matched term, $R(0)$, which contains the energy of the channel segments. As shown in section 4.4.2, the unmatched terms $R(\tau)$ with $\tau \in \{D, 2D\}$ can be ignored if we choose $D > \tau_0$, where τ_0 is a certain correlation length, often very small (less than a nanosecond) for typical UWB channels, and dependent on channel statistics and antenna responses.

The oversampling process (by integrate and dump with $T_{sam} < T_f \ll T_h$) actually divides the spreading channel into $L_h = \lfloor \frac{T_h}{T_{sam}} \rfloor$ segments (or sub-channels). Each segment has its own "channel energy" and "channel autocorrelation function". The original channel $h(t)$ is now replaced by L_h parameters related to the energy of the channel segments (with a little abuse of notation):

$$h[n] = \int_{(n-1)T_{sam}}^{nT_{sam}} h^2(t)dt \qquad n = 1, \cdots, L_h\,. \tag{5.3}$$

Define the corresponding TR-UWB "channel" power vector as

$$\mathbf{h} = [h[1], \cdots, h[L_h]]^T\,. \tag{5.4}$$

After stacking all discrete samples together in a vector $\mathbf{x}_0$ and ignoring the cross-terms in (5.2), we have a generic data model for a single frame as

$$\mathbf{x}_0 = \mathbf{h} \cdot s_0\,. \tag{5.5}$$

This is a very simple approximate data model for a single frame, based on some statistical properties of the UWB channels and the ultra-wideband nature of the signal and the antennas. As shown later in simulations, this approximation suffers almost no BER performance loss while helps reduce the complexity in data model and receiver algorithms. Based on this generic model, data models for multiple frames, multiple users, and multiple reference delays can be readily derived.

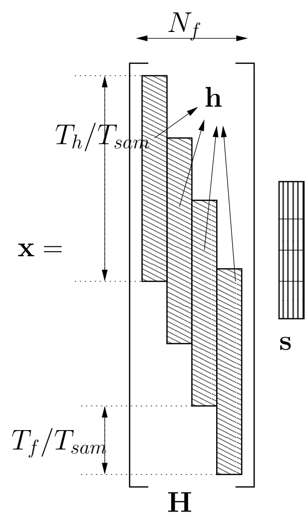

Figure 5.2: *Data model for multiple frames*

5.2.2 Multiple frames

We extend the preceding model to the transmission of N_f consecutive frames. Each frame has duration T_f, and is assigned a data bit s_j in the polarity of its second pulse, delayed by D from the first pulse. Let us recall that the frame period T_f is much shorter than the channel length T_h so that there always exists inter-frame interference (IFI). Since a single delay is used for all frames, the receiver structure remains the same as in Fig. 5.1.

Since we have more than one frame, apart from the matched term and the unmatched terms within every frame, there appear new cross-terms between frames. These cross-terms can also be expressed in terms of the autocorrelation functions of the channel segments. However, the correlation length in the cross-terms are much longer, comparable to the frame length. Therefore, they can be ignored or treated as a noise-like signal.

However, although all the cross-terms can be safely ignored, we still have the matched term that spreads over some next frames because $T_h \gg T_f$. These overlapping parts are IFIs and can be modeled in a channel matrix $\mathbf{H}$ in the data model for multiple frames as

$$\mathbf{x} = \mathbf{H}\mathbf{s} + \text{noise} \tag{5.6}$$

where $\mathbf{x}$ is the stacking of all received samples, $\mathbf{s}$ is the unknown data vector $\mathbf{s} = [s_1 \cdots s_{N_f}]^T$, and $\mathbf{H}$ is the channel matrix that contains shifted versions of the "channel" vector $\mathbf{h}$ in (5.4). The relation is illustrated in Fig. 5.2. The IFI effect is also visible in this figure from the fact that many rows in $\mathbf{H}$ have more than one nonzero entry.

We can further improve the accuracy of this data model by including the unmatched terms (with correlation length D) of equation (5.2). The improved data model becomes

$$\mathbf{x} = \mathbf{H}\mathbf{s} + \mathbf{B}\mathbf{1} + \text{noise}\,, \tag{5.7}$$

where $\mathbf{B}$ has the same structure as $\mathbf{H}$, containing shifted versions of the "unmatched" vector $\mathbf{b} = [b_1, b_2, \cdots, b_{L_h}]^T$, where

$$b_n := R(D, n) + R(D, n - \frac{D}{T_{sam}})\,.$$

However, as shown later in simulations (Section 5.5.2), little gain is obtained if the model in (5.7) is used for receiver design, even if D is quite small. Therefore, it is sufficient to use the approximate data model in (5.6).

5.2.3 Effect of timing synchronization

UWB communication systems often have stringent requirements on synchronization because of ultra-short pulses. However, in TR-UWB schemes, the analog processing can be kept data-independent as we can easily deal with synchronization issues only after sampling, in the digital domain.

Suppose the full data packet (consisting of multiple frames) is not synchronously sampled, which means that there is an offset G at the beginning of the packet. We can always express the offset as

$$G = G' T_{sam} + g$$

where G' is an integer and g the remainder that satisfies the condition: $0 \leq g < T_{sam}$.

The integer G' is incorporated in the data model as G' zero padding rows at the top of the channel matrix $\mathbf{H}$. The offset fraction g causes small changes to the channel vector $\mathbf{h}$, with entries

$$h[n] = \int_{(n-1)T_{sam}}^{nT_{sam}} h^2(t-g)dt\,, \qquad n = 1, \cdots, L_h\,.$$

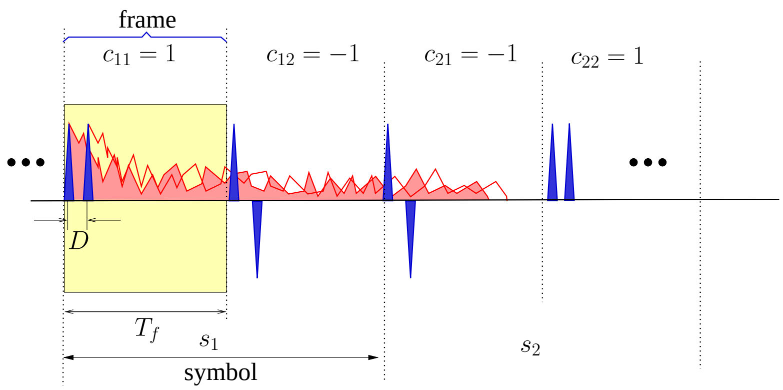

Figure 5.3: *Pulse sequence structure*

Since no assumption was made on the unknown channel vector $\mathbf{h}$, we can still model the whole system as in (5.6) in the same way as before.

Our receiver algorithms will require G' to be known. If G' is unknown, there are techniques as in [23, 24] that can jointly estimate the unknown offset integer G' and detect the data symbols. In this paper, we will not study in detail these synchronization algorithms.

The implication of the preceding discussion is that by using integrate and dump with oversampling, the proposed TR-UWB scheme is robust against timing errors up to a sampling period. The offset fraction g is absorbed in the unknown channel vector, while the complete synchronization algorithm to estimate the offset integer G' can be implemented in the DSP part, which simplifies the analog part of the receiver.

5.3 Data model

The preceding preliminary models are extended to the reception of a batch of multiple symbols.

5.3.1 Single user, single delay

Consider the transmission of a packet of N_s data symbols $\mathbf{s} = [s_1 \cdots s_{N_s}]^T$, where each symbol $s_i \in \{+1, -1\}$ is "spread" over N_f frames of duration T_f. The spacing between two pulses in one frame is fixed at D. Each frame is assigned a known user code $c_{ij} \in \{+1, -1\}, j = 1, \cdots, N_f$. The code varies from frame to frame, and can

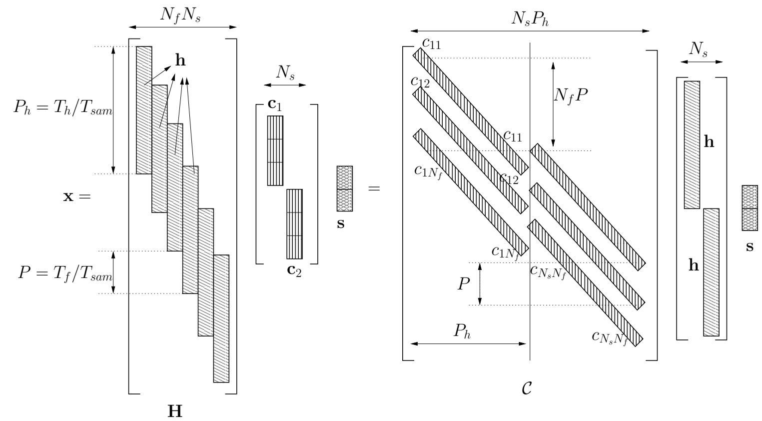

Figure 5.4: *The data model for the single user, single delay case with no offset*

vary from symbol to symbol similar to the long code concept in CDMA. The receiver still has the simple structure with only one correlator as illustrated in Fig. 5.1. The structure of the transmitted pulse sequence is illustrated in Fig. 5.3.

The received signal at the antenna output is

$$y(t) = \sum_{i=1}^{N_s} \sum_{j=1}^{N_f} [h(t-((i-1)N_c+j-1)N_f T_f) + s_i c_{ij} h(t-((i-1)N_c+j-1)N_f T_f - D)] \tag{5.8}$$

where $\mathbf{c}_i = [c_{i1}, \cdots, c_{iN_f}]^T$ is the code vector for the i-th symbol s_i.

At the multiplier output, the signal $x(t) = y(t)y(t-D)$ will be integrated and dumped at the oversampling rate $P = T_f/T_{sam}$. Due to uncorrelated channels, as concluded in section 4.4.1 the unmatched terms and the cross-terms can be ignored for the purpose of receiver design. The data model in (5.6) can be easily extended to include the code c_{ij}. The resulting discrete samples $x[n] = \int_{(n-1)T_{sam}}^{nT_{sam}} x(t)dt$, $n = 1, \cdots, (N_s N_f - 1)P + T_h/T_{sam}$ are stacked into a column vector $\mathbf{x}$, which can be expressed as (see the left part of Fig. 5.4)

$$\mathbf{x} = \mathbf{H}\mathrm{diag}\{\mathbf{c}_1, \cdots, \mathbf{c}_{N_s}\}\mathbf{s} + \text{noise} \tag{5.9}$$

where, as before, $\mathbf{H}$ contains shifted versions of the “channel” vector $\mathbf{h}$, and the ‘diag’ operator puts the vectors $\mathbf{c}_1, \cdots, \mathbf{c}_{N_s}$ into a block diagonal matrix.

One important result is that the data model in (5.9) can also be rewritten in another form (as visually illustrated in blocks in Fig. 5.4) ,

$$\mathbf{x} = \mathcal{C}(\mathbf{I}_{N_s} \otimes \mathbf{h})\mathbf{s} + \text{noise} \tag{5.10}$$

where $\otimes$ denotes the Kronecker product and $\mathcal{C}$ is the code matrix of size $((N_f N_s - 1)T_f + T_h)/T_{sam} \times (T_h N_s)/T_{sam}$, with entries taken from $\mathbf{c}_i$ and structure illustrated in Fig. 5.4. This form of data model will be used to derive the data model for multiuser, multi-delay cases.

5.3.2 Multiple users, single delay

Now we derive the data model for an asynchronous multiuser system where the k-th user is characterized by a code matrix $[\mathbf{c}_{k1}, \cdots, \mathbf{c}_{k,N_s}]$, channel vector $\mathbf{h}_k$, and offset $G_k = G'_k T_{sam} + g_k$, $0 \le g_k < T_{sam}$. The code and the integer G'_k are known, the channel $\mathbf{h}_k$ and g_k are unknown. Since each user goes through a different channel, we can safely assume that two different channels are uncorrelated, which means that all the cross-terms between two users' channels are noise-like. Therefore, the received signal will be modeled as

$$\begin{aligned} \mathbf{x} &= \sum_{k=1}^{K} \mathbf{H}_k \text{diag}\{\mathbf{c}_{k1}, \cdots, \mathbf{c}_{kN_s}\}\mathbf{s}_k + \text{noise} \\ &= \sum_{k=1}^{K} \mathcal{C}_k(\mathbf{I} \otimes \mathbf{h}_k)\mathbf{s}_k + \text{noise} \end{aligned}$$

where $\mathbf{H}_k$, $\mathcal{C}_k$ are the channel matrix and code matrix for the k-th user. They have structure as in Fig. 5.4, except that the time offset G_k shows up as G'_k zero padding rows at the top of the matrices $\mathbf{H}_k$ and $\mathcal{C}_k$. The effect of the offset fraction g_k is not visible in the model (as discussed earlier in Section 5.2.3, the values of the entries of the channel vector $\mathbf{h}_k$ are slightly changed).

The multiuser data model can be straightforwardly derived as

$$\mathbf{x} = \mathcal{C}\mathcal{H}\mathbf{s} + \text{noise} \tag{5.11}$$

where $\mathcal{C} = [\mathcal{C}_1 \cdots \mathcal{C}_K]$ is the known code matrix; $\mathcal{H} = \text{diag}\{\mathbf{I} \otimes \mathbf{h}_1, \cdots, \mathbf{I} \otimes \mathbf{h}_K\}$ is the unknown channel matrix, in which $\mathbf{h}_k$ contains the unknown channel coefficients; and $\mathbf{s} = [\mathbf{s}_1^T \cdots \mathbf{s}_K^T]^T$ contains the unknown source symbols.

5.3.3 Multiple users, multiple delays

In the previous sections, we used a fixed delay between the two pulses in a doublet (frame) to simplify the mathematical expressions and the receiver structure. However, the fixed delay D will cause spikes at $1/D$ frequency intervals in the spectrum

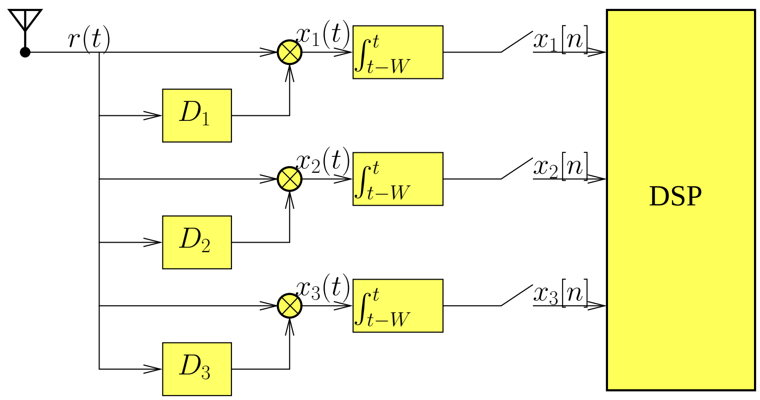

Figure 5.5: *Receiver structure with multiple correlators*

of the received UWB signal, which may conflict with spectral masks. To mitigate this problem, the delay between two pulses in a doublet can be made to vary from frame to frame, according to a known pattern. From a signal processing viewpoint, the use of multiple delays will improve equalization and multiuser separation performance, as it improves the conditioning of the matrix $\mathcal{CH}$ by making it taller.

Let the spacing between two pulses in a frame be d_{ij}^k seconds (corresponding to the k-th user, i-th symbol, j-th frame). As before, we choose the delay d_{ij}^k to be very small compared to the frame period and the channel length, i.e., $d_{ij}^k \ll T_f < T_h$. The values of all the delays d_{ij}^k are chosen from a finite set $d_{ij}^k \in \{D_1, D_2, \cdots, D_M\}$, of which the pattern is known to the receiver.

In the receiver, we use a bank of correlators, each followed by an "integrate and dump" operator as shown in Fig.5.5. The signals at the outputs will be processed in the DSP part of the receiver.

We have M equations corresponding to the M branches of correlators $D_1, \cdots, D_M$. In the single user case, each equation has a similar expression to (5.9) and (5.10),

$$\mathbf{x}^{(m)} = \mathbf{H}^{(m)}\text{diag}\{\mathbf{c}_1', \cdots, \mathbf{c}_{N_s}'\}\mathbf{s} + \text{noise}, \qquad m = 1, \cdots, M, \tag{5.12}$$

where $\mathbf{x}^{(m)}$ is a vector containing the received samples of the m-th branch, and $\mathbf{H}^{(m)}$ is similar to $\mathbf{H}$ as before. The code vector $\mathbf{c}_i'$ has entries corresponding to each user, frame and delay. If the delay matches the delay code, the entry contains the corresponding chip value $\{+1, -1\}$, otherwise the entry is 0.

In the data model, we should take into account that all the branches share the same "channel" coefficients $\mathbf{h}$ and the symbol values $\mathbf{s}$. To this end, we first rewrite the data model of a single branch that corresponds to delay D_m (5.12) in the "code" by "channel" by "data" form, as

$$\mathbf{x}^{(m)} = \mathcal{C}^{(m)}(\mathbf{I} \otimes \mathbf{h})\mathbf{s} + \text{noise}, \qquad m = 1, \cdots, M, \tag{5.13}$$

where $\mathcal{C}^{(m)}$ is a code matrix with structure as before, but with nonzero entries only for frames that have delay codes that match delay D_m.

Now, stacking all received samples in all branches into a column vector, since the channel and source symbols are the same for all branches, the data model for a single user, multi-delay receiver becomes

$$\mathbf{x} = \mathcal{C}(\mathbf{I} \otimes \mathbf{h})\mathbf{s} + \text{noise} \tag{5.14}$$

where

$$\mathcal{C} = \begin{bmatrix} \mathcal{C}^{(1)} \\ \vdots \\ \mathcal{C}^{(M)} \end{bmatrix}.$$

From this equation, the data model for multiuser, multi-delay receiver case can be straightforwardly derived in a similar way as presented in the previous section. The multiuser multi-delay data model becomes

$$\mathbf{x} = \begin{bmatrix} \mathcal{C}_1^{(1)} & \cdots & \mathcal{C}_K^{(1)} \\ \vdots & \ddots & \vdots \\ \mathcal{C}_1^{(M)} & \cdots & \mathcal{C}_K^{(M)} \end{bmatrix} \begin{bmatrix} \mathbf{I} \otimes \mathbf{h}_1 & & \mathbf{0} \\ & \ddots & \\ \mathbf{0} & & \mathbf{I} \otimes \mathbf{h}_K \end{bmatrix} \begin{bmatrix} \mathbf{s}_1 \\ \vdots \\ \mathbf{s}_K \end{bmatrix} =: \mathcal{C}\mathcal{H}\mathbf{s} \tag{5.15}$$

where $\mathcal{C}_k^{(m)}$ is the code matrix corresponding to the k-user, m-th correlator branch. This matrix contains information regarding the user's chip code, delay code, and time offset.

By using a property of the Kronecker product: $(\mathbf{I} \otimes \mathbf{h}_k)\mathbf{s}_k = (\mathbf{s}_k \otimes \mathbf{I})\mathbf{h}_k$, the data model above ($\mathbf{x} = \mathcal{C}\mathcal{H}\mathbf{s}$) can be rewritten in another form ($\mathbf{x} = \mathcal{C}\mathcal{S}\mathbf{h}$) as

$$\mathbf{x} = \begin{bmatrix} \mathcal{C}_1^{(1)} & \cdots & \mathcal{C}_K^{(1)} \\ \vdots & \ddots & \vdots \\ \mathcal{C}_1^{(M)} & \cdots & \mathcal{C}_K^{(M)} \end{bmatrix} \begin{bmatrix} \mathbf{s}_1 \otimes \mathbf{I} & & \mathbf{0} \\ & \ddots & \\ \mathbf{0} & & \mathbf{s}_K \otimes \mathbf{I} \end{bmatrix} \begin{bmatrix} \mathbf{h}_1 \\ \vdots \\ \mathbf{h}_K \end{bmatrix} =: \mathcal{C}\mathcal{S}\mathbf{h}. \tag{5.16}$$

The two forms of the data model in (5.15) and (5.16) will be used to derive the iterative algorithms to jointly detect the data symbols and estimate the channel vectors of all users.

5.3.4 Remarks

The oversampling included in the integrate and dump process gives us multiple samples per frame. This reduces the individual channel multipath parameters into $L_h = T_h/T_{sam}$ channel coefficients (corresponding to the energies of the channel segments). The oversampling rate P is a flexible parameter that can be used to improve the performance of the system at the expense of computational complexity.

By introducing multiple delays, we add more diversity to the system. The role of multiple delays is similar to that of multiple antennas in "conventional" communication systems, e.g. CDMA. The difference is that multiple antennas give rise to different channels (more unknown parameters), whereas the bank of multiple delays (in the receiver) shares the same "channel". In general, the larger the number of possible delays M, the better performance the receiver algorithm can achieve. However, M is limited by constraints on data rate in relation to channel length and channel correlation properties. For example, let τ_0 be the shortest correlation length so that the unmatched terms can be ignored (cf. section 4.4.2), then a set of minimal delay values is $\{D_1, \cdots, D_M\} = \{\tau_0, 2\tau_0, \cdots, M\tau_0\}$. The distance between the last pulse in a frame and the first pulse in the next frame should be larger than $D_M = M\tau_0$. Thus, we should have $T_f > 2M\tau_0$. If the frame length is fixed at T_f, the maximum number of delays will be $M = \lfloor \frac{T_f}{2\tau_0} \rfloor$.

5.4 Receiver algorithms

5.4.1 Alternating least squares receiver algorithm

In section 5.3, we have established linear data models for either the single user or multiple users case. In each case, the data model can be expressed in two common forms,

$$\mathbf{x} = \mathcal{C}\mathcal{H}\mathbf{s} \tag{5.17}$$

$$\mathbf{x} = \mathcal{C}\mathcal{S}\mathbf{h} \tag{5.18}$$

where $\mathcal{H}$, $\mathcal{S}$ are matrices with known structures, constructed from the channel vector $\mathbf{h}$ and source symbols vector $\mathbf{s}$, respectively. In this equation, $\mathbf{x}$ is the (known) data sample vector, $\mathcal{C}$ is the known code matrix, while $\mathbf{s}$ and $\mathbf{h}$ are the unknowns.

Based on these two forms of the data model, the alternating least squares (ALS) algorithm can be implemented as below.

With an initial channel estimate $\mathbf{h}^{(0)}$, for iteration index $i = 1, 2, \cdots$ until convergence,

- keeping the channel $\mathbf{h}^{(i-1)}$ fixed, construct the $\mathcal{H}$ matrix, and estimate the source symbols via

$$\mathbf{s}^{(i)} = (\mathcal{C}\mathcal{H})^{\dagger}\mathbf{x}\,,$$

  where $(\cdot)^{\dagger}$ indicates the Moore-Penrose pseudo-inverse (in this case equal to the left inverse),

- keeping the source symbols $\mathbf{s}^{(i)}$ fixed, construct the $\mathcal{S}$ matrix, and estimate the channel coefficients via

$$\mathbf{h}^{(i)} = (\mathcal{C}\mathcal{S})^{\dagger}\mathbf{x}\,.$$

After these iterations, step 1 is repeated once more to get the final estimate of the source symbols. Hard decisions can be used in step 1 to further improve the performance.

Although this is an iterative algorithm that repeatedly uses matrix inversion operations $(\mathcal{C}\mathcal{H})^{\dagger}$ and $(\mathcal{C}\mathcal{S})^{\dagger}$, we will discuss in section 5.4.4 that, by exploiting the sparse structures of these matrices, we can efficiently implement these operations.

5.4.2 Initialization—A blind algorithm

The ALS algorithm needs an initial channel estimate. As later shown in simulations, the quality of this initial estimate is decisive for the overall performance of the iterative algorithm. Therefore, a fairly good initial estimate of the channel is needed. One idea is that (in view of the definition (5.3)), the channel vector can be roughly approximated by the channel delay profile. However, in the following, we will introduce a simple blind algorithm, which is similar to the algorithm in [66] (see chapter 6).

From equation (5.15), if the code matrix is tall (this implies the condition $M((N_sN_f-1)T_f+T_h)/T_{sam} > KT_hN_s/T_{sam}$) we can pre-multiply both sides of (5.15) with the left-inverse of this known code matrix. The resulting multiuser equation can be decomposed into K single user equations,

$$\mathbf{x}'_k \approx (\mathbf{I}\otimes\mathbf{h}_k)\mathbf{s}_k\,, \quad k=1,\cdots,K\,,$$

where $\mathbf{x}'_k$ is the k-th segment of $\mathbf{x}' = \mathcal{C}^{\dagger}\mathbf{x}$.

After restacking the vector $\mathbf{x}'_k$ into a matrix $\mathbf{X}'_k$ of size $L_h \times N_s$ as in [66], we have

$$\mathbf{X}'_k \approx \mathbf{h}_k\mathbf{s}_k^T\,.$$

Subsequently, the channel vector $\mathbf{h}_k$ and the source symbols $\mathbf{s}_k$ of the k-th user are found, up to an unknown scaling, by taking a rank-1 approximation of $\mathbf{X}'_k$. This requires the computation of the SVD of $\mathbf{X}'_k$ and keeping the dominant component.

5.4.3 Training-based algorithm

In certain cases where the data is transmitted in a long packet, through a channel with fairly constant statistics, we can use a few training symbols to further improve the performance while sacrificing a small portion of the data rate. E.g., UWB indoor channels are commonly known to be less varying in time, especially in its channel delay profile which is relevant in our case. With training available, the ALS algorithm is readily adapted. Firstly, based on the known data symbols, we can estimate the channel vector. This estimated channel vector can be used in a zero-forcing receiver to detect the unknown data symbols, etc. It can even be used as the initial channel estimate in the next data packet, which will require no training. This might also help to avoid the local convergence point that may otherwise occur in ALS algorithms.

5.4.4 Computational complexity

The proposed algorithms are all two-step iterations. The complexity of one iteration is derived here. For simplicity of the expressions, we assume that all users have the same parameters and time offsets. As before, $L_h = \frac{T_h}{T_{sam}}$ is the channel length in terms of number of samples. Let $L = \frac{T_h}{T_f} = \frac{L_h}{P}$ be the channel length in terms of frames, assumed an integer number here.

1. *Given the channel coefficients* $\mathbf{h}$, *estimate the source symbols* $\mathbf{s}$ *by solving* $\mathbf{x} = \mathcal{CH}\mathbf{s}$ *(equation (5.17)).* This is done by the following steps:

$$\begin{array}{lll} \text{Compute } \mathbf{T} = \mathcal{CH} & : & KN_sN_fLP \quad \text{operations} \\ \text{Compute } \mathbf{y} = \mathbf{T}^H\mathbf{x} & : & KN_sMP(N_f + L) \\ \text{Compute } \mathbf{M} = \mathbf{T}^H\mathbf{T} & : & K^2N_sMP(N_f + L + \frac{L^2}{N_f}) \\ \text{Solve for } \mathbf{s} \text{ in } \mathbf{Ms} = \mathbf{y} & : & N_sK^3(2 + \frac{L}{N_f})^2 \end{array}$$

   In the estimation of the complexities, one can use the fact that $\mathbf{T}$ is a permutation of a block-Sylvester matrix, with structure as shown in Fig. 5.6. As a result, $\mathbf{M} = \mathbf{T}^H\mathbf{T}$ is a permutation of a block banded matrix, of size $KN_s \times KN_s$, and with bandwidth $B = K\lfloor(2 + \frac{L}{N_f})\rfloor$. This sparsity structure should be exploited when computing $\mathbf{M}$ and when solving for $\mathbf{s}$ via a sparse LU factorization and backsubstitution (as introduced in chapter 2).

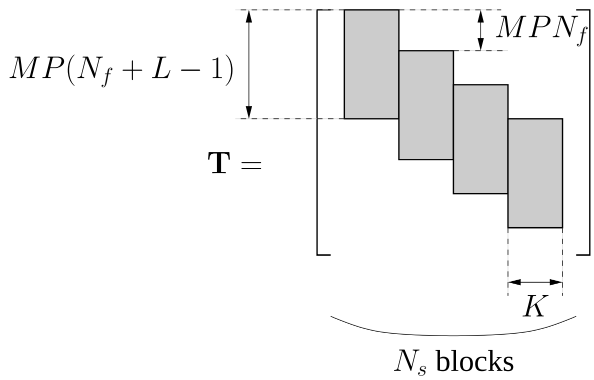

Figure 5.6: *Structure of* **T** *(after permutations)*

The dominant operation is the computation of $\mathbf{M}$. Thus, the order of complexity of the estimation of $\mathbf{s}$ is $K^2N_sMP(N_f+L+\frac{L^2}{N_f})$.

2. *Given* $\mathbf{s}$, *estimate the channel coefficients* $\mathbf{h}$ *by solving* $\mathbf{x} = \mathcal{CS}\mathbf{h}$ *(equation (5.18)).* This is done by the following steps:

Compute $\mathbf{T} = \mathcal{CS}$	:	(only composition)
Compute $\mathbf{y} = \mathbf{T}^H\mathbf{x}$	:	KN_sN_fLP additions
Compute $\mathbf{M} = \mathbf{T}^H\mathbf{T}$	:	$K^2N_sN_fPL^2$ additions
Solve for $\mathbf{h}$ in $\mathbf{Mh} = \mathbf{y}$	:	K^2PL^2 operations

In the estimation of the complexities, we used the fact that $\mathbf{T}$ is very sparse with entries $\{0, \pm 1\}$. Each column has only N_sN_f nonzero entries. $\mathbf{M}$ is of size $KLP \times KLP$ and has a multiband structure: only each P-th diagonal is nonzero. Consequently, the inversion problem in the last step can be split into P independent inversion problems.

In total, the complexity is $K^2N_sN_fPL^2$ additions plus K^2PL^2 multiply/additions.

Overall, solving for $\mathbf{s}$ gives the dominant complexity. One iteration thus has a complexity of order $K^2N_sMP(N_f+L+\frac{L^2}{N_f})$ operations. Per estimated symbol per user, the complexity is $KMP(N_f+L+\frac{L^2}{N_f})$. Compare this to a single antenna CDMA multiuser decorrelating receiver, which has complexity per user per symbol of order KN_f or LN_f, depending on the type of receiver as discussed in chapter 6 and [15]. The increased complexity (factor MP) is due to the multi-branch nature of the TR-UWB receiver structure, and would be similar to the use of multiple antennas.

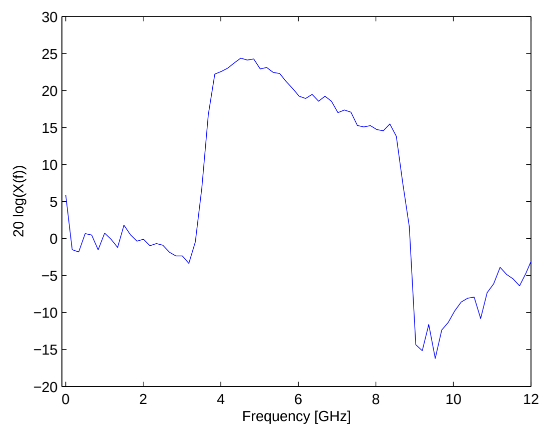

Figure 5.7: *Frequency response of a practical antenna*

5.5 Simulations

5.5.1 Setup

We simulate an asynchronous multiuser TR-UWB system with $K = 3$ equal powered users transmitting Gaussian monocycle pulses of width 0.2 ns. The spacing between two pulses in a doublet may vary in frames, symbols and users, with values taken from the set $\{1, 2, 3, 4\}$ ns. In one user's data packet, we transmit $N_s = 10$ symbols, each symbol consists of $N_f = 10$ frames with duration $T_f = 30$ ns. All the users' symbols and codes are generated randomly. Each user signal is delayed by a random (but known) offset of up to one frame duration, rounded to an integer number of samples. The sampling rate is $T_{sam} = T_f/P$ and depends on the chosen over-sampling rate, which can be $P \in \{3, 6, 15\}$ samples per frame.

We use the IEEE channel models (CM1, CM2) which are always longer than the frame period, implying that inter-frame interference (IFI) does exist. The non-ideal antenna effect is also included, i.e. a measured antenna response is convolved with the channel and the pulse. The frequency response of the antenna is shown in Fig. 5.7 [41]. The energy of the resulting channel is normalized to $\int_0^\infty h(t)^2 dt = 1$.

Monte Carlo runs are used to compare the BER vs. signal to noise ratio (SNR) and channel mean squared error (MSE) vs. SNR plots between various algorithms under different situations. A reference curve for the BER vs. SNR plot is the performance of the zero-forcing receiver when the channel coefficients are completely known.

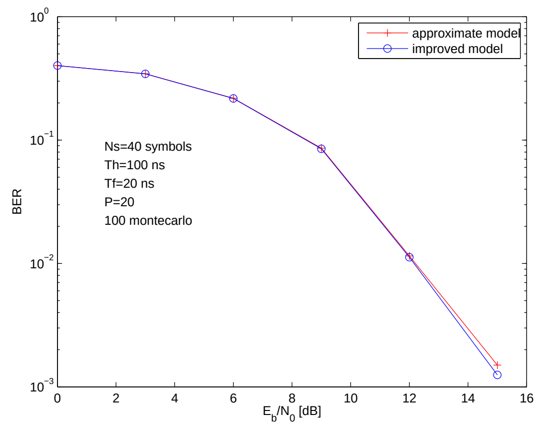

Figure 5.8: *Comparison of the performance of a ZF receiver based on the approximate data model (5.6) vs. one based on the improved data model (5.7).*

Here, SNR is defined as the pulse energy spread by a normalized channel over the noise spectral density, and channel MSE is defined as the mean squared error of the estimate of the "channel" vector $\mathbf{h}$, i.e., the average of $\|\hat{\mathbf{h}} - \mathbf{h}\|^2$.

With the parameters given above, one iteration in the iterative algorithm for CM2 case has the complexity of order $K^2 N_s M P(N_f + L + \frac{L^2}{N_f}) = 3^2 \cdot 10 \cdot 4 \cdot 6 \cdot (10 + 4 + 4^2/10) = 33696$ operations for 10 bits.

5.5.2 The accuracy of the data model

In Section 5.2.2, we have shown two data models: one where all cross-terms due to non-matching delays were ignored (equation (5.6)), and one where cross-terms over a distance D were incorporated (equation (5.7)). In chapter 4, we have analytical and simulated results to show that the unmatched terms are very small compared to matched terms at a certain correlation length $\tau > \tau_0$. In this section, we will indirectly check whether that approximation is sufficient by comparing the BER performance for the zero-forcing receiver when the channel coefficients are completely known under two cases: ignoring the unmatched terms ($\hat{\mathbf{s}} = \mathbf{H}^\dagger \mathbf{x}$), and taking the unmatched terms into account ($\hat{\mathbf{s}} = \mathbf{H}^\dagger(\mathbf{x} - \mathbf{B1})$).

Fig. 5.8 compares the BER vs. SNR plots for the IEEE channel model CM2. It can be seen that although the improved data model has better performance, the gap is negligible. Meanwhile, the approximate data model has fewer unknowns, and thus results in a less complex receiver algorithm. Therefore, we can conclude that it is

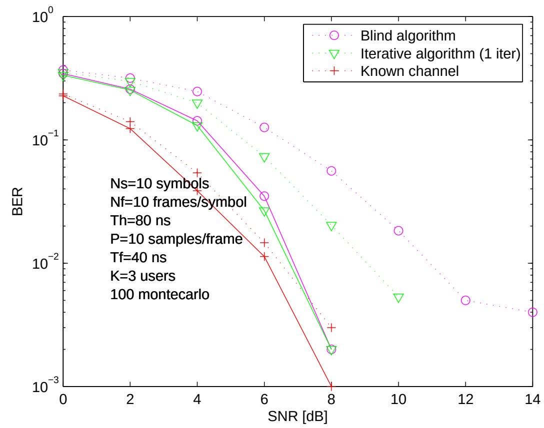

(*a*)

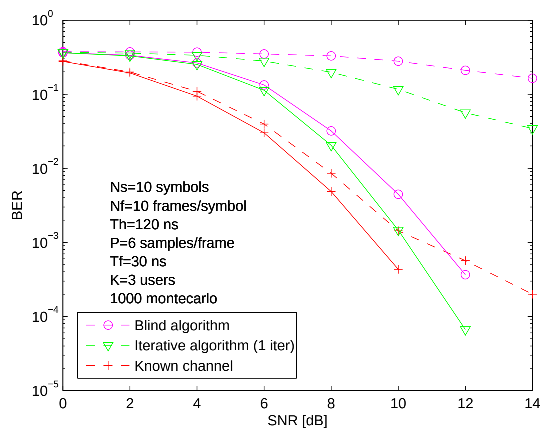

(*b*)

Figure 5.9: *BER vs. SNR performance comparison between single delay (dashed lines) and multi-delay (solid lines) schemes for* (*a*) *CM1, and* (*b*) *CM2.*

sufficient to use the approximate data model.

5.5.3 Single delay vs. multiple delays

Fig. 5.9 shows the BER performance gain of the multiple delay scheme (with $M = 4$ different delays in total) compared to the single delay scheme for the IEEE channel models: CM1 and CM2. The solid lines denote the multiple delay case, the dashed lines denote the single delay case. For CM1, the gain can be 2 dB (for the blind algorithm used for initialization) or 4 dB (for the iterative algorithm) at BER $= 10^{-2}$.

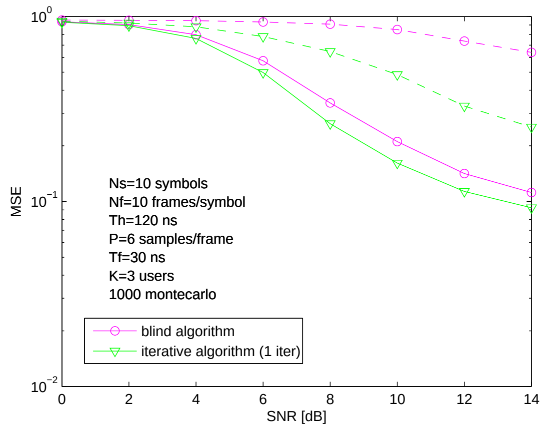

Figure 5.10: *MSE vs. SNR performance comparison between single delay (dashed lines) and multi-delay (solid lines) schemes for CM2*

The gaps widen as SNR increases. In the CM2 case, the performance difference is even more visible. The same conclusion can be drawn from the MSE vs. SNR curves in Fig. 5.10.

The reason is, similar to multiple antenna communication systems, that by using M correlation banks at the receiver, we can gather more information to help detect the data symbols and estimate the channel coefficients. More specifically, the code matrix $\mathcal{C}$ and the matrices $\mathcal{CH}$, $\mathcal{CS}$ are M times taller, which will improve the algorithms' performance and eliminate the BER flooring effect in the high SNR region.

By having $M = 4$ delays, the curves of the blind algorithm can be quite close to the reference curve (ZF receiver with known channel), the difference is only less than 1 dB. The iterative algorithm does not improve much in this case. It will show more improvement under more extreme situations, e.g., when the code matrix $\mathcal{C}$ is wide or barely tall.

It can also be seen that the performance degrades from LOS-CM1 to NLOS-CM2 channel. This is because we keep the same system parameters for both cases (actually the CM2 case has even shorter frame period and lower sampling rate), while the CM2 channel has much longer delay spread, which causes more severe IFI and IPI effects.

From simulation results in Fig. 5.9(a) and Fig. 5.9(b), the iterative algorithm is only slightly better than the blind algorithm when multiple delays are used. In this specific case, the performance of the blind algorithm is already quite close to the "reference" curve (the gap is less than 1 dB for LOS and 2 dB for NLOS). However, in

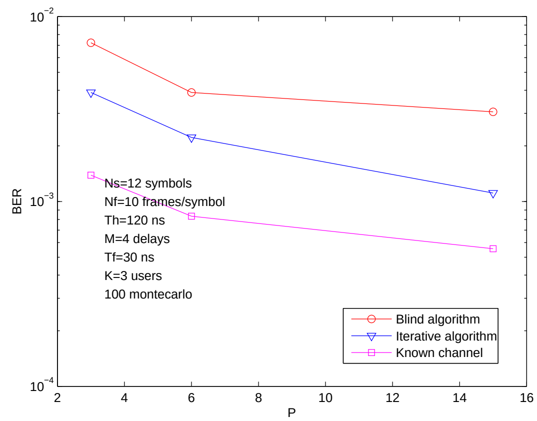

Figure 5.11: *BER vs. P plots for CM2, SNR=20dB*

a more challenging situation where the code matrix **C** is barely tall, the improvement will be more visible (as seen in the NLOS case compared to LOS case).

Note that in Fig. 5.9, the curve for known channel (single delay) has a knee at 10 dB. The reason is that even when the channel is known, we only the compute the matched terms i.e. entries of vector **h** and ignore the unmatched terms. For longer channels, i.e. NLOS case as in Fig. 5.9(b), it might happen for some random channel realizations that the unmatched terms causes some model error, which is more visible in high SNR region. However, as multiple delays are used, this effect reduces because the matched terms add together while the unmatched terms cancel among themselves. This effect is shown in the better reference curve for multiple delays.

5.5.4 BER vs. oversampling P

Fig. 5.11 illustrates how the BER performance changes with respect to the oversampling rate $P = 3, 6, 15$ samples per frame at a given SNR value (10 dB). It can be seen that the performance improves as P increases. This is because of the presence of IFI and multiuser interference (MUI) in the system. The more samples per frame, the better we can resolve IFI and MUI. Moreover, it is known that integration over long frame intervals accumulates the noise power in the tail areas of the channel. Therefore, by dividing a frame into more sub-intervals (larger P), we can indirectly deal with the noise problem better by processing the individual sub-intervals in parallel.

Fig. 5.11 shows that the BER performance does not increase linearly with P, and there is little gain when $P > 6$, while the frame period is kept fixed at $T_f = 30$ns. Because P is directly related to the integration period: $T_{sam} = T_f/P$, the higher the oversampling rate P, the shorter the integration period T_{sam}. As discussed in chapter 4 and illustrated in Fig. 4.7(a),4.7(b), the model error will increase if we reduce the integration length T_{sam} (or increase P) but at the same time, we gain some IFI/ISI resolving ability (because of getting more samples per frame). These effects combined explain the curve in Fig. 5.11.

5.6 Transceiver design issues

To conclude the chapter, we will take into account some of the implications in this chapter for the design of a practical TR-UWB system. What are the constraints on the system parameter values?

A first constraint is posed by the receiver bandwidth, which is limited by spectral masks or antenna design constraints. E.g., the antenna response shown in Fig. 5.7 has a bandwidth of about 5 GHz. The finite bandwidth determines the correlation distance τ_0, as discussed in section 4.4.2. In the receiver algorithm design, we ignored all correlations beyond τ_0. For the preceding antenna response, we found that we can safely choose $\tau_0 = 1$ ns. Therefore, according to the conclusions in section 4.4.2, the most closely spaced set of possible delays is $\{D_1, \cdots, D_M\} = \{1, 2, 3, \cdots\}$ ns.

The number of delays M is often constrained by practical considerations: the analog delay lines do take physical space in the receiver, and the receiver algorithm's complexity increases linearly with M. Therefore, we can often afford only a limited number of delays, say, $M \leq 5$.

Two constraints restrict the choice of the frame size T_f. Firstly, the last pulse of a frame must not overlap with the first pulse of the next frame, even after a maximal delay D_M. Therefore,

$$T_f > 2M\tau_0 \,.$$

Secondly, for the blind initialization algorithm described in section 5.4.2 to work, the code matrix $\mathcal{C}$ must be invertible, hence tall, which implies the condition: $M((N_s N_f - 1)T_f + T_h)/T_{sam} > KT_h N_s/T_{sam}$. This can be approximately reduced to:

$$MN_f T_f > KT_h \,.$$

This expression defines a trade-off between the coding gain (or the symbol period $T_s = N_f T_f$) and the number of users K given the number of delays M and the channel length T_h.

If our aim is to have as high-rate system as possible, then we would set $K = 1$ user, and $N_f = 1$ chips/symbol. The two preceding inequalities give

$$\frac{T_h}{T_f} < M < \frac{1}{2}\frac{T_f}{\tau_0}$$

which leads to

$$T_f > \sqrt{2T_h\tau_0}\,.$$

This provides a limit on the data rate. For example, if $T_h = 80$ ns and $\tau_0 = 1$ ns, then $T_f > 13$ ns. To have an integer M, we choose T_f a bit larger, e.g., $T_f = 15$ ns corresponding to a data rate of about 66 Mbps. It follows that $M \in \{6, 7\}$.

To illustrate the role of the antenna, we consider the case when it has a lower bandwidth e.g. 1 GHz with the same center frequency. τ_0 will increase, e.g. to 4 ns, which reduces the maximum data rate from 66 Mbps to about 38.5 Mbps with $M = 3$, for a channel length $T_h = 80$ ns. Approximately, the rate change is about the square root of the antenna bandwidth change.

We can further increase the maximum data rate by improving the constraint on the receiver algorithm. The constraint is based on the inversion of $\mathcal{C}$ in the blind algorithm while the constraint is much more relax on the iterative algorithm ($\mathcal{CH}$ and $\mathcal{CS}$ are much taller than $\mathcal{C}$), if the initial estimate is not important (e.g. replaced by training).

The oversampling rate P can be chosen based on the trade-off between the BER performance (shown in simulations) and the receiver's complexity (shown in section 5.4.4). Computationally, oversampling (P) and multiple delays (M) play almost equivalent roles. Both give rise to a multi-branch model. The difference is in the complexity of the analog hardware: oversampling requires faster samplers, whereas multiple delays require more circuitry that runs in parallel. Increasing the code length (N_f) does not cost additional hardware but lowers the data rate and improves the BER performance as usual.

5.7 Conclusions

In this chapter, by oversampling (with multiple samples per frame), we established a signal processing data model that includes all the interference terms, i.e. interpulse interference (IPI), interframe interference (IFI), intersymbol interference (ISI) and multiuser interference (MUI). The decorrelating multiuser receiver, followed by an iterative algorithm, can effectively resolve all these interferences without much increase in complexity, which results in a higher data rate compared to other TR-UWB systems. The performance can be further improved by employing multiple reference delays, which simulates multiple antenna systems. The use of oversampling and the structure of the data model imply that the proposed scheme is robust against timing error (up to a sampling period T_{sam}), while a synchronization algorithm (to estimate the unknown offset which is an integer number of T_{sam}) for a similar model was already developed [23]. The problems of imperfect antenna and pulse distortion, and how they affect the system parameters are also addressed. Finally, by allowing to change the oversampling rate P according to the trade-off between performance and complexity, this scheme can be considered as a feasible and flexible bridge between the RAKE scheme (which samples at Nyquist rate) and the “traditional” TR-UWB scheme (which samples at frame / symbol rate).

Published as: Q.H. Dang and A-J van der Veen – *"A Low-Complexity Blind Multiuser Receiver for Long-Code WCDMA,"* EURASIP Journal on Wireless Communications and Networking, vol. 2004, no. 1, pp. 113–122, August 2004.

Chapter 6

Signal processing model and receiver algorithms for WCDMA

If you have built castles in the air, your work need not be lost; that is where they should be. Now put the foundations under them.

Henry David Thoreau

Since first introduced as an advanced multiple access technology for mobile communications almost two decades ago, Code Division Multiple Access (CDMA) has become a typical example of how signal processing can be successfully applied in communications. New research results on CMDA technology are still continuously published these days, and CDMA in turn keeps inspiring and influencing the way signal processing is implemented in many new wireless communication systems including UWB radio.

In this chapter, we study in detail the underlying concepts of the signal processing models and receiver algorithms presented in earlier (UWB) chapters in the context of a novel multiuser long-code WCDMA system.

It will be shown that, by exploiting the linear relations between different model parameters (users' codes, channel coefficients, users' symbols, etc. in this CDMA case), the data model can be established in various forms: different matrices' structures and parameters, different multiplication orders. The detection and estimation task is reduced to a clear and compact mathematic equation (in matrix form) to be solved. As a result, the extensions to the multiple user and multiple antenna cases are quite straightforward.

Depending on the specific tasks and situations, the most suitable forms can be used to derive effective receiver algorithms. More specifically, instead of employing more complex techniques based on second-order moment matching, a simple blind decorrelating algorithm based on the simple rank-one singular value decomposition (SVD) can be derived by building the data model in a appropriate (matrix) form where the known code matrix is separated from the unknown parameters. The way of deriving the signal processing data model by some matrix manipulations like this has been used extensively in all the data models developed for UWB radio in the thesis.

The Alternating Least Square (ALS) algorithm, which has been implemented repeatedly in the previous chapters about UWB radio, is now studied in more details in a similar CDMA system. Its performance is evaluated under different initializations, and its *quick convergence rate (by only a few iterations) is shown by simulation. Moreover, the algorithms' complexities can be significantly reduced by exploiting the sparse structures of all the matrices in our signal processing data model.*

6.1 Introduction

Long-code (or aperiodic code) DS-CDMA systems are currently being used in the IS-95 mobile communication network standard and have been adopted in several third-generation standards such as UMTS. Originally, the receivers proposed for such systems were based on the RAKE structure, i.e. banks of matched filters which correlate the received data with the desired user's code, followed by a combining of the outputs (RAKE fingers). Since multi-user interference is not completely canceled, the performance is degraded, especially when the network is heavily loaded and power control imperfect. It is therefore interesting to look at multi-user receivers.

Channel estimation and multiuser detection for long code wideband CDMA has not seen the same levels of attention as its short-code equivalent, yet has been considered by a number of authors and is receiving renewed interest. A first classification of the available literature can be made according to the assumptions posed on the scenario:

- Narrowband versus wideband propagation channels—here we consider wideband channels, for which equalization is needed.
- Uplink versus downlink scenarios—we will consider only the uplink. The downlink case is different because users are perfectly synchronized, orthogonal and with the same propagation channel, and only a single user needs to be decoded.
- Synchronous and asynchronous transmissions—we consider the asynchronous case.
- Training-based channel estimation algorithms versus blind algorithms—we consider the blind case.

The complexity of the problem greatly depends on these assumptions. E.g., in the case of synchronous transmissions and delay spreads of at most a few chips, the receiver can drop the samples that have intersymbol interference (ISI) [71,51,49,84]. This decouples the problem and allows symbol-by-symbol processing.

For asynchronous systems, Buzzi and Poor [10, 11] consider non-blind channel estimation using training symbols for all users; they also consider sequential interference cancelation (SIC) techniques with a complexity quadratic in the code length/processing gain (the algorithm proposed in this paper has linear complexity). With known or iteratively estimated symbols, the channel estimation step in [10] and also [8, 68] is comparable to our scheme. In these papers, a large matrix inversion with a complexity cubic in the number of users and processing gain is avoided by iterative techniques (gradient descent), leading to a quadratic complexity.

Blind techniques based on second order moment matching (i.e., stochastic techniques) have appeared in [85, 48, 27, 61, 79, 26, 76]. These rely on the convergence of time averages, which often requires hundreds of symbols. Other approaches are based on iterative optimization of a likelihood function [46,82], which tends to have a very high complexity. Several other approaches are valid only for the downlink, e.g. [71], see also [77] which contains an extensive reference list.

The algorithms in this paper continue on the blind multi-user joint symbol-channel estimation techniques in [65, 67] and can be called *deterministic*, since no statistical model of the sources is assumed. In these papers, Tong, Van der Veen et al. considered an uplink receiver algorithm (DRR) where the base station knows all codes. By constructing and inverting a code matrix, a blind decorrelating RAKE and MMSE receiver was derived to estimate the channel and desired user symbols, based on all samples in a frame. After the decorrelating step, the users are treated independently, which is computationally advantageous but gives suboptimal performance when compared to an informed multi-user MMSE receiver. This is because of two reasons. Firstly, due to the code inversion, the noise becomes correlated among symbols and users. This reduces the performance of the subsequent single-user estimation and detection step. A second and more important reason is that code inversion followed by channel inversion is suboptimal, and gives more noise enhancement than the inversion of the product of the code and channel matrices. In this paper, we take these effects into account.

We propose to use the single-user channel estimates from the DRR as an initial point for an iterative symbol/channel estimation algorithm which also considers the noise correlations. This can be done on a per-user basis, or, with better performance, jointly in a multi-user fashion. In heavily loaded systems, this algorithm shows a significant improvement over the current decorrelating RAKE receiver and the conventional RAKE receiver.

The proposed multi-user algorithm is by itself not a very surprising result: similar iterative receivers are known for short-code (periodic code) CDMA systems, e.g., the PIC (parallel interference cancelation) receivers, and for long-code CDMA an iterative blind receiver that appears to be related to ours was proposed in [68]. Such receivers usually act on symbol-by-symbol data, whereas the proposed algorithm

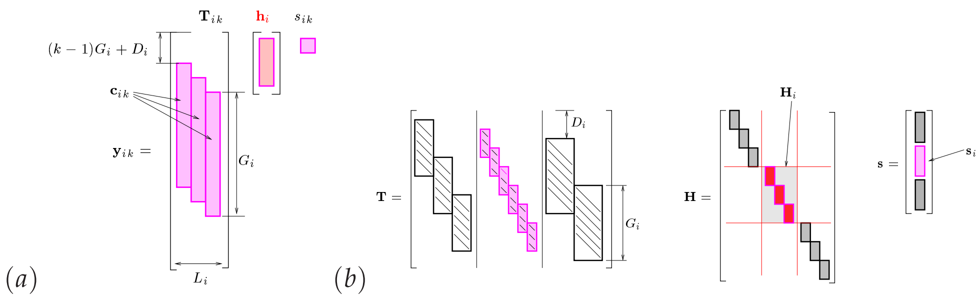

Figure 6.1: (a) *Effect of a single transmitted symbol on the received data vector* $\mathbf{y}$*,* (b) *structure of the code matrix* $\mathbf{T}$*, channel matrix* $\mathbf{H}$*, symbol vector* $\mathbf{s}$.

acts on a slot of data (M symbols). What is new here is the observation that the blind DRR (or the related blind RAKE) receiver provides a very good initial point for the iteration, and the observation that an efficient implementation for the algorithm is possible. A direct implementation has a complexity that grows with M^3, and would soon be prohibitive. However, the matrices to be inverted are sparse and structured (they are related to a band matrix after permutations). As in [67], we consider the use of time-varying state space theory developed by Dewilde and Van der Veen [20] to implement matrix multiplications, QR factorizations, and matrix inversions.[1] We will demonstrate that the resulting complexity of the iteration is similar to that of the DRR, i.e., linear in the number of transmitted symbols M and linear in the code length (coding gain) G. For large M, the complexity is of order GK per estimated symbol per user, where K is the number of users. The conventional RAKE receiver has complexity GL per estimated symbol per user, where L is the channel length in chips. Hence, the proposed algorithm is not much more complex, and certainly feasible.[2]

The outline of the chapter is as follows. Section 6.2 gives the data model and describes the blind receiver algorithm from [67]. Section 6.3 derives the proposed algorithms, in both multi-user and single-user fashion. Section 6.4 derives the complexity of the algorithms, and section 6.5 shows the performance by simulations. Finally, section 6.6 gives the conclusions.

[1] This theory for time-varying systems should be regarded as a computational framework applicable to *any* matrix, potentially even of infinite size, and not be confused with the modeling of long-code CDMA systems as a time-varying system as is sometimes done in the literature. There are connections, e.g., between these matrix inversion techniques and Kalman filtering.

[2] To put these numbers in perspective, note that for the WCDMA system applied in UMTS, a slot has size $MG = 2560$ chips, the variable spreading gain is $G = 4, \cdots, 256$ chips and hence $M = 640, \cdots, 10$ symbols. The channel length is $L = 4$ to 8 chips (suburban) up to 80 chips (hilly terrain) [38].

6.2 Problem statement and preliminary results

6.2.1 Data model

We consider the same data model as in in [67]. The context is the uplink of a slotted system with K asynchronous users. In a slot, the i-th user transmits a vector $\mathbf{s}_i$ consisting of M_i symbols s_{ik}. Each symbol s_{ik} is spread by an aperiodic code (vector) $\mathbf{c}_{ik}$ of length G_i. After multipath propagation over a channel with length L_i chips and relative delay D_i (asynchronism), pulse-shaped matched filtering and chip-rate sampling, the receiver stacks the received samples in a slot in a vector $\mathbf{y}$. The contribution of s_{ik} to $\mathbf{y}$ is a linear combination of the transmitted signal $\mathbf{c}_{ik}s_{ik}$, plus delays of it, properly scaled by the L_i channel coefficients collected in a vector $\mathbf{h}_i$, or

$$\mathbf{y}_{ik} = \mathbf{T}_{ik}\mathbf{h}_i s_{ik}\,, \quad k = 1, \cdots, M_i\,,$$

which is illustrated in figure 6.1(a). $\mathbf{T}_{ik}$ is a Toeplitz matrix whose L_i columns consist of shifts of the code vector $\mathbf{c}_{ik}$. Including all K users and the noise, we have

$$\begin{aligned} \mathbf{y} &= \mathbf{THs} + \mathbf{w} \qquad (6.1)\\ \mathbf{T} &:= [\mathbf{T}_1, \cdots, \mathbf{T}_K] \\ \mathbf{H} &:= \operatorname{diag}(\mathbf{I}_{M_1} \otimes \mathbf{h}_1, \cdots, \mathbf{I}_{M_K} \otimes \mathbf{h}_K)\,, \end{aligned}$$

where the i-th user's code matrix is $\mathbf{T}_i := [\mathbf{T}_{i1}, \cdots, \mathbf{T}_{i,M_i}]$, the channel matrix $\mathbf{H}$ is block diagonal with $\mathbf{I} \otimes \mathbf{h}_i$ as the i-th block, vector $\mathbf{s}$ is a stacking of all symbol vectors of all users, as illustrated in figure 6.1(b). $\mathbf{w}$ is a vector representing the additive Gaussian noise.

$\mathbf{T}$ has size $\max(M_iG_i + D_i + L_i - 1) \times \sum_1^K(M_iL_i)$, and $\mathbf{H}$ has size $\sum_1^K(M_iL_i) \times \sum_1^K(M_i)$. For convenience, we will usually consider the case of users with equal parameters, but the general case is certainly not ruled out.

In the derivations of the algorithms, we will make the following assumptions:

(A1) The code matrix $\mathbf{T}$ is known. This implies that the receiver knows the codes, the user delay offsets D_i, and the number of paths L_i of all users.

(A2) $\mathbf{TH}$ is tall and full column rank, which (for users with equal parameters) implies $K < G$, i.e., the number of users is less than the processing gain. We will also require another matrix to be tall ($\mathbf{TS}$ in (6.8)), which will imply $KL < MG$.

For initialization using the DRR, we need to require moreover that $\mathbf{T}$ is tall and full column rank, which implies $KL < G$ (for users with equal parameters).

(A3) The noise $\mathbf{w}$ is white Gaussian, with unknown variance σ^2.

The problem we consider is, given the code matrix $\mathbf{T}$ and the received data vector $\mathbf{y}$, to find good estimates of all users' source symbols $\mathbf{s}$ and all channel coefficients $\mathbf{h}$, where

$$\mathbf{h} = [\mathbf{h}_1^H, \cdots, \mathbf{h}_K^H]^H$$

is the stacking of all users' channels $\mathbf{h}_i$.

6.2.2 Decorrelating RAKE Receiver algorithm (DRR)

As introduced in [67], the Decorrelating RAKE Receiver (DRR) algorithm first applies a decorrelating matched filter, or $\mathbf{T}^\dagger = (\mathbf{T}^H\mathbf{T})^{-1}\mathbf{T}^H$, to the vector of received data $\mathbf{y}$. This removes all multi-user interference. The output of the decorrelating matched filter is given by

$$\mathbf{u} = \mathbf{T}^\dagger\mathbf{y} = \mathbf{H}\mathbf{s} + \mathbf{n}\,, \tag{6.2}$$

where $\mathbf{n} = \mathbf{T}^\dagger\mathbf{w}$ is a colored noise vector. The new noise covariance matrix is

$$\mathbf{R}_n := \mathrm{E}\,(\mathbf{n}\mathbf{n}^H) = \sigma^2(\mathbf{T}^H\mathbf{T})^{-1}\,. \tag{6.3}$$

Since $\mathbf{H}$ is block diagonal, the filter output can be separated into individual user contributions. Split $\mathbf{u}$ into K segments $\mathbf{u}_i$, one for each user, then

$$\mathbf{u}_i = (\mathbf{I} \otimes \mathbf{h}_i)\mathbf{s}_i + \mathbf{n}_i, \quad i = 1, \cdots, K\,. \tag{6.4}$$

By unstacking the vector $\mathbf{u}_i$ into a matrix $\mathbf{U}_i$, we obtain the model

$$\mathbf{U}_i = \mathbf{h}_i\mathbf{s}_i^T + \mathbf{N}_i, \quad i = 1, \cdots, K\,. \tag{6.5}$$

The channel estimation proceeds by taking a rank-1 decomposition of $\mathbf{U}_i$, via a singular value decomposition. The dominant left singular vector is an estimate of $\mathbf{h}_i$, and the corresponding right singular vector determines the symbols $\mathbf{s}_i$ up to an unknown scaling. Since the noise $\mathbf{N}_i$ is not white, a prewhitening can improve the decomposition [67]; unfortunately, it is not possible to prewhiten each column of $\mathbf{U}_i$ separately because it would destroy the rank-1 property.

A blind RAKE receiver is obtained in a similar way, but by setting $\mathbf{u} = \mathbf{T}^H\mathbf{y}$ in equation (6.2).

With an initial channel estimate $\mathbf{h}^{(0)}$ obtained in this way, it was also briefly mentioned in [67] that further refinements can be obtained in a two-step iterative fashion, i.e., an Alternating Least Squares algorithm similarly to the ILSP algorithm [63]. Based on (6.5),

1. Given $\mathbf{h}_i^{(k-1)}$, solve

$$\begin{aligned}\mathbf{s}_i^{(k)} &= \arg\min_{\mathbf{s}_i} \|\mathbf{U}_i - \mathbf{h}_i^{(k-1)}\mathbf{s}_i^T\|^2 \\ &= \frac{1}{\|\mathbf{h}_i^{(k-1)}\|^2} \cdot (\mathbf{h}_i^{(k-1)H}\mathbf{U}_i)^T .\end{aligned}$$

   Subsequently round the entries of $\mathbf{s}_i^{(k)}$ to the nearest elements of the alphabet.

2. Keeping $\mathbf{s}_i^{(k)}$ fixed, solve

$$\begin{aligned}\mathbf{h}_i^{(k)} &= \arg\min_{\mathbf{h}_i} \|\mathbf{U}_i - \mathbf{h}_i^{(k-1)}\mathbf{s}_i^T\|^2 \\ &= \frac{1}{\|\mathbf{s}_i^{(k)}\|^2} \cdot \mathbf{U}_i\mathbf{s}_i^{(k)} .\end{aligned}$$

Although this algorithm was proposed in [67], its performance was not shown.

6.2.3 Discussion

To simplify the initial estimation of the channel, the preceding derivation from [67] ignored most of the information on the noise covariance matrix $\mathbf{R}_n$, namely the noise correlations among the users, and the symbol-by-symbol temporal correlations. Also the iterative refinement did not take any noise correlation properties into account. Our aim will be to improve the estimation by taking the complete noise model into account. As it turns out, the elegant rank-1 channel estimation property is hard to generalize. However, using the DRR or the blind RAKE to obtain an initial channel estimate, we can improve the estimates by straightforward multi-user two-step iterations, discussed in the next section.

6.3 Joint source-channel estimation

Our derivations will use the following lemma.

1. LEMMA. *Let* $\mathbf{h}$ *and* $\mathbf{s}$ *be vectors of length L and M, respectively. Then* $(\mathbf{I}_M \otimes \mathbf{h})\mathbf{s} = (\mathbf{s} \otimes \mathbf{I}_L)\mathbf{h}$.

*Proof:*Using the multiplicative property of Kronecker products, $(\mathbf{A} \otimes \mathbf{B})(\mathbf{C} \otimes \mathbf{D}) = (\mathbf{AC} \otimes \mathbf{BD})$, we immediately obtain

$$\begin{aligned}(\mathbf{I}_M \otimes \mathbf{h})\mathbf{s} \;&=\; (\mathbf{I}_M \otimes \mathbf{h})(\mathbf{s} \otimes 1) \;=\; \mathbf{s} \otimes \mathbf{h} \\ &=\; (\mathbf{s} \otimes \mathbf{I}_L)(1 \otimes \mathbf{h}) \;=\; (\mathbf{s} \otimes \mathbf{I}_L)\mathbf{h} .\end{aligned}$$

□

6.3.1 Single-user estimation with noise whitening

Consider the single-user model (6.4). The covariance of the noise $\mathbf{n}_i$ is denoted by $(\mathbf{R}_n)_i$, and is known: it is a submatrix of $\mathbf{R}_n = \sigma^2(\mathbf{T}^H\mathbf{T})^{-1}$. We first whiten the noise,

$$\tilde{\mathbf{u}}_i := (\mathbf{R}_n)_i^{-1/2}\mathbf{u}_i = (\mathbf{R}_n)_i^{-1/2}(\mathbf{I}\otimes\mathbf{h}_i)\mathbf{s}_i + \tilde{\mathbf{n}}_i\,,$$

where $\tilde{\mathbf{n}}_i$ is white noise. Using the lemma, we can now introduce a similar Alternating LS algorithm to estimate $\mathbf{s}_i$ and $\mathbf{h}_i$ in turns, for each user i separately:

1. Given $\mathbf{h}_i^{(k-1)}$, solve

$$\begin{aligned}\mathbf{s}_i^{(k)} &= \arg\min_{\mathbf{s}_i} \|\tilde{\mathbf{u}}_i - (\mathbf{R}_n)_i^{-1/2}(\mathbf{I}\otimes\mathbf{h}_i^{(k-1)})\mathbf{s}_i\|^2 \\ &= \big((\mathbf{R}_n)_i^{-1/2}(\mathbf{I}\otimes\mathbf{h}_i^{(k-1)})\big)^{\dagger}\tilde{\mathbf{u}}_i\,.\end{aligned}$$

   Subsequently, round the entries of $\mathbf{s}_i^{(k)}$ to the nearest elements of the alphabet.

2. Keeping $\mathbf{s}_i^{(k)}$ fixed, solve

$$\begin{aligned}\mathbf{h}_i^{(k)} &= \arg\min_{\mathbf{h}_i} \|\tilde{\mathbf{u}}_i - (\mathbf{R}_n)_i^{-1/2}(\mathbf{s}_i^{(k)}\otimes\mathbf{I})\mathbf{h}_i\|^2 \\ &= \big((\mathbf{R}_n)_i^{-1/2}(\mathbf{s}_i^{(k)}\otimes\mathbf{I})\big)^{\dagger}\tilde{\mathbf{u}}_i\,.\end{aligned}$$

In comparison to the original single-user iterative algorithm, the performance is expected to be better, since the noise correlations of the data vector are taken into account. On the other hand, correlations among users are still ignored. Also, the noise enhancement due to the preprocessing with $\mathbf{T}^{\dagger}$ is not avoided.

6.3.2 Iterative multi-user estimation

Compared to the single-user estimation algorithms, it is known that joint detection algorithms can achieve significant performance gains, at the expense of increased complexity. We will derive such an algorithm in this section, then verify its complexity in the next section.

Consider the original data model in (6.1). We can formulate the channel/data estimation problem as a typical Least Squares problem: find $\mathbf{h}$ and $\mathbf{s}$ to minimize $\|\mathbf{y}-\mathbf{THs}\|^2$, where $\mathbf{H} = \mathrm{diag}(\mathbf{I}\otimes\mathbf{h}_1,\cdots,\mathbf{I}\otimes\mathbf{h}_K)$. In the presence of white Gaussian noise, this LS cost function is also optimal in a maximum likelihood sense.

Before we show the iteration, we use the lemma to rewrite the cost function also as a function of $\mathbf{h}$, i.e., $\|\mathbf{y}-\mathbf{TSh}\|^2$, where

$$\mathbf{S} = \mathrm{diag}(\mathbf{s}_1\otimes\mathbf{I}_{L_1},\cdots,\mathbf{s}_K\otimes\mathbf{I}_{L_K})\,. \tag{6.6}$$

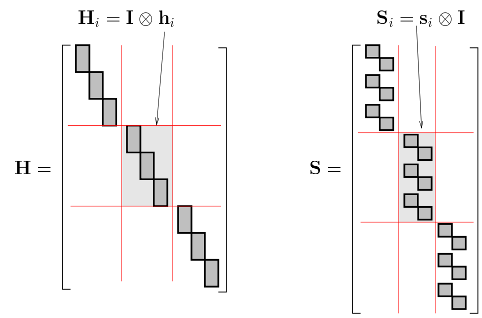

Figure 6.2: *Structure of* (a) *matrix* $\mathbf{H}$ *and* (b) *matrix* $\mathbf{S}$

The structure of $\mathbf{S}$ is shown in figure 6.2(b).

With a good initial channel estimate, $\mathbf{h}^{(0)}$ say, we can use the following iteration to improve the estimate. For iteration index $k = 1, 2, \cdots$ until convergence, do

1. Keeping the channel $\mathbf{h}^{(k-1)}$ fixed, solve

$$\begin{aligned} \mathbf{s}^{(k)} &= \arg\min_{\mathbf{s}} \|\mathbf{y} - \mathbf{T}\mathbf{H}^{(k-1)}\mathbf{s}\|^2 \\ &= (\mathbf{T}\mathbf{H}^{(k-1)})^{\dagger}\mathbf{y} \\ &= (\mathbf{H}^{(k-1)^H}\mathbf{T}^H\mathbf{T}\mathbf{H}^{(k-1)})^{-1}\mathbf{H}^{(k-1)^H}\mathbf{T}^H\mathbf{y}\,, \end{aligned} \tag{6.7}$$

   Subsequently, round the entries of $\mathbf{s}_i^{(k)}$ to the nearest elements of the alphabet.

2. Keeping the source symbols $\mathbf{s}^{(k)}$ fixed, solve

$$\begin{aligned} \mathbf{h}^{(k)} &= \arg\min_{\mathbf{h}} \|\mathbf{y} - \mathbf{T}\mathbf{S}^{(k)}\mathbf{h}\|^2 \\ &= (\mathbf{T}\mathbf{S}^{(k)})^{\dagger}\mathbf{y} \\ &= (\mathbf{S}^{(k)^H}\mathbf{T}^H\mathbf{T}\mathbf{S}^{(k)})^{-1}\mathbf{S}^{(k)^H}\mathbf{T}^H\mathbf{y}\,. \end{aligned} \tag{6.8}$$

After the iterations, step 1 is repeated once more to get the final estimate of the source symbols. Assuming the decisions are correct, the algorithm will approach the multi-user Linear MMSE solution with the channel estimated from completely known symbols.

Although written differently, the second estimation step is similar to other batch training-based techniques proposed for long-code CDMA, cf. [10, 68].

As an alternating projection algorithm, it is known that it will converge monotonically to a local optimum. Generally, the algorithm only completely converges after a number of iterations. However, with an initial estimate of the channel provided by the DRR or the blind RAKE discussed in section 6.2.2, the algorithm rapidly converges with only 1 iteration. Because in this formulation the noise is not colored, the final estimates can be much better than that of the initial single-user algorithms that have to work with incomplete noise models.

Apart from this, a second reason why this algorithm is expected to have better performance is that it uses inverses $(\mathbf{TH})^\dagger$ and $(\mathbf{TS})^\dagger$ of taller matrices, whereas the previous algorithm implicitly worked with $\mathbf{H}^\dagger\mathbf{T}^\dagger$ for computing the symbol estimates. While $\mathbf{H}^\dagger\mathbf{T}^\dagger$ is a valid left inverse of $\mathbf{TH}$, it is not the minimum-norm left inverse, hence it can give unnecessary noise enhancement.

Another advantage is that the algorithm's performance can still be stable even when $\mathbf{T}$ is not tall, i.e. in heavily loaded cases. In that case, the algorithm needs to be initialized by the blind RAKE channel estimation algorithm (i.e., use $\mathbf{T}^H$ rather than $\mathbf{T}^\dagger$ in equation (6.2)).

6.3.3 Multiple receive antennas

In the near future, many base stations will be equipped with multiple antennas. We indicate how the two-step iteration have to be modified to take this into account. The multi-antenna version for DRR was shown in [67].

Consider a case where d receive antennas are used. No structure is imposed on this antenna array. Let $\mathbf{y}_j$, $\mathbf{H}_j$ and $\mathbf{w}_j$ be the received vector, channel matrix and noise vector for the j-th antenna, respectively. Applying the identity $\mathbf{TH}_j\mathbf{s} = \mathbf{TSh}_j$, we have the two versions of the data model

$$\begin{aligned}
\begin{bmatrix} \mathbf{y}_1 \\ \mathbf{y}_2 \\ \vdots \\ \mathbf{y}_d \end{bmatrix} &= \begin{bmatrix} \mathbf{TH}_1 \\ \mathbf{TH}_2 \\ \vdots \\ \mathbf{TH}_d \end{bmatrix} \mathbf{s} + \begin{bmatrix} \mathbf{w}_1 \\ \mathbf{w}_2 \\ \vdots \\ \mathbf{w}_d \end{bmatrix} \\
&= (\mathbf{I}_d \otimes (\mathbf{TS})) \begin{bmatrix} \mathbf{h}_1 \\ \mathbf{h}_2 \\ \vdots \\ \mathbf{h}_d \end{bmatrix} + \begin{bmatrix} \mathbf{w}_1 \\ \mathbf{w}_2 \\ \vdots \\ \mathbf{w}_d \end{bmatrix}
\end{aligned} \tag{6.9}$$

where $\mathbf{h}_j$ is the stacking of all channel vectors for the j-th antenna.

In the first step of the iterative algorithm, where source symbols are estimated from known channel vectors using (6.9), we need to apply the inverse of $[(\mathbf{TH}_1)^T(\mathbf{TH}_2)^T\cdots(\mathbf{TH}_d)^T]^T$ to the data vector. Since this matrix is d times taller than before, its conditioning is expected to be much better so that the estimation of $\mathbf{s}$ is significantly improved. In the second step, estimating the channels from known source symbols using (6.9), the matrix to be inverted, $\mathbf{I}_d \otimes (\mathbf{TS})$, has the same conditioning as the matrix $(\mathbf{TS})$ in the single-antenna case. Actually, each channel is estimated independently from the source symbols, which means that no gain is obtained in this step. However, since the symbols are estimated at higher accuracy, the overall performance improvement over the single antenna case is significant, even after only one iteration.

6.4 Computational complexity

In this section, the computational complexity of the two-step iterative algorithm is discussed. In summary, one iteration of the algorithm consists of the following steps:

1. Given the channel coefficients $\mathbf{h}$, estimate the source symbols $\mathbf{s}$ by solving $\mathbf{y} = \mathbf{THs} + \mathbf{w}$,
2. With known source symbols $\mathbf{s}$, estimate the channel coefficients $\mathbf{h}$ by solving $\mathbf{y} = \mathbf{TSh} + \mathbf{w}$.

For simplicity of the expressions, all users are assumed to have equal parameters. We compute the complexity of a direct implementation, one that exploits the sparse structure of $\mathbf{T}$ (many zero entries), and one that uses this sparse structure *and* the fact that the nonzero entries occur in bands.

6.4.1 Direct computation

$\mathbf{T}$ has size $GM \times MKL$, whereas $\mathbf{H} : MKL \times MK$ and $\mathbf{S} : MKL \times KL$. Therefore, computation of $\mathbf{T}' := \mathbf{T} \cdot \mathbf{H}$ (size $GM \times MK$) costs order $GM \cdot MKL \cdot MK = GM^3K^2L$ operations, and similarly computation of $\mathbf{T}'' := \mathbf{TS}$ (size $GM \times KL$) costs order $GM^2K^2L^2$.

The computation of $\hat{\mathbf{s}} := (\mathbf{T}')^{\dagger}\mathbf{y}$ can be implemented in two ways:

1. Via $(\mathbf{T}'^H\mathbf{T}')^{-1} \cdot \mathbf{T}'^H\mathbf{y}$. The computation of $\mathbf{T}'^H \cdot \mathbf{T}'$ costs order $GM(MK)^2$ operations, inversion of this matrix costs $(MK)^3$ operations, computation of $\mathbf{T}'^H\mathbf{y}$ costs $GM \cdot MK$ operations, application of $(\mathbf{T}'^H\mathbf{T}')^{-1}$ to this vector another $(MK)^2$. In total, order $GM^3K^2 + (MK)^3$.
2. Via QR-factorization of $\mathbf{T}' = \mathbf{QR}$, subsequently $\mathbf{v} = \mathbf{Q}^H\mathbf{y}$ and $\hat{\mathbf{s}} = \mathbf{R}^{-1}\mathbf{v}$ implemented via backsubstitution. Computation of the QR factorization costs order $GM(MK)^2$, computation of $\mathbf{v}$ costs order $GM \cdot MK$, backsubstitution costs order $(MK)^2$. In total, order GM^3K^2.

Similarly, the complexity of $\hat{\mathbf{h}} = (\mathbf{T}'')^{\dagger}\mathbf{y}$ is

1. Via $(\mathbf{T}''^H\mathbf{T}'')^{-1} \cdot \mathbf{T}''^H\mathbf{y}$: order $GM(KL)^2 + (KL)^3$,
2. Via QR-factorization of $\mathbf{T}'' = \mathbf{QR}$: order $GM(KL)^2$.

6.4.2 Computation using sparse structure of T, H, and S

In the direct computation, we did not recognize the fact that many entries of $\mathbf{T}$, $\mathbf{H}$ and $\mathbf{S}$ are zero. Each row of $\mathbf{T}$ has only KL nonzero entries, whereas $\mathbf{H}$ and $\mathbf{S}$ are block diagonal and a permutation of a block-diagonal matrix, respectively. Exploiting this, the computation of $\mathbf{T}' := \mathbf{T} \cdot \mathbf{H}$ costs order $GMKL$ operations, and also the computation of $\mathbf{T}'' := \mathbf{TS}$ costs order $GMKL$. In the latter case, we can also recognize the fact that these are integer operations (the entries of $\mathbf{T}$ and $\mathbf{S}$ are typically ± 1 or some other finite alphabet).

In the computation of $\hat{\mathbf{s}} := (\mathbf{T}')^{\dagger}\mathbf{y}$ using the sparse structure of $\mathbf{T}'$, we cannot use the technique via QR-factorization because it destroys the structure. Each row of $\mathbf{T}'$ has only K nonzero entries, each column has G nonzero entries. Via $(\mathbf{T}'^H\mathbf{T}')^{-1} \cdot \mathbf{T}'^H\mathbf{y}$, the computation of $\mathbf{T}'^H \cdot \mathbf{T}'$ costs order $G(MK)^2$ operations, inversion of this matrix still costs $(MK)^3$ operations, computation of $\mathbf{T}'^H\mathbf{y}$ costs GMK operations, and the application of $(\mathbf{T}'^H\mathbf{T}')^{-1}$ to this vector costs $(MK)^2$. In total, order $G(MK)^2 + (MK)^3$.

Unfortunately, this direct computation cannot use backsubstitution, hence the complete matrix $(\mathbf{T}'^H \cdot \mathbf{T}')^{-1}$ is formed even if it is applied only to a single vector. There are iterative techniques (e.g., conjugate gradient, cf. the channel estimation techniques reported in [10, 8]) that compute an approximation to the result, they have complexity of order $(MK)^2$. The total complexity would then be $G(MK)^2 + (MK)^2$, or of order $G(MK)^2$.

In the computation of $\hat{\mathbf{h}} = (\mathbf{T}'')^{\dagger}\mathbf{y}$, no advantage is obtained because $\mathbf{T}''$ is a full matrix. We can recognize, however, that $\mathbf{T}''$ has integer entries, hence computation of $(\mathbf{T}''^H\mathbf{T}'')^{-1}$ costs order $\alpha(KL)^2$, where α is the complexity of adding GM integer numbers. If approximate iterative techniques are used for applying the inverse, then the total complexity becomes order $(KL)^2$. This is similar to the complexity of the channel estimation step in [10] and [8].[3]

6.4.3 Computation via time-varying state space representations

A matrix-vector multiplication $\mathbf{y} = \mathbf{Tu}$ can be regarded as a time-varying system $\mathbf{T}$, which has input signal $\mathbf{u}$ and produces $\mathbf{y}$ as the output. Such a system can be

[3] Note that, in the cited papers, it was assumed that no synchronization is available and hence the channel length was taken equal to the code length. Therefore, they reported a complexity of $(KG)^2$.

Table 6.1: *Computational complexity of the two-step iterative algorithm*

Implementation:	direct	sparse **T**, **H**, **S**	state space
symbol estimation:			
$\mathbf{T}' = \mathbf{TH}$	GM^3K^2L	$GMKL$	$GMKL$
$\hat{\mathbf{s}} = (\mathbf{T}')^\dagger \mathbf{y}$	GM^3K^2	$G(MK)^2$	GMK^2
channel estimation:			
$\mathbf{T}'' = \mathbf{TS}$	$GM^2K^2L^2$	$GMKL$	$\times$ $[GMKL]$
$\hat{\mathbf{h}} = (\mathbf{T}'')^\dagger \mathbf{y}$	$GM(KL)^2$	$(KL)^2$	$\times$ $[(KL)^2]$
Total per iteration:	GM^3K^2L	$G(MK)^2$	$GMKL + GMK^2$

realized using time-varying state space equations,

$$\begin{cases} \mathbf{x}_{n+1} &= \mathbf{A}_n \mathbf{x}_n + \mathbf{B}_n \mathbf{u}_n \\ \mathbf{y}_n &= \mathbf{C}_n \mathbf{x}_n + \mathbf{D}_n \mathbf{u}_n \end{cases} \tag{6.10}$$

where $\mathbf{x}_n$ is a state-vector that carries information from one stage to the next. This representation shows in some more detail how the entries of $\mathbf{y} = \mathbf{Tu}$ are computed one-by-one. A complete theory based on this can be found in [20]. In [67], this theory was applied to the efficient inversion of the code matrix $\mathbf{T}$ in the current application. Essentially, efficient computations are possible because $\mathbf{T}$ has many zero entries *and* they occur in bands, a result of the FIR channel assumption. Therefore, the channel inversion can have a lower complexity: the QR factorization, application of $\mathbf{Q}^H$ and $\mathbf{R}^{-1}$ via backsubstitution can all be done using the state space realization.[4] It is also shown that the realization of $\mathbf{T}$ has GM stages, and in the n-th stage, $[\mathbf{C}_n,\ \mathbf{D}_n]$ are directly specified in terms of the nonzero entries of the n-th row of $\mathbf{T}$, whereas $[\mathbf{A}_n,\ \mathbf{B}_n]$ are shift matrices (similar to identity matrices).

Without repeating the derivations of [67], we mention the resulting complexities. Computation of a state space realization of $\mathbf{T}' = \mathbf{T} \cdot \mathbf{H}$ costs order $GMKL$ operations, and the result is a realization with GM stages, each with K nonzero entries. Computation of the QR-factorization of $\mathbf{T}'$ costs GMK^2 operations, applying $\mathbf{Q}^H$ or $\mathbf{R}^{-1}$ to a vector via backsubstitution costs GMK operations. In total, the complexity is of order $GMKL + GMK^2$ operations. This is a factor M less than in the preceding section, even if here the *exact* solution is computed.

In the computation of $\hat{\mathbf{h}} = (\mathbf{T}'')^\dagger \mathbf{y}$, no specific advantage of using state-space

[4] This inversion technique is closely related to Kalman filtering, e.g., both are connected to a Riccati equation. A difference is that the Kalman filter is placed in a stochastic context.

realizations is obtained because $\mathbf{T}''$ is not sparse. In this case, the complexity of the preceding section will be assumed.

6.4.4 Summary

The preceding complexities are summarized in table 6.1. For $K > L$, the dominant term in the complexity is of order GMK^2, contributed by the symbol estimation step. Per estimated symbol per user, the complexity is GK. This can be compared to the complexity of a RAKE receiver (computing $\mathbf{u} = \mathbf{T}^H\mathbf{y}$), which is $GMKL$, or GL per estimated symbol per user. This suggests that the two-step algorithm does not cost much more, hence is feasible to implement in practice. If $K < L$, the dominant complexity is $GMKL$, of the same order as for the RAKE.

To put this in further perspective, we mention the complexity of a few other proposed algorithms. The Bayesian approach in [82] has a complexity of GL^2 per symbol per user per iteration (about 50–100 iterations are needed). The Kalman filter receiver structure in [47] requires GKL^2 per symbol per user, a known channel is assumed. The reported complexity of the approach in [79] is G^2L^2 per user, for the channel estimation step only.

6.5 Simulation results

Simulations are used to compare the proposed algorithms to the blind RAKE receiver and the DRR. We simulate a long-code CDMA uplink with $K = 8$ equal-power users transmitting BPSK symbols in frames of length $M = 10$ symbols, spread by randomly generated codes with gain $G = 32$. All channels have lengths $L = 3$, have a random delay to model asynchronism, and all channel coefficients are equal power, complex normal random numbers. 100 Monte Carlo runs are used to derive the performance statistics.

Only a single iteration of the two-step algorithm is used. The well-known phase ambiguity problem in blind estimation is easily solved by using a single training pilot symbol or by differential encoding.

6.5.1 Channel estimation mean square error comparison

The channel mean square errors (MSEs) of the various algorithms are compared for varying signal-to-noise ratio (SNR). The reference curve is the linear MMSE receiver with known source symbols.

Fig. 6.3(a) shows the results. It is seen that the proposed iterative algorithms (multi-user estimation, either initialized by DRR or RAKE) have significant gains

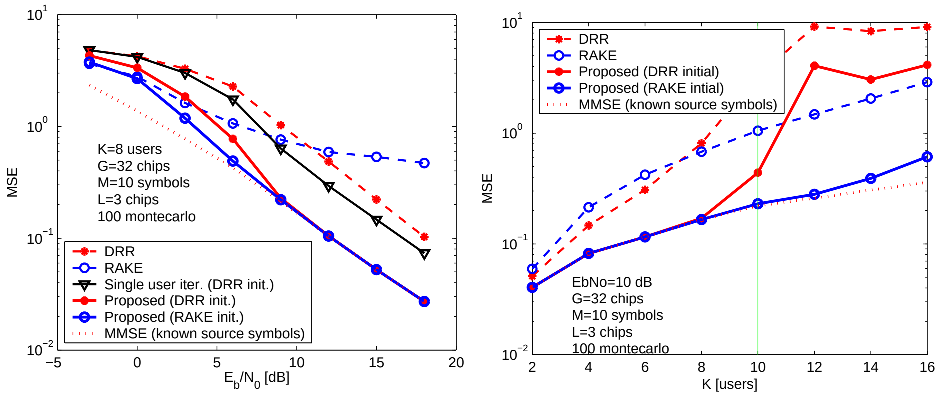

Figure 6.3: (a) *Channel estimation error (MSE) vs. SNR, and* (b) *vs. number of users (K)*

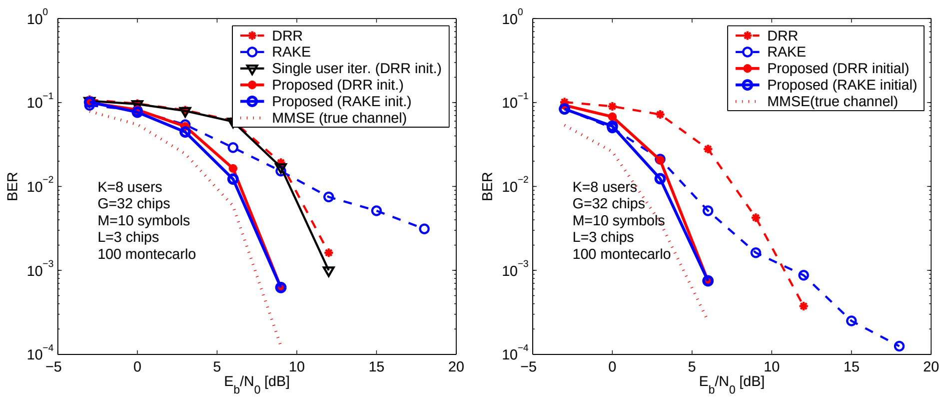

Figure 6.4: *BER vs. SNR.* (a) *single antenna;* (b) *two antennas*

over the DRR and especially over the conventional RAKE receiver. When the SNR is sufficiently high (SNR$>$ 9dB), their performance is almost the same as the ideal Linear MMSE receiver (computed from known symbols) with gain of about 7 dB over the DRR.

When the noise is strong, the proposed algorithm initialized by RAKE seems to be the better candidate than the one with DRR as the initial estimate. This is attibuted to the noise enhancement of $\mathbf{T}^{\dagger}$, since $\mathbf{T}$ is not very tall. Consequently, as the SNR increases the gap between the two curves reduces quickly to zero.

In addition, the iterative single-user estimation version of the proposed algorithm also has a good performance with gain of about 2 dB over the DRR. However, separate simulations showed that the noise whitening did not give any improvement in MSE over the unwhitened iterative DRR (its curve is not shown for clarity).

Fig. 6.3(b) shows how the algorithms' performance changes with respect to the number of users (K) while the SNR is kept fixed at a moderate level, 10 dB. When K is small, the proposed curves are nearly identical to the MMSE receiver. Since DRR requires $\mathbf{T}$ to be tall, the maximal number of users for DRR is given by $K_0 = \lfloor G/L \rfloor$. When approaching this limit ($K \approx 7$ to 8 so that $\mathbf{T}$ is barely tall), the performance of DRR starts to deteriorate: the conditioning of $\mathbf{T}$ becomes poor and $\mathbf{T}^\dagger$ will significantly amplify the noise. The two-step algorithm initialized by DRR still has a good performance. However, when $K \geq K_0 = 10$, its performance degrades drastically while the algorithm initialized by RAKE still maintains a good performance. Its curve gradually detaches from the MMSE curve as K increases.

It can be interpreted from the preceding results that our proposed multi-user algorithm converges rapidly, and even a single iteration can have significant improvement in channel estimation, and can be comparable to the linear MMSE receiver. Moreover, the proposed algorithm is rather independent of the initial estimate when the system is not heavily loaded. When the number of users K becomes critical, initialization by the blind RAKE is the preferred choice because it does not suffer from sudden noise enhancement.

6.5.2 Bit error rate (BER) comparison

We next study the BER performance of the various algorithms. The reference curve indicates the performance of the linear MMSE receiver based on true channel coefficients. Fig. 6.4(a) corresponds to figure 6.3(a) and shows that the multi-user version of the proposed multi-user algorithm has significant improvement over the DRR. The gain is approximately 4 dB at BER$= 10^{-2}$, and slightly increases when the BER decreases. The single-user noise-whitened iterative version, despite its rather good performance in channel estimation, is only slightly better than its corresponding DRR (the gain is about 1 dB). Without noise whitening, however, the BER results of the original iterative algorithm in section 6.2.2 were slightly worse than the non-iterative DRR (curves not shown for clarity), therefore, the whitening step is advisable.

The proposed multi-user algorithm seems to have the same BER when the SNR is high enough, independent of its initialization by the DRR or by the blind RAKE. However, when the noise is strong, the iterations initialized by RAKE have a slightly better performance because they do not suffer from noise enhancement in case $\mathbf{T}$ is not tall.

Finally, Fig. 6.4(b) shows the performance of the multiple antenna versions of each of the proposed algorithms. Compared with the corresponding MMSE receiver, the performance gap is wider than in the single-antenna case. This is in accordance with our discussion in section 6.3.3.

6.6 Conclusion

We have derived a multi-user joint source-channel estimation for long-code CDMA, which is the combination of the blind (decorrelating) RAKE receiver with an iterative symbol/channel estimation algorithm. The algorithm shows a significant improvement over the decorrelating RAKE receiver and the conventional RAKE receiver. The gain is especially impressive in heavily loaded systems, even if the noise is strong.

Using time-varying state space realizations, we showed that the proposed algorithm can be efficiently implemented, especially if the number of symbols in a slot is relatively large. Per estimated symbol per user, the complexity is of order GK, whereas the complexity of a RAKE receiver is GL, where G is the code length, K the number of users, and L the channel length in chips (assuming $K > L$ and the number of symbols in a slot sufficiently large). Thus, the proposed scheme has a complexity that is similar to that of the RAKE receiver.

Moreover, this chapter also shows how signal processing techniques can be implemented in a more general communication system, i.e. multiuser CDMA: Proper matrix manipulations can simplify the data model and ease the estimation / detection algorithms, and the matrices' sparse structures in the data models can be exploited to reduce the receiver's complexity, even the iterative ALS algorithm. Next chapter is another example of this concept when signal processing techniques are used to mitigate the narrowband interference in a TR-UWB scheme.

Part of this chapter was published as: Q.H. Dang and A-J van der Veen – *"Narrowband Interference Mitigation for a Transmit-Reference Ultra-Wideband Receiver,"* 14th European Signal Processing Conference (EUSIPCO), Sept 2006.

Chapter 7

Narrowband interference mitigation

Narrowband interference (NBI) is of specific concern in transmitted reference ultra-wideband (TR-UWB) communication systems. We the consider NBI problem in higher data rate applications where oversampling is used to resolve significant inter-frame interferences (IFIs) caused by the fact that the frame period is much shorter than the channel length. We formulate an approximate data model that includes the dominant NBI terms. For a certain range of the interference power, the receiver algorithm based on this model can mitigate the NBI effect.

7.1 Introduction

Due to its ultra-wide bandwidth nature, an UWB signal needs to coexist with signals from other narrowband systems. UWB interference to existing narrowband systems is limited by the FCC mask. Meanwhile, the narrowband interference to the UWB system is an open problem, especially in the transmit-reference (TR) scheme.

Although several research papers on TR-UWB have appeared, not many consider the presence of narrow band interference (NBI). The correlation operation in TR-UWB receivers makes it difficult to investigate and thus eliminate the NBI effect. In [55], statistics of the cross terms (due to the correlation operation) "NBI by NBI" and "NBI by data" were studied, where a "code" is used to mitigate the NBI when its frequency is known. In [73], a data model and some receiver algorithms were derived to deal with NBI in low data rate applications with no inter-frame interference. Both mentioned papers make use of a long integration time to average out some of the NBI effects. In this chapter, we will analyze the effect of NBI in a high data rate application context, where the integration is much shorter, i.e. with several samples per frame. An approximate signal processing data model, which exploits the high data rate and narrowband nature, is proposed. Subsequently, the performance improvement of the receiver algorithm based on this model is shown.

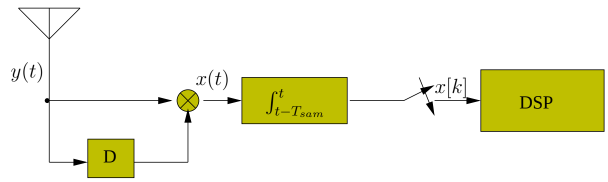

Figure 7.1: *Autocorrelation receiver*

7.2 Derivation and evaluation of the cross-terms

We consider the NBI problem for the higher data rate TR-UWB scheme, in which the inter-frame interference (IFI) is present, i.e. the frame rate T_f much less than the channel length T_h, and oversampling is used. For simplicity and clarity reasons, only a single user, single delay system is considered: each frame contains a doublet (two subsequent pulses spaced by D), each doublet is associated with a symbol value s_i. The assumed channel is specified as uncorrelated dense multipath in a typical UWB indoor environment.

The receiver structure is reduced to the simplest structure as in Fig. 7.1. The received signal at the antenna output is

$$y(t) = \sum_{i=1}^{\infty} \sqrt{E_p}[h(t-(i-1)T_f) + s_i h(t-(i-1)T_f - D)] + \gamma(t) \tag{7.1}$$

where the normalized composite channel $h(t) = h_p(t) * g(t) * a(t)$ is the convolutional product of the physical channel $h_p(t)$, the UWB pulse shape $g(t)$ and the antenna template $a(t)$. E_p is the transmitted pulse energy, and $\gamma(t)$ is the narrowband interference (NBI)

$$\gamma(t) = \sqrt{2N_I} v(t) \cos(2\pi f_I t + \theta)$$

where $v(t)$, f_I and θ are respectively the baseband signal (with normalized unit power), carrier frequency and random (uniformly distributed) phase of the NBI. N_I is the average NBI power.

It should be noted that, in order to highlight the relation between signal strength and the interference power, the new terms are now included in our equations: E_p - the transmitted pulse energy, and N_I - the average NBI power, while all other terms are normalized.

At the multiplier output, the signal $x(t) = y(t)y(t-D)$ is integrated and dumped at the oversampling rate $P = T_f/T_{sam}$. The resulting discrete signal $x[k]$ will include three cross-terms: the "data by data" term $x^{(1)}[k]$, the "data by NBI" term $x^{(2)}[k]$ and the "NBI by NBI" term $x^{(3)}[k]$.

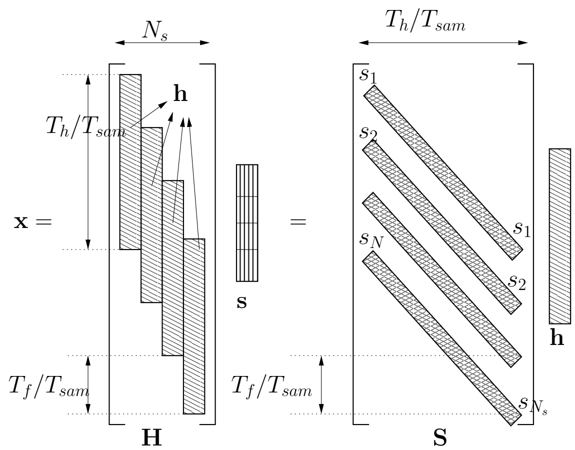

Figure 7.2: *Two forms of the data model for* $\mathbf{x}^{(1)}$

The first term "data by data" for one frame can be written as

$$x^{(1)}[k] = E_p h[k] \tag{7.2}$$

where $h[k]$ is defined (with some abuse of notation) as

$$h[k] = \int_{(k-1)T_{sam}}^{kT_{sam}} h^2(t)dt$$

Putting all samples $x^{(1)}[k]$ into a vector and taking IFI into account, we arrive a familiar model as derived in previous chapters

$$\mathbf{x}^{(1)} = E_p \mathbf{H}\mathbf{s}$$

where $\mathbf{H}$ contains the shifted versions of vector $\mathbf{h}$ with entries $h[k], k = 1, \cdots, \frac{T_h}{T_{sam}}$. The structure of the "channel" matrix $\mathbf{H}$ is illustrated in Fig. 7.2.

Now we will look at the second and the third term in $x[k]$ that deal with the NBI signal. First, since $v(t)$ is narrowband ($B \ll \frac{1}{T_{sam}}$), we can assume that it is constant during one integration period T_{sam}: $v_k = v(t)$ for $(k-1)T_{sam} < t \leq kT_{sam}$. Therefore, the "NBI by NBI" term can be expressed as

$$\begin{aligned}x^{(3)}[k] &:= 2N_I \int_{(k-1)T_{sam}}^{kT_{sam}} v(t)\cos(2\pi f_I t+\theta)v(t-D)\cos(2\pi f_I(t-D)+\theta)dt \\ &= N_I v_k^2 \int_{(k-1)T_{sam}}^{kT_{sam}} [\cos(2\pi f_I(2t-D)+2\theta)+\cos(2\pi f_I D)]dt \\ &= N_I v_k^2 T_{sam}\cos(2\pi f_I D) + N_I v_k^2 \int_{(k-1)T_{sam}}^{kT_{sam}} \cos(2\pi f_I(2t-D)+2\theta)dt\end{aligned}$$

The second term in the equation above is always less than $N_I v_k^2 \cdot \frac{1}{\pi(2f_I)}$, where $\frac{1}{\pi(2f_I)}$ is the maximum value of the integration of a zero-mean cosine wave of frequency $(2f_I)$ (over half a cycle). When T_{sam} is in the order of a nanosecond while the NBI carrier f_I is in the GHz range ($T_{sam} \gg 1/(2f_I)$), this can help increase the dominance of the first term. Unfortunately, since the value of $\cos(2\pi f_I D)$ can be arbitrary small, the condition on T_{sam} and f_I is not enough to make any conclusion about the relative magnitudes of the two terms. In the worst case, when $T_{sam}\cos(2\pi f_I D) \gg \frac{1}{\pi(2f_I)}$, the "NBI by NBI" term can be approximated as a constant with a small fluctuation ϵ_k

$$x^{(3)}[k] \approx N_I v_k^2 T_{sam}\cos(2\pi f_I D) + \epsilon_k \tag{7.3}$$

The "data by NBI" term for one frame can be expressed as

$$\begin{aligned}&x^{(2)}[k] := \sqrt{E_p}\int_{(k-1)T_{sam}}^{kT_{sam}}[h'(t)\gamma(t-D)+h'(t-D)\gamma(t)]dt \\ &= \sqrt{E_p N_I}\sqrt{2}v_k \int_{(k-1)T_{sam}}^{kT_{sam}}[h'(t)\cos(2\pi f_I(t-D)+\theta)+h'(t-D)\cos(2\pi f_I t+\theta)]dt\end{aligned}$$

where $h'(t) = h(t) + s_i h(t-D)$. Note that although we have cross-terms from other frames, they can be ignored due to the highly uncorrelated channel. The question is whether this term is relatively small compared to the "NBI by NBI" term, and how it relates to the signal to interference ratio (SIR).

Let us define

$$x_I[k,\tau_1,\tau_2] := \sqrt{E_p N_I}\sqrt{2}v_k \int_{(k-1)T_{sam}}^{kT_{sam}} h(t-\tau_1)\cos(2\pi f_I(t-\tau_2)+\theta)dt\,,$$

then we have

$$\begin{aligned}x^{(2)}[k] &= x_I[k,0,D] + s_i x_I[k,D,D] + x_I[k,D,0] + s_i x_I[k,2D,0] &(7.4)\\ &= (x_I[k,0,D] + x_I[k,D,0]) + s_i(x_I[k,D,D] + x_I[k,2D,0]) &(7.5)\end{aligned}$$

The expression for $x^{(2)}[k]$ in (7.4) contains four different terms, but they all have the form $x_I[k, \tau_1, \tau_2]$ (with differences only in the time-delay parameters τ_1, τ_2). Therefore, to simplify the expression, instead of directly comparing the "data by data" term to the "data by NBI" term, we can compare two vectors $\mathbf{x}_I$ and $\mathbf{x}_p$, with entries for $k = 1, \cdots, (T_h/T_{sam})$

$$\begin{aligned} x_I[k] &= \sqrt{E_p N_I}\sqrt{2}v_k \int_{(k-1)T_{sam}}^{kT_{sam}} h(t)\cos(2\pi f_I t + \theta)dt && (7.6) \\ x_p[k] &= E_p \int_{(k-1)T_{sam}}^{kT_{sam}} h^2(t)dt && (7.7) \end{aligned}$$

where $x_p[k]$ are the values of the "data by data" term i.e. the desired signal considered for a single frame only (and data symbol equal to 1), and $x_I[k]$ is actually $x_I[k, \tau_1, \tau_2]$ with τ_1, τ_2 set to zeros.

Define the signal to interference ratio as SIR $:= E_p/(T_f N_I)$. Note that in this definition, SIR should not be misunderstood as the exact symbol energy over the interference power because we may have several frames per symbol and the IFI effect, not to mention that one frame in this case has two pulses (doublet).

From equation (7.6), the ratio between the norms of the two vector $\mathbf{x}_p$ and $\mathbf{x}_I$ relates to the SIR as

$$\frac{\|\mathbf{x}_p\|}{\|\mathbf{x}_I\|} = \sqrt{\text{SIR}} \cdot \Gamma$$

where Γ is a factor depending on the channel and its correlation to the NBI characteristics (mostly the NBI carrier frequency f_I).

In Fig. 7.3 and 7.4, we compare these two vectors (entry-wise) for the channel models CM1 and CM3 (the results are averaged over 100 realizations) that include the UWB pulse shape and antenna effect for different sampling intervals at SIR $= 0$ dB. Here we only provide the simulation result because the sampling period T_{sam}, due to oversampling, is not long enough to make any statistical assumptions. It can be seen that, entry-wise at SIR $= 0$ dB, the "NBI by NBI" term is much smaller than the "data by data" term. Moreover, as we increase the integration interval T_{sam}, the effect of the "data by NBI" term will reduce.

For the overall comparison (between the norms), the values of the factor Γ are

$$\Gamma \approx \begin{cases} 11.7 & \text{for CM1, } T_{sam} = 1\text{ns} \\ 13.4 & \text{for CM1, } T_{sam} = 2\text{ns} \\ 19.2 & \text{for CM1, } T_{sam} = 4\text{ns} \\ 9.2 & \text{for CM3, } T_{sam} = 1\text{ns} \\ 11.1 & \text{for CM3, } T_{sam} = 2\text{ns} \\ 17.0 & \text{for CM3, } T_{sam} = 4\text{ns} \end{cases}$$

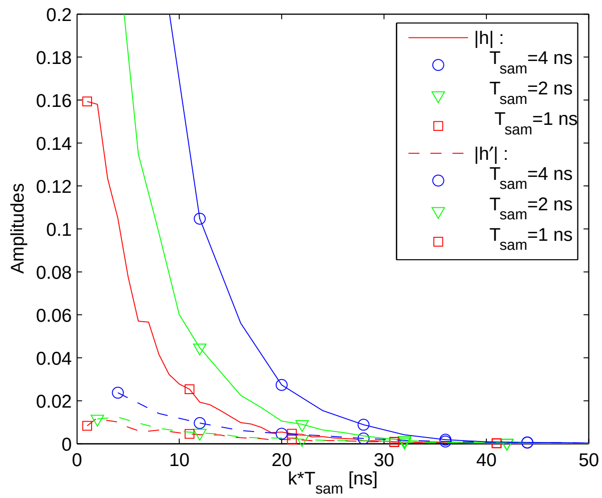

Figure 7.3: *Entry-wise comparison between* $\mathbf{x}_p$ *and* $\mathbf{x}_I$ *(CM1, SIR=0dB)*

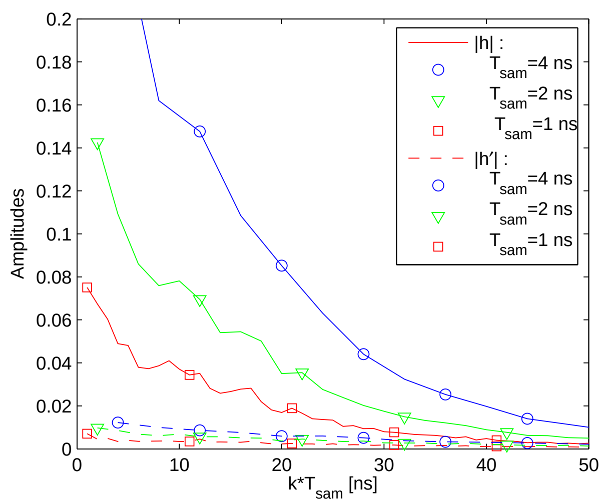

Figure 7.4: *Entry-wise comparison between* $\mathbf{x}_p$ *and* $\mathbf{x}_I$ *(CM3, SIR=0dB)*

The conclusion that $\|\mathbf{x}_I\| \ll \|\mathbf{x}_p\|$ at SIR $= 0$ dB can also be explained from the fact that in $x_p[k]$ we integrate a positive parameter $h^2(t)$, while in $x_I[k]$ the parameter

$h(t)\cos(2\pi f_I t + \theta)$ to be integrated can be randomly either positive or negative. As a result, the $x_p[k]$ are proportional to the energies of the channel segments while the $x_I[k]$ are just noise-like.

Meanwhile, at SIR = 0 dB, from equations (7.2) and (7.3), we can easily see that the third term "NBI by NBI" term is at least comparable to the first "data by data" term. Therefore, we can conclude that, in a certain SIR range, the "data by NBI" term can be ignored. The data model can be written as

$$\mathbf{x} = E_p \mathbf{H}\mathbf{s} + N_I \mathbf{v} \tag{7.8}$$

where $\mathbf{v} = T_{sam}\cos(2\pi f_I D)[v_1^2, v_2^2, \cdots]^T$.

7.3 NBI mitigation algorithms

In our data model (7.8), all the parameters on the right hand side are unknowns (more unknowns than received samples), which makes it hard, if not impossible, to find a good estimation solution. Luckily, due to high data rate and the fact that the interference is narrowband, the frame period T_f is much smaller than the reciprocal of the bandwidth of the NBI baseband signal. Therefore, it is reasonable to assume that all entries of vector $\mathbf{v}$ are approximately constant over one frame period. For example, a NBI signal of 10 MHz bandwidth (or 100 ns coherence time) can be assumed constant over one frame duration $T_f = 10$ ns. This assumption reduces the number of unknowns in $\mathbf{v}$ by a factor of P (the number of samples we take per frame $T_f = PT_{sam}$), which, for sufficiently large P, makes it possible to solve the problem iteratively.

With this assumption, the NBI vector can be expressed as

$$\begin{aligned} \mathbf{v} &= \mathbf{v}' \otimes \mathbf{1}_P & (7.9)\\ &= \mathbf{J}\mathbf{v}' & (7.10) \end{aligned}$$

where $\mathbf{J} = \mathbf{I} \otimes \mathbf{1}_P$, and $\mathbf{v}' = [v_1', v_2', \cdots]^T$, while v_i' is the value of the NBI parameter in the i-th frame:

$$v_i' = T_{sam}\cos(2\pi f_I D) v_{i1}^2 = T_{sam}\cos(2\pi f_I D) v_{i2}^2, \cdots$$

We can rewrite (7.8) in two forms, as illustrated in Fig. 7.2, namely

$$\begin{aligned} \mathbf{x} = \mathbf{H}\mathbf{s} + \mathbf{J}\mathbf{v}' &= [\mathbf{H} \quad \mathbf{J}][\mathbf{s}^T \quad \mathbf{v}'^T]^T & (7.11)\\ &= [\mathbf{S} \quad \mathbf{J}][\mathbf{h}^T \quad \mathbf{v}'^T]^T . & (7.12) \end{aligned}$$

In these equations we drop the scale terms E_p, N_I to simplify the expressions (they can be embedded in the unknown coefficients).

An iterative ALS estimation algorithm for $\mathbf{h}$, $\mathbf{s}$ and $\mathbf{v}'$ can be straightforwardly implemented as discussed previously in chapter 5 and chapter 6. The initial channel estimate can be obtained by using a training sequence (assume that the first few data symbols are known).

From equation (7.9), we can easily modify the "reduced" data model for the case where the NBI baseband signal $v(t)$ is constant over more than one frame (by changing the dimensions of vectors $\mathbf{v}'$ and $\mathbf{1}_P$ accordingly). The corresponding algorithm can be readily derived. Moreover, it should also be noted that the data model and the receiver algorithm are derived for the "noise-free" case, which means we ignore 5 cross terms that includes noise among the total number of 9 terms. In the simulation section discussed next, we will consider over which range of parameters this approximation is valid.

7.4 Simulation

We simulate the transmission of a TR-UWB scheme at high symbol rate. The frame period is $T_f = 20$ ns. Since there is only one frame per symbol, the symbol rate is 50 Mbps. UWB Gaussian monocycles of width 0.2 ns are transmitted through different IEEE channel models that take into account the nonideal antenna response. The delay between two pulses in one doublet is $D = 0.5$ ns. The channel length can be 100 ns (for CM1) up to 300 ns (for CM4).

We use 1000 Monte Carlo runs to compare the BER vs SIR (signal to interference ratio) plots of receiver algorithms when we take the NBI effect into account and when we ignore it, i.e., use the same algorithm and model but set the NBI term to zero (set $\mathbf{v}' = 0$ in equation (7.11)). To emphasize the difference, we implement two receiver algorithms when we have perfect channel estimation, i.e. the channel vector $\mathbf{h}$ is known. Note that we have much less unknown channel parameters now (compared to number of all of the "real" channel taps), which can be easily estimated by some training symbols.

In Fig. 7.5 and Fig. 7.6, we can see that in the low SIR region i.e. strong NBI signal, with our data model, we can significantly improve the BER performance, which can be as much as 5 dB. However, as the NBI signal strength decreases, the improvement also reduces, until a certain threshold SIR $\approx 0 \div 5$dB (depending on the channel model and noise power) we obtain no gain anymore. After that, the old receiver algorithm, which ignores the NBI effect, outperforms the new one. This is foreseeable because when the NBI is small enough, it can be neglected or regarded

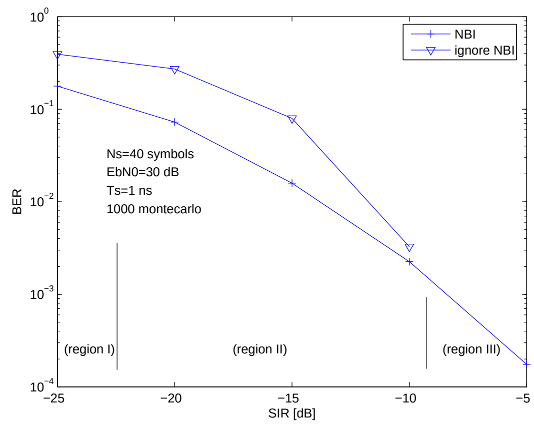

Figure 7.5: *BER vs. SIR plots for IEEE channel model CM1, SNR=30dB*

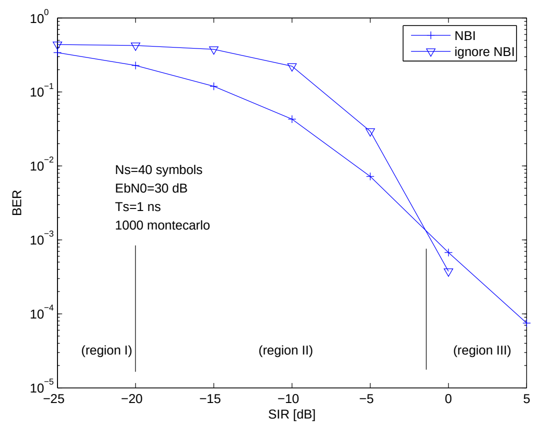

Figure 7.6: *BER vs. SIR plots for IEEE channel CM2, SNR=30dB*

as part of noise, therefore the old algorithm prevails as the number of parameters it needs to estimate is only half of that of the new algorithm (more specifically, the matrix it needs to invert is two times more tall than the other).

For a better understanding, we will look more detail into the BER vs. SIR performance with different values of the noise power. Fig. 7.7 and Fig. 7.8 show the plots

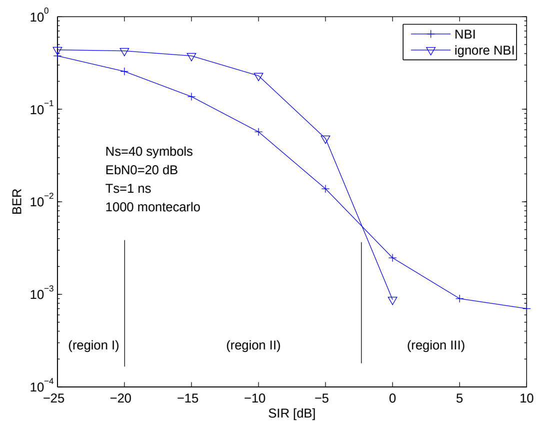

Figure 7.7: *BER vs. SIR plots for IEEE channel model CM1, SNR=20dB*

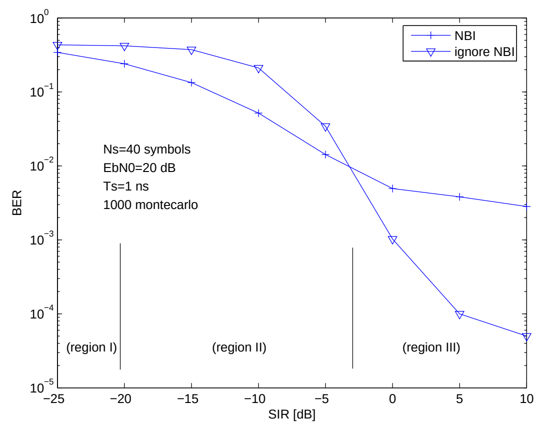

Figure 7.8: *BER vs. SIR plots for IEEE channel CM2, SNR=20dB*

when SNR=20dB. We can see that as the noise increases, its effect will be more visible than the NBI. The floor effect in high SIR region is the performance limit under the current noise power.

We can roughly divide the SIR range into three regions as follows. The high SIR region (III) is when the NBI signal is weak enough to be regarded as noise, which supports the receiver algorithm that ignores the NBI effect. The low SIR region (I) is when the NBI signal is so strong that the cross term "NBI by data" becomes significant, which will destroy the data model in (7.8). This explains why the performances of the algorithms are limited in this region. The "middle" SIR region (II) satisfies the data model, which gives expected superior performance of the algorithm that deals with the NBI signal.

7.5 Conclusions

An approximate data model has been derived to deal with the NBI problem in a TR-UWB communication system. Simulation results show that at a certain range of signal-to-interference ratio (SIR) we can mitigate the NBI effect. However, the model will not be valid anymore when the NBI signal is too strong, which results in significant increase in the cross-terms: NBI by data and NBI by noise. In this case, we may have to filter the NBI signal out before it enters the autocorrelation receiver [43].

Chapter 8

Conclusions

In the thesis, Ultra-Wideband radio has been thoroughly investigated from a signal processing perspective. Data models and their accompanying receiver algorithms have been developed for transmit-reference UWB under two main contexts: a robust low rate scheme, and a feasible and flexible higher rate scheme. Various practical issues and system design discussions have been included. The signal processing "core" of the thesis is introduced in a multiuser long code WCDMA system where matrix manipulations and algorithms are derived and implemented with reasonable complexities.

8.1 Main contributions

The thesis's main contributions are presented in relation to the questions stated previously in section 1.2.

The most important contribution, in the author's opinion, is the proposed scheme in chapter 5 for a higher rate TR-UWB system. It is a direct answer to the question #1: *"How to design a transceiver scheme for IR-UWB that uses sub-Nyquist sampling frequencies to reduce the receiver's complexity while it can still resolve IPI and IFI to achieve relatively high data rates?"*. The use of oversampling (with integrate and dump) not only helps resolve IFI (by dividing channel into multiple segments) but also allows a flexible tradeoff between various system parameters e.g. BER performance, data rate (bandwidth efficiency), complexity, number of users, which is an effective response to question #2 (*"Is there a third solution that neither ignores channel estimation nor estimates all the individual multipath channel coefficients, while providing a good and flexible trade-off between performance and complexity?"*). The design of the signal processing data model and receiver algorithms eases the system extension to multiple users, multiple delays, to narrowband interference mitigation, which at the same time solves both question #3 (*"How to build a IR-UWB scheme that effectively deals with NBI and other hardware imperfection issues?"*) and question #4 (*"How to derive efficient linear signal processing models and receiver algorithms to include multiple users and have an acceptable complexity?"*).

It should also be highlighted that, for practical antennas (of which the bandwidth is not as ultra-wide as that of the UWB pulses), those with smoother transition slopes in frequency domain have better performance, in term of allowing higher data rates, than the "ideal" rectangular shape.

Another notable contribution is the robust TR-UWB scheme. It can resolve IPI (question #1) and provide an exact signal processing model for a low rate UWB system, which works with any random channel. The unknown channel coefficients are presented in new channel matrices, of which the entries relate to the channel autocorrelation function at different lags. These channel matrices not only helps the estimation/detection problems (in question #2) but they are also robust against small discrepancies in delays between transmitter and receiver (question #3).

Last but not least, the "core" signal processing techniques applied throughout this thesis introduce elegant and coherent tools to deal with different communication systems, e.g. WCDMA and UWB. By collecting samples and putting them into matrices, the "visual" and structural representation of the matrices enables appropriate rearrangement and other mathematical manipulations on these matrices, which significantly eases the blind estimation and detection problems. The iterative algorithm (alternating Least Squares) further improves the performance without much increase in complexity. Also by exploiting the structural sparsity of the matrices, the receiver algorithms' complexities can be reduced significantly.

8.2 Future directions

Synchronization

. Although already considered and referred to, synchronization is not directly treated in this thesis. A synchronization algorithm developed for the low rate TR-UWB scheme in chapter 3 was published in [24] (originated from [25]). The same idea can be applied to estimate the unknown offsets (integer number of sampling period) but still needs some modifications for the specific data model in chapter 5. However, this algorithm is rather complex, and it does both synchronization and symbol detection at the same time, which may be unnecessary and unfavorable in some real-time, autonomous systems.

The use of oversampling in the higher rate scheme (chapter 5) implies a maximum time resolution equal to the sampling period T_{sam}, while the design of data model and receiver algorithm guarantees a robust system against a timing error ϵ less than a sampling period. This suggests to oversample in even lower rate systems to increase time resolution in synchronization algorithms.

Also in chapter 5, no assumption is made on the unknown channel vector (including the unknown offset ϵ). If a training (data) sequence is transmitted, we can use the same data model to estimate the channel vector. Comparing this resulting estimated channel vector with a known channel delay profile would give valuable information on the offset.

Applications in sensor networks

In low rate sensor networks, the autonomous devices are inactive most of the time, they should only "wake up" when a "real" signal arrives (from other devices/users or from the sensors) so that they do not waste energy on idle time. A simple and low complexity acquisition algorithm (including synchronization) is needed.

In localization applications, although ultra-short pulses can penetrate walls and other obstacles, the resulting NLOS channels cause problems in localization algorithms. Also, a fine synchronization typically below 1ns is a strong requirement for a higher resolution localization. By making use of oversampling and deriving proper signal processing models/algorithms, these problems can be solved.

Bibliography

[1] "Homepage of IEEE 802.15.3c task group," tech. rep., IEEE 802.15 WPAN Millimeter Wave Alternative PHY Task Group 3c (TG3c).

[2] "Homepage of IEEE 802.15.4a task group," tech. rep., IEEE 802.15 WPAN Low Rate Alternative PHY Task Group 4a (TG4a).

[3] "FCC notice of proposed rule making, revision of part 15 of the commission's rules regarding ultra-wideband transmission systems," Tech. Rep. ET-Docket 98-153, Federal Communications Commission, Washington, D.C., Apr. 2002.

[4] "United states frequency allocation chart," tech. rep., National Telecommunications and Information Administration, Oct. 2003.

[5] "Harmonise radio spectrum use for ultra-wideband systems in the european union," tech. rep., European Electronic Communications Committee, Copenhagen, Denmark, Mar. 2005.

[6] S. R. Aedudola, S. Vijayakumaran, and T. F. Wong, "Acquisition of direct-sequence transmitted reference ultra-wideband signals," *IEEE Journal on Selected Areas in Communications*, vol. 24, pp. 759–765, Apr. 2006.

[7] S. Bagga, L. Zhang, W. Serdijin, J. Long, and E. Busking, "A quantized analog delay for an IR-UWB quadrature downconversion autocorrelation receiver," in *IEEE International Conference on Ultra Wideband, ICU*, (Zurich (CH)), Sept. 2005.

[8] S. Bhashyam and B. Aazhang, "Multiuser channel estimation and tracking for long-code CDMA systems," *IEEE Transactions on Communications*, vol. 50, pp. 1081–1090, July 2002.

[9] J. Brown and H. Piper, "Output charactersitic function for an analog crosscorrelator with bandpass inputs," *IEEE Transactions on Information Theory*, Jan. 1967.

[10] S. Buzzi and H. Poor, "Channel estimation and multiuser detection in long-code CDMA systems," *IEEE J. Sel. Areas Comm.*, vol. 19, pp. 1476–1487, Aug. 2001.

[11] S. Buzzi and H. Poor, "On parameter estimation in long-code CDMA systems: Cramer-rao bounds and least squares algorithms," *IEEE Transactions on Signal Processing*, vol. 51, pp. 545–559, Feb. 2003.

[12] D. Cassioli, M. Win, and A. Molisch, “The ultra-wide bandwidth indoor channel: From statistical model to simulations,” *IEEE Journal on Selected Areas in Communications*, vol. 20, pp. 1247–1257, Aug. 2002.

[13] J. Choi and W. Stark, “Performance of ultra-wideband communications with suboptimal receivers in multipath channels,” *IEEE Journal on Selected Areas in Communications*, vol. 20, pp. 1754–1766, Dec. 2002.

[14] D. Coppersmith and S. Winograd, “Matrix multiplication via arithmetic progressions,” in *Proceedings of the 19th annual ACM Conference on Theory of Computing*, Apr. 1987.

[15] Q. Dang and A. van der Veen, “A low-complexity blind multi-user receiver for long-code WCDMA,” *EURASIP J. Wireless Comm. Netw.*, vol. 2004, pp. 113–122, Aug. 2004.

[16] Q. Dang and A. van der Veen, “Resolving inter-frame interference in a transmit-reference UWB communication system,” in *International Conference on Acoustics, Speech, and Signal Processing, ICASSP*, (Toulouse, France), 2006.

[17] Q. Dang and A. van der Veen, “A decorrelating multiuser receiver for TR-UWB communication systems,” *IEEE Journal on Selected Topics in Signal Processing*, vol. 1, pp. 431–442, 2007.

[18] Q. Dang and A. van der Veen, “Signal processing model and receiver algorithms for a higher rate multiuser TR-UWB communication system,” in *International Conference on Acoustics, Speech, and Signal Processing, ICASSP*, (Honolulu, HI), 2007.

[19] Q. Dang, A. van der Veen, A. Trindade, and G. Leus, “Signal model and receiver algorithms for a transmit-reference ultra-wideband communication system,” *IEEE Journal on Selected Areas in Communications*, Apr. 2006.

[20] P. Dewilde and A. van der Veen, *Time-Varying Systems and Computations*. Dordrecht, The Netherlands: Kluwer Academic Publishers, 1998.

[21] R. Djapic, *Synchronization and packet separation in wireless ad-hoc networks*. PhD thesis, Delft University of Technology, Dec. 2006.

[22] R. Djapic, G. Leus, and A. van der Veen, “Blind synchronization in asynchronous UWB networks based on the transmit-reference scheme,” in *Asilomar Conf. on Signals, Systems, and Computers*, Nov. 2004.

[23] R. Djapic, G. Leus, A. van der Veen, and A. Trindade, “Blind synchronization in multiuser transmit-reference UWB systems,” in *EUSIPCO*, (Antalya (T)), Eurasip, Sept. 2005.

[24] R. Djapic, G. Leus, A. van der Veen, and A. Trindade, “Blind synchronization in asynchronous ultra wideband (uwb) networks based on the transmit-reference scheme,” *EURASIP Journal on Wireless Communications and Networking*, vol. 2006, pp. Article ID 37952, 14 pages, 2006. doi:10.1155/WCN/2006/37952.

[25] R. Djapic, A. van der Veen, and L. Tong, “Synchronization and packet separation in wireless ad hoc networks by known modulus algorithms,” *IEEE Journal on Selected Areas in Communications*, vol. 23, pp. 51–64, Jan. 2005.

[26] C. Escudero, U. Mitra, and D. Slock, "A Toeplitz displacement method for blind multipath estimation for Long Code DS/CDMA signals," *IEEE Trans. Signal Processing*, vol. SP-48, pp. 654–665, March 2001.

[27] Y. C. et al, "Reduced-dimension blind space-time 2-D rake receivers for DS-CDMA communication systems," *IEEE Trans. Signal Processing*, vol. 48, pp. 1521–1536, June 2000.

[28] J. Foerster, "Channel modeling sub-committee report final," tech. rep., IEEE P802.15 Working Group for Wireless Personal Area Networks (WPANs), 2003.

[29] J. Foerster and Q. Li, "Uwb channel modeling contribution from intel," tech. rep., IEEE P802.15 Working Group for Wireless Personal Area Networks (WPANs), 2002.

[30] S. Franz and U. Mitra, "Generalized UWB transmitted reference systems," *IEEE Journal on Selected Areas in Communications*, vol. 24, pp. 780–786, Apr. 2006.

[31] E. Funk, S. Saddow, L. Jasper, and A. Lee, "Time coherent ultra-wideband pulse generation using photoconductive switching," *Digest of the LEOS Summer Topical Meetings*, pp. 55–56, 1995.

[32] R. Gagliardi, "A geometrical study of transmitted reference communication systems," *IEEE Transactions on Communication Technology*, pp. 118–123, Dec. 1964.

[33] G. Golub and C. V. Loan, *Matrix Computations*. Baltimore, Maryland: The Johns Hopkins University Press, 1990.

[34] G. Golub and C. Reinsch, "Singular value decomposition and least squares solutions," *Numerische Mathematik*, vol. 14, pp. 403–420, 1970.

[35] G. Hingorani and J. Hancock, "A transmitted reference system for communication in random channels," *IEEE Transactions on Communication Technology*, Sept. 1965.

[36] R. Hoctor and H. Tomlinson, "Delay-hopped transmitted-reference RF communications," in *IEEE Conference on Ultra Wideband Systems and Technologies*, pp. 265–270, 2002.

[37] R. Hoctor and H. Tomlinson, "An overview of delay-hopped, transmitted-reference RF communications," Tech. Rep. 2001CRD198, GE Research & Development Center, Jan. 2002.

[38] H. Holma and A. Toskala, *WCDMA for UMTS*. West Sussex, England: John Wiley & Sons, second ed., 2002.

[39] S. Hoyos and B. Sadler, "Frequency-domain implementation of the transmitted-reference ultra-wideband receiver," *IEEE Transactions on Microwave Theory and Techniques*, vol. 54, pp. 1745–1753, June 2006.

[40] S. Hoyos, B. Sadler, and G. Arce, "Monobit digital receivers for ultrawideband communications," *IEEE Transactions on Wireless Communications*, vol. 4, pp. 1337–1344, July 2005.

[41] Z. Irahhauten, G. J. Janssen, H. Nikookar, A. Yarovoy, and L. P. Ligthart, "UWB channel measurements and results for office and industrial environments," in *IEEE International Conference on Ultra Wideband, ICU*, (MA), Sept. 2006.

[42] Z. Irahhauten, H. Nikookar, and G. Janssen, “An overview of ultra wide band indoor channel measurements and modeling,” *IEEE Microwave and Wireless Components Letters*, vol. 14, pp. 386–388, Aug. 2004.

[43] Z. Irahhauten, A. Yarovoy, G. J. Janssen, H. Nikookar, and L. P. Ligthart, “Suppression of noise and narrowband interference in UWB indoor channel measurements,” in *IEEE International Conference on Ultra Wideband, ICU*, (Zurich (CH)), Sept. 2005.

[44] G. Leus and A. J. van der Veen, “Noise suppression in UWB transmitted reference system,” in *IEEE Signal Processing Workshop on Signal Processing Advances in Wireless Communications, SPAWC*, (Lisboa, Portugal), July 2004.

[45] G. Leus and A. J. van der Veen, “A weighted autocorrelation receiver for transmitted reference ultra wideband communications,” in *IEEE Signal Processing Workshop on Signal Processing Advances in Wireless Communications, SPAWC*, (NY), June 2005.

[46] K. Li and H. Liu, “Channel estimation for DS-CDMA with aperiodic spreading codes,” in *Proc. 1999 ICASSP*, pp. 2535–1538, Mar 1998.

[47] T. J. Lim, L. K. Rasmussen, and H. Sugimoto, “An asynchronous multiuser cdma detector based on the kalman filter,” *IEEE Journal on Selected Areas in Communications*, vol. 16, no. 9, p. 17111722, 1998.

[48] H. Liu and M. Zoltowski, “Blind equalization in antenna array CDMA systems,” *IEEE Trans. Signal Processing*, vol. 45, p. 161172, Jan. 1997.

[49] P. Liu and Z. Xu, “Linear multiuser detection for uplink long-code CDMA systems,” in *International Conference on Acoustics, Speech, and Signal Processing, ICASSP*, Apr. 2003.

[50] V. Lottici, A. DAndrea, and U. Mengali, “Channel estimation for ultrawideband communications,” *IEEE Journal on Selected Areas in Communications*, vol. 20, no. 9, p. 16381645, 2002.

[51] M. Melvasalo and V. Koivunen, “Blind channel estimation in multicode CDMA system with antenna array,” in *IEEE Proc. Sensor Array and Multichannel Signal Processing Workshop*, pp. 565 – 569, Aug. 2002.

[52] A. Molisch, J. Foerster, and M. Pendergrass, “Channel models for ultrawideband Personal Area Networks,” *IEEE Personal Communications Magazine*, vol. 10, pp. 14–21, Dec. 2003.

[53] T. K. Moon and W. C. Stirling, *Mathematical Methods and Algorithms for Signal Processing*. Prentice Hall, 1999.

[54] I. Oppermann, M. Hamalainen, and J. Iinatti, *UWB: Theory and Applications*. West Sussex, England: John Wiley & Sons, first ed., 2004.

[55] M. Pausini and G. Janssen, “On the narrowband interference in transmitted reference UWB receivers,” in *ICU*, (Zurich (CH)), Sept. 2005.

[56] J. Proakis, *Digital Communications*. McGraw Hill, 4 ed., 2001.

[57] C. Rushforth, “Transmitted-reference techniques for random or unknown channels,” *IEEE Transactions on Information Theory*, Jan. 1964.

[58] A. Saleh and R. Valenzuela, "A statistical model for indoor multipath propagation," *IEEE Journal on Selected Areas in Communications*, vol. 5, pp. 128–137, Feb. 1987.

[59] H. Schantz and L. Fullerton, "The diamond dipole: A gaussian impulse antenna," in *Proceedings of IEEE International Symposium on Antennas and Propagation*, vol. 4, (Boston,MA), pp. 100–103, 2001.

[60] A. Schranzhofer, "Acquisition for a transmitted reference uwb receiver," Master's thesis, Delft University of Technology, 2007.

[61] N. Sidiropoulos and R. Bro, "User separation in DS-CDMA Systems with unknown Long PN Spreading Codes," in *IEEE Signal Processing Workshop on Signal Processing Advances in Wireless Communications, SPAWC*, (Annapolis, MD.), pp. 194–197, May 1999.

[62] V. Strassen, "Gaussian elimination is not optimal," *Numerische Mathematik*, vol. 13, pp. 354–356, Aug. 1969.

[63] S. Talwar, M. Viberg, and A. Paulraj, "Blind separation of synchronous co-channel digital signals using an antenna array. i. algorithms," *IEEE Transactions on Signal Processing*, vol. 44, no. 5, p. 11841197, 1996.

[64] Z. Tian and G. Giannakis, "Ber sensitivity to timing offset in ultra wideband communications," in *IEEE Signal Processing Workshop on Signal Processing Advances in Wireless Communications, SPAWC*, 2003.

[65] L. Tong, A. van der Veen, and P. Dewilde, "Channel estimation for long-code WCDMA," in *Proc. IEEE ISCAS*, (Scotsdale (AZ)), IEEE, May 2002.

[66] L. Tong, A.-J. van der Veen, P. Dewilde, and Y. Sung, "Blind decorrelating rake receivers for long-code WCDMA," *IEEE Transactions on Signal Processing*, vol. 51, pp. 1642–1655, June 2003.

[67] L. Tong, A.-J. van der Veen, P. Dewilde, and Y. Sung, "Blind decorrelating RAKE receivers for long-code WCDMA," *to appear, IEEE Tr. Signal Processing*, vol. 51, Jan. 2003.

[68] M. Torlak, B. Evans, and G. Xu, "Blind estimation of FIR channels in CDMA systems with aperiodic spreading sequences," in *Proc. 31st. Asilomar Conf. Sig. Systems and Computers*, (Montery, CA), pp. 495–499, Oct 1997.

[69] A. Trindade, Q. Dang, and A. van der Veen, "Signal processing model for a transmit-reference UWB wireless communication system," in *IEEE Conference on Ultra Wideband Systems and Technologies*, (Reston, Virginia), Oct. 2003.

[70] N. van Stralen, A. Dentinger, K. Welles, R. Gauss, R. Hoctor, and H. Tomlinson, "Delay hopped transmitted reference experimental results," in *IEEE Conference on Ultra Wideband Systems and Technologies*, pp. 93–98, 2002.

[71] A. Weiss and B. Friedlander, "Channel estimation for DS-CDMA downlink with aperiodic spreading codes," *IEEE Transactions on Communications*, vol. 47, pp. 1561–1569, Oct 1999.

[72] M. Win and R. Scholtz, "Characterization of ultra-wide bandwidth wireless indoor channels: a communication-theoretic view," *IEEE Journal on Selected Areas in Communications*, vol. 20, no. 9, p. 16131627, 2002.

[73] K. Witrisal and Y. D. Alemseged, "Narrowband interference mitigation for differential UWB systems," in *Asilomar Conference on Signals, Systems, and Computers*, (California, US), 2005.

[74] K. Witrisal, G. Leus, M. Pausini, and C. Krall, "Equivalent system model and equalization of differential impulse radio UWB systems," *IEEE Journal on Selected Areas in Communications*, vol. 23, pp. 1851–1862, Sept. 2005.

[75] K. Witrisal, M. Pausini, and A. Trindade, "Multiuser interference and inter-frame interference in UWB transmitted reference systems," in *IEEE Conference on Ultra Wideband Systems and Technologies*, (Kyoto, Japan), May 2004.

[76] Z. Xu, "Computationally efficient multiuser detection for aperiodically spreading CDMA systems," in *International Conference on Acoustics, Speech, and Signal Processing, ICASSP*, May 2001.

[77] Z. Xu, P. Liu, and M. Zoltowski, "Diversity-assisted channel estimation and multiuser detection for downlink CDMA with long spreading codes," *IEEE Transactions on Signal Processing*, vol. 52, pp. 1492–1500, Jan. 2004.

[78] Z. Xu and B. M. Sadler, "Multiuser transmitted reference ultra-wideband communication systems," *IEEE Journal on Selected Areas in Communications*, vol. 24, pp. 766–772, Apr. 2006.

[79] Z. Xu and M. Tsatsanis, "Blind channel estimation for long code multiuser CDMA systems," *IEEE Trans.Signal Processing*, vol. 48, pp. 988–1001, April 2000.

[80] L. Yang and G. Giannakis, "Blind UWB timing with a dirty template," in *International Conference on Acoustics, Speech, and Signal Processing, ICASSP*, (Montreal, Canada), 2004.

[81] L. Yang and G. Giannakis, "Optimal pilot waveform assisted modulation for ultra-wideband communications," *IEEE Transactions on Wireless Communications*, vol. 3, pp. 1236–1249, 2004.

[82] Z. Yang and X. Wang, "Blind turbo multiuser detection for long-code multipath CDMA," *IEEE Transactions on Signal Processing*, vol. 50, pp. 112–125, Jan. 2002.

[83] H. Zhang and D. Goeckel, "Generalized transmit-reference UWB systems," in *IEEE Conference on Ultra Wideband Systems and Technologies*, (Reston, VA), Oct. 2003.

[84] Y. Zhang and R. Zhang, "Blind mmse multipath combining for long-code CDMA systems," in *International Conference on Acoustics, Speech, and Signal Processing, ICASSP*, Apr. 2003.

[85] M. Zoltowski, Y. Chen, and J. Ramos, "Blind 2D RAKE receivers based on space-time adaptive MVDR processing for IS-95 CDMA system," in *Proceedings of the 15th IEEE MILCOM*, (Atlanta, GA), pp. 618–622, Oct 1996.

Index

Summary

This thesis mainly focuses on signal processing algorithms for transmit-reference (TR) schemes in Impulse Radio Ultra-Wideband (IR-UWB) systems. Data models and receiver algorithms are developed under various situations: single-user / multiuser, with interframe interferences (IFI), and narrowband interference (NBI). Sub-Nyquist sampling and oversampling are used to reduce the receiver complexity and at the same time provide a more flexible and feasible solution to channel estimation in UWB. The core signal processing model and algorithm are presented in a more general WCDMA system.

Firstly, a novel TR-UWB scheme is proposed to deal with ranndom UWB channel by modeling and estimating the channel correlation matrix. By using the whole channel matrix, the model is shown to be much more accurate than the original TR-UWB scheme exploiting only the main diagonal of this matrix. Another advantage is that the proposed scheme is robust again a small discrepancy in the delay lines.

Based on statistics of typical UWB channels (both measured and theoretical channels), an even higher data rate TR-UWB is motivated and developed. Oversampling (with integrate and dump) is used to resolve IFIs. Signal processing models and algorithms are derived for both single-user and multiuser cases, with multiple delays serving a similar role to multiple antennas in other wireless communication systems.

The core signal processing techniques is introduced in a multiuser WCDMA context. By visual representations and matrix manipulations in building data models, an iterative receiver based on Alternating Least Squares (ALS) algorithm can be easily implemented. This iterative algorithm is shown to be converge quickly after a few iterations. The receiver algorithm's complexity can be reduced by exploiting matrices' sparse structures.

Finally, the statistics of additional terms caused by NBI is analyzed and simulated. It is shown under certain circumstances, these interference terms can be modeled and subsequently mitigated by signal processing algorithms.

Samenvatting

Dit proefschrift behandelt vooral signaalbewerkingsalgoritmes voor "transmit-reference" (TR) modulatietechnieken voor pulsgebaseerd ultra-breedband (UWB) systemen. Data modellen en ontvanger-algoritmes worden afgeleid voor diverse situaties: een gebruiker en meerdere gebruikers, met interframe interferentie (IFI) en smalbandige interferentie (NBI). Sampling onder de Nyquist limiet en oversampling worden gebruikt om de complexiteit van de ontvanger te reduceren en tegelijkertijd een flexibelere en realiseerbare oplossing te bieden voor het kanaalschattingsprobleem in UWB. Het basismodel en algoritme worden ook getoond voor een meer algemeen WCDMA systeem.

Om te beginnen wordt een nieuw TR-UWB modulatieschema voorgesteld dat rekening houdt met willekeurige UWB kanalen door middel van het schatten van de kanaalcorrelatiematrix. Doordat de hele kanaalmatrix gebruikt wordt is het model veel nauwkeuriger dan het originele TR-UWB systeem dat enkel de hoofddiagonaal van die matrix benut. Een ander voordeel is dat het voorgestelde systeem robust is voor kleine afwijkingen in de gebruikte RF vertragingslijnen.

Gebaseerd op de statistieken van typische UWB kanalen (zowel gemeten kanalen als theoretische modellen) wordt een TR-UWB systeem voorgesteld met zelfs hogere transmissiesnelheden. Oversampling wordt gebruikt om het IFI probleem te overkomen. Signaalbewerkingsmodellen en algoritmen worden afgeleid voor zowel een gebruiker als meerdere gebruikers, met meerdere vertragingslijnen die dezelfde rol spelen als het gebruik van meerdere antennes in draadloze communicatiesystemen.

Het basis signaalbewerkingsalgoritme wordt ook getoond voor een WCDMA systeem met meerdere gebruikers. Door een inzichtelijke afleiding van het datamodel kan een iteratief algoritme gebaseerd op alternerende kleinste kwadraten eenvoudig geimplementeerd worden. Dit iteratieve algoritme convergeert snel, al na een paar iteraties. De complexiteit van het algoritme kan verminderd worden door gebruikmaking van de nulstructuren in de matrices.

Tot slot worden de statistieken van de extra kruistermen veroorzaakt door NBI geanalyseerd en bestudeerd via simulaties. Het volgt dat, onder bepaalde omstandigheden, deze extra termen gemodeleerd kunnen worden en vervolgens onderdrukt door middel van signaalbewerkingstechnieken.

Acknowledgments

First of all, I would like to thank my supervisor and promotor, Prof. dr. ir. Alle-Jan van der Veen, for his thoughtful guidance from the days I did my M.Sc thesis. It was him who gave me the opportunity to enroll as a PhD student. From him I learned not only in-depth knowledge in linear algebra but also a strong devotion to science. Alle-Jan aroused my interest in other disciplines, and taught me to have a much broader view at problems from different perspectives. He encouraged me in other hobbies like photography, and even helped me to translate the propositions and summary of this thesis into Dutch. Thanks again, Alle-Jan!

Thanks to the committee members for spending time and effort to review this thesis and provide me with insightful remarks! Thank you, Geert, not only because you are in the committee, but also because of interesting discussions and generous helps from you, despite my shyness, through out all these years.

If I can only name one friend from our group here, then it must be you - Tang. Although we seemed to be a bit quiet officemates, you were not just a Dutch interpreter to me. Whether it was about my “social” alienation, my career disorientation, or the problems I had in writing this thesis, your understanding and your willingness to help were invaluable. Thank you very much, Tang!

I owe many thanks to Laura Bruns and Laura Zondervan for providing me with excellent working facilities and organizing memorable outdoor activities. Thanks to Antoon for repeatedly reinstalling Linux OS and other software on request. Thanks to my PhD fellows - Antonio, Relja, Zoubir, Marco, Eelco, Bas, Filip, Kun, Claude, Vijay, Sayit, and Yiyin - for your support, your collaboration and the fun we had together.

Six years in Delft would have been pretty boring without my Vietnamese friends. The community is so big that I cannot possibly name all of them here. Many thanks to Linh, who was my classmate, my roommate, and my (football) teammate. Your help in printing this thesis is highly appreciated. Little Khoai and your parents should not be forgotten for throwing delightful parties. Big applause to Dong & Linh, Trinh, Hoang for sharing a fancy apartment with me recent years. The weekend dinners with beef steaks and French wines, followed by noisy Karaoke nights were a great source of entertainment and inspiration to me.

Distant friends have been vital to me during all these years. Ly, Hang, GT, HA, QA, MA, and Ha were not only great links between me and Vietnam, but also opened new horizons for me in their many other “worlds”, and for those, thanks a lot. Last but not least, special thanks to Tra for being my companion these days, your love and support are always priceless!

Quang Hieu Dang

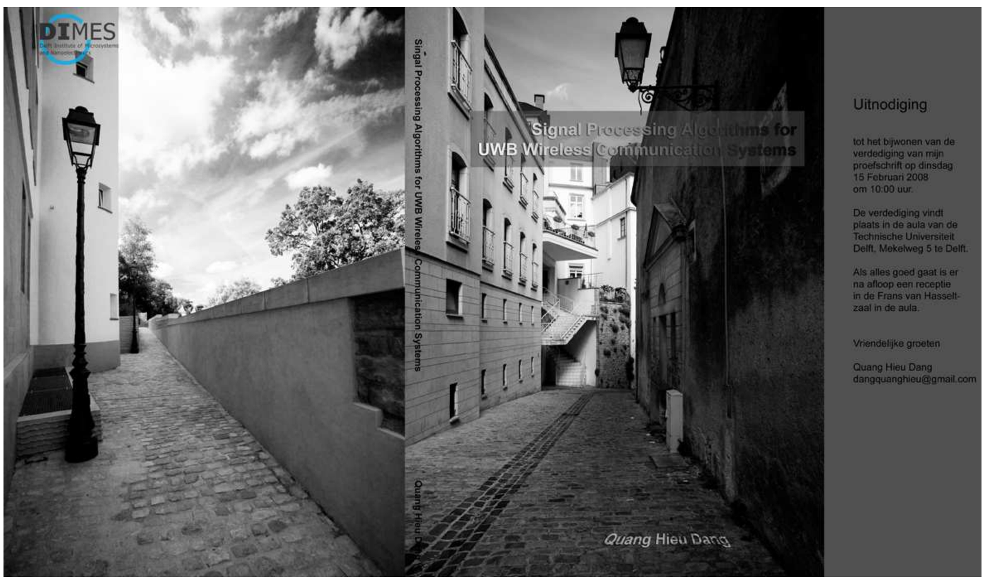

Figure 8.1: *The beloved unused cover with my photos taken in Europe.*